Final Report

THERMAL POLLUTION MATHEMATICAL MODEL

(Volume Two of Seven Volumes)

VERIFICATION OF ONE-DIMENSIONAL NUMERICAL MODEL AT LAKE KEOWEE

by
Samuel S. Lee, Subrata Sengupta,
and Emmanuel V. Nwadike
Department of Mechanical Engineering
University of Miami

Volume II

August 1980

Final Report

THERMAL POLLUTION MATHEMATICAL MODEL

(Volume Two of Seven Volumes)

VERIFICATION OF ONE-DIMENSIONAL NUMERICAL MODEL AT LAKE KEOWEE

Volume II

by

Samuel S. Lee, Subrata Sengupta
and Emmanuel V. Nwadike
Department of Mechanical Engineering
University of Miami
Coral Gables, Florida 33124

Prepared for

National Aeronautics and Space Administration
and
Environmental Protection Agency
(NASA Contract NAS 10-9410)

August 1980

STANDARD TITLE PAGE

1. Report No.	2. Government Accession No.	3. Recipient's Catalog No.
CR-165623		

4. Title and Subtitle	5. Report Date
Thermal Pollution Math Model Volume II, Verification of One-Dimensional Numerical Model at Lake Keowee	6. Performing Organization Code TR 43-4
7. Author(s) Drs. Samuel Lee and Subrata Sengupta; Emmanuel V. Nwadike	8. Performing Organization Report No.
9. Performing Organization Name and Address John F. Kennedy Space Center Kennedy Space Center, Florida 32899 Project Manager: Roy A. Bland Code PT-FAP	10. Work Unit No. 11. Contract or Grant No. NAS10-9410
12. Sponsoring Agency Name and Address National Aeronautics and Space Administration and Environmental Protection Agency Research Triangle Park, N.C.	13. Type of Report and Period Covered Final 14. Sponsoring Agency Code

15. Abstract

A one-dimensional model for studying the thermal dynamics of cooling lakes has been developed and verified. The model is essentially a set of partial differential equations which are solved by finite difference methods. The model includes the effects of variation of cross-sectional area with depth, surface heating due to solar radiation absorbed at the upper layer and internal heating due to the transmission of solar radiation to the sub-surface layers. The exchange of mechanical energy between the lake and the atmosphere is included through the coupling of thermal diffusivity and wind speed. The effects of discharge and intake by power plants are also included.

The numerical model was calibrated by applying it to Cayuga Lake. The performance was very good. The model was then verified through a long term simulation using Lake Keowee data base. The comparison between measured and predicted vertical temperature profiles for the nine years is good. The physical limnology of Lake Keowee is presented through a set of graphical representations of the measured data base.

16. Key Words
Thermal Pollution
Math Models
Nuclear or Fossil Fuel Power Plants
Waste Heat

17. Bibliographic Control	18. Distribution
Announce in Star Category 43	Unlimited

19. Security Classif.(of this report)	20. Security Classif.(of this page)	21. No. of Pages	22. Price
None	None		

KSC FORM 16-272NS (REV. 7/78)

PREFACE

This final report is the summary of a two-year effort portraying the development, calibration and verification of a one-dimensional variable cross-sectional area numerical model. This is one of the publications of the thermal pollution group at the University of Miami.

This effort covers the applications of this model to Cayuga Lake in New York and Lake Keowee in South Carolina. The conclusions and derivations are accompanied by an abundance of figures and tables. These figures and tables are presented in such a way as to make it possible for use in calibrating or verifying other one-dimensional models.

This work was conducted under funding from National Aeronautics and Space Administration (NASA), Kenedy Space Center and the Environmental Protection Agency (EPA).

ABSTRACT

A one-dimensional model for studying the thermal dynamics of cooling lakes has been developed and verified. The model is essentially a set of partial differential equations which are solved by finite difference methods. The model includes the effects of variation of cross-sectional area with depth, surface heating due to solar radiation absorbed at the upper layer and internal heating due to the transmission of solar radiation to the sub-surface layers. The exchange of mechanical energy between the lake and the atmosphere is included through the coupling of thermal diffusivity and wind speed. The effects of discharge and intake by power plants are also included.

The numerical model was calibrated by applying it to Cayuga Lake. The performance was very good. The model was then verified through a long term simulation using Lake Keowee data base. The comparison between measured and predicted vertical temperature profiles for the nine years is good. The physical limnology of Lake Keowee is presented through a set of graphical representations of the measured data base.

CONTENTS

Foreword .....
Preface ii
Abstract iii
Figures iv
Tables xi
Symbols xii
Acknowledgments xiii

1. Introduction 1
2. Conclusions 3
3. Recommendations 4
4. The Mathematical Model 5
   Description 5
   Boundary conditions 8
   Numerical method 9
5. Model Calibration 12
   Cayuga Lake application 12
   Input quantities 12
   Results 15
6. Model Verification 24
   Lake Keowee application 24
   Input quantities 24
   Results 25

References 57
Appendices 59

A. Derivation of the Mathematical Model 60
B. Measured Temperature Profiles Plots (1971-1978), Stations 500 through 506 68
C. Averaged Temperature Profiles, Stations 500 through 506 . 125

FIGURES

Number		Page
1	Vertical temperature profiles, Cayuga Lake	17
2	Vertical temperature profiles, Cayuga Lake	18
3	Vertical temperature profiles, Cayuga Lake	19
4	Stratification cycle cylindrical domain, Cayuga Lake	20
5	Stratification cycle paraboloid domain, Cayuga Lake	21
6	Variation of eddy diffusivity with depth cylindrical domain, Cayuga Lake	22
7	Variation of eddy diffusivity with depth paraboloid domain, Cayuga Lake	23
8	Map of Lake Keowee	34
9	Temperature profiles, Lake Keowee, 1971	35
10	Temperature profiles, Lake Keowee, 1972	36
11	Temperature profiles, Lake Keowee, 1973	37
12	Temperature profiles, Lake Keowee, 1974	38
13	Temperature profiles, Lake Keowee, 1975	39
14	Temperature profiles, Lake Keowee, 1976	40
15	Temperature profiles, Lake Keowee, 1977	41
16	Temperature profiles, Lake Keowee, 1978	42
17	Temperature profiles, Lake Keowee, 1979	43
18	Lake Keowee discharge vs no discharge, 1971	44
19	Lake Keowee discharge vs no discharge, 1972	45

FIGURES

Number		Page
20	Lake Keowee discharge vs no discharge, 1973	46
21	Lake Keowee discharge vs no discharge, 1974	47
22	Lake Keowee discharge vs no discharge, 1975	48
23	Lake Keowee discharge vs no discharge, 1976	49
24	Lake Keowee discharge vs no discharge, 1977	50
25	Lake Keowee discharge vs no discharge, 1978	51
26	Lake Keowee discharge vs no discharge, 1979	52
27	Variation of eddy diffusivity with depth	53
28	Monthly variation of the depth of the thermocline	54
29	Temporal variation of the surface exchange coefficient	55
30	Stratification cycle, Lake Keowee	56
B-1	Lake Keowee measured temperature profiles, 1971, Station 500	69
B-2	Lake Keowee measured temperature profiles, 1972, Station 500	70
B-3	Lake Keowee measured temperature profiles, 1973, Station 500	71
B-4	Lake Keowee measured temperature profiles, 1974, Station 500	72
B-5	Lake Keowee measured temperature profiles, 1975, Station 500	73
B-6	Lake Keowee measured temperature profiles, 1976, Station 500	74
B-7	Lake Keowee measured temperature profiles, 1977, Station 500	75
B-8	Lake Keowee measured temperature profiles, 1978, Station 500	76

FIGURES

Number		Page
B-9	Lake Keowee measured temperature profiles, 1971, Station 501	77
B-10	Lake Keowee measured temperature profiles, 1972, Station 501	78
B-11	Lake Keowee measured temperature profiles, 1973, Station 501	79
B-12	Lake Keowee measured temperature profiles, 1974, Station 501	80
B-13	Lake Keowee measured temperature profiles, 1975, Station 501	81
B-14	Lake Keowee measured temperature profiles, 1976, Station 501	82
B-15	Lake Keowee measured temperature profiles, 1977, Station 501	83
B-16	Lake Keowee measured temperature profiles, 1978, Station 501	84
B-17	Lake Keowee measured temperature profiles, 1971, Station 502	85
B-18	Lake Keowee measured temperature profiles, 1972, Station 502	86
B-19	Lake Keowee measured temperature profiles, 1973, Station 502	87
B-20	Lake Keowee measured temperature profiles, 1974, Station 502	88
B-21	Lake Keowee measured temperature profiles, 1975, Station 502	89
B-22	Lake Keowee measured temperature profiles, 1976, Station 502	90
B-23	Lake Keowee measured temperature profiles, 1977, Station 502	91
B-24	Lake Keowee measured temperature profiles, 1978, Station 502	92

FIGURES

Number		Page
B-25	Lake Keowee measured temperature profiles, 1971, Station 503	93
B-26	Lake Keowee measured temperature profiles, 1972, Station 503	94
B-27	Lake Keowee measured temperature profiles, 1973, Station 503	95
B-28	Lake Keowee measured temperature profiles, 1974, Station 503	96
B-29	Lake Keowee measured temperature profiles, 1975, Station 503	97
B-30	Lake Keowee measured temperature profiles, 1976, Station 503	98
B-31	Lake Keowee measured temperature profiles, 1977, Station 503	99
B-32	Lake Keowee measured temperature profiles, 1978, Station 503	100
B-33	Lake Keowee measured temperature profiles, 1971, Station 504	101
B-34	Lake Keowee measured temperature profiles, 1972, Station 504	102
B-35	Lake Keowee measured temperature profiles, 1973, Station 504	103
B-36	Lake Keowee measured temperature profiles, 1974, Station 504	104
B-37	Lake Keowee measured temperature profiles, 1975, Station 504	105
B-38	Lake Keowee measured temperature profiles, 1976, Station 504	106
B-39	Lake Keowee measured temperature profiles, 1977, Station 504	107
B-40	Lake Keowee measured temperature profiles, 1978, Station 504	108

FIGURES

Number		Page
B-41	Lake Keowee measured temperature profiles, 1971, Station 505	109
B-42	Lake Keowee measured temperature profiles, 1972, Station 505	110
B-43	Lake Keowee measured temperature profiles, 1973, Station 505	111
B-44	Lake Keowee measured temperature profiles, 1974, Station 505	112
B-45	Lake Keowee measured temperature profiles, 1975, Station 505	113
B-46	Lake Keowee measured temperature profiles, 1976, Station 505	114
B-47	Lake Keowee measured temperature profiles, 1977, Station 505	115
B-48	Lake Keowee measured temperature profiles, 1978, Station 505	116
B-49	Lake Keowee measured temperature profiles, 1971, Station 506	117
B-50	Lake Keowee measured temperature profiles, 1972, Station 506	118
B-51	Lake Keowee measured temperature profiles, 1973, Station 506	119
B-52	Lake Keowee measured temperature profiles, 1974, Station 506	120
B-53	Lake Keowee measured temperature profiles, 1975, Station 506	121
B-54	Lake Keowee measured temperature profiles, 1976, Station 506	122
B-55	Lake Keowee measured temperature profiles, 1977, Station 506	123
B-56	Lake Keowee measured temperature profiles, 1978, Station 506	124

FIGURES

Number		Page
C-1	Lake Keowee averaged measured temperature profiles, Stations 501-506, 1971	126
C-2	Lake Keowee averaged measured temperature profiles, Stations 501-506, 1972	127
C-3	Lake Keowee averaged measured temperature profiles, Stations 501-506, 1973	128
C-4	Lake Keowee averaged measured temperature profiles, Stations 501-506, 1974	129
C-5	Lake Keowee averaged measured temperature profiles, Stations 501-506, 1975	130
C-6	Lake Keowee averaged measured temperature profiles, Stations 501-506, 1976	131
C-7	Lake Keowee averaged measured temperature profiles, Stations 501-506, 1977	132
C-8	Lake Keowee averaged measured temperature profiles, Stations 501-506, 1978	133

TABLES

Number		Page
1	Oconee Nuclear Station Condenser Cooling Water Flowrate (m^3/min)	27
2	Oconee Nuclear Station Condenser Temperature Rise, ΔT (°C)	28
3	Monthly Average Flowrates (m^3/sec) - Lake Keowee Hydro Station	29
4	Lake Jocassee Hydro Flows (cfs)	30
5	Lake Keowee, Wind Speed (cm/sec)	31
6	Lake Keowee Gross Solar Radiation (Langleys)	32
7	Lake Keowee Dewpoint Temperature (°C)	33

SYMBOLS

z	Vertical coordinate measured upward from the deepest point of the lake. As a subscript it marks the vertical component of a vector.
h	Depth of the lake
$A(z)$	Horizontal cross-sectional area at height Z
$I(z)$	Bottom-surface source of mass per unit area
$Q(z)$	Bottom-surface source of heat per unit area
T	Temperature
ρ	Density of water
V_z	Vertical velocity
K_z	Eddy diffusivity
K_{zo}	Eddy diffusivity under neutral condition
$W^* = (\tau_s/\rho)$	Friction velocity
σ_1	Empirical constant
R_i	Richardson number
T_s	Surface temperature
q_B	Bottom surface heat flux
α_v	Volumetric coefficient of expansion of water
τ_s	Surface shear stress
C_p	Heat capacity
$H(z)$	Heat source/unit volume
A_1	Average value of W^*
A_2	Half the annual variation of W^*
C_1, C_2, C_3, C_4, C_5	Phase angles
ϕ_o	Solar radiation incident on the water surface
A_2	Average value of ϕ_o
B_2	Half the annual variation of ϕ_o
η	Extinction coefficient
β	Absorption coefficient
Q_p	Volumetric discharge
ΔT	Condenser temperature change
T_D	Discharge temperature
q_s	Surface heat flux
K_s	Surface heat exchange coefficient
T_E	Equilibrium temperature
A_3	Average value of T_E
B_3	Half the annual variation of T_E
B	Lake surface radius
$\frac{dA}{dz}$	Area variation with depth

ACKNOWLEDGMENTS

This work was supported by a contract from the National Aeronautics and Space Administration (NASA-KSC) and the Environmental Protection Agency (EPA-RTP).

The authors express their sincere gratitude for the technical and managerial support of Mr. Roy A. Bland, the NASA-KSC project manager of the contract, and the NASA-KSC remote sensing group. Special thanks are also due to Dr. Theodore G. Brna, the EPA-RTP project manager, for his guidance and support of the experiments, and to Mr. S. B. Hager, Chief Engineer, Civil-Environmental Division, and Mr. William J. McCabe, Assistant Design Engineer, both from the Duke Power Company, Charlotte, North Carolina, and their data collection group for data acquisition. The support of Mr. Charles H. Kaplan of EPA was extremely helpful in the planning and reviewing of this project.

SECTION 1

INTRODUCTION

Deep bodies of water provide a convenient source of condenser cooling water supply to electric generating power plants. One of the problems associated with this, that has gained increasing importance in recent years is the thermal pollution caused by the discharge of waste heat from these power plants. The degradation of the quality of these waters usually occurs through the direct influence of the increased temperature on aquatic life or through the lowering of the amount of dissolved oxygen and other biochemical effects.

In temperate regions most deep bodies of water develop a thermocline during their annual heating cycle. A warmer epilimnion at the top is isolated from a cooler hypolimnion below by severe stable gradients (thermocline). Convective transport and heat addition caused by power plant discharge result in disturbances in the thermocline.

The formation time, phasing, depth and severity of the thermocline are crucial factors affecting the bio-chemical processes in an aquatic ecosystem. The nutrient levels, species spectra and physical characteristics are quite different in the two distinct domains below and above the thermocline. This stratification is believed to be caused by nonlinear interaction between the wind-generated turbulence and stable buoyancy gradients. While being heated from above, a basin forms stable stratification thereby inhibiting wind-generated turbulence. During early spring, most temperate lakes exhibit a nearly homothermal temperature distribution with a temperature of about 4°C (which is the temperature of maximum density for water) extending all the way to the bottom. As the air above the lake begins to warm, the lake receives heat, at an increasingly rapid rate. During the early part of the warming season, the lake continues to remain nearly homothermal, since the heat that is received at the surface layers is transported to the deeper layers by wind-induced currents and turbulence. As the rate of heating of the lake continues to increase, the rate at which heat is received at the surface layers soon exceeds the rate of heat removal to the deeper layers, and the temperature of the surface layers begins to increase. During this period the temperature decreases monotonically with increasing depth. As heating continues, a point of inflexion develops in the temperature profile separating an upper well-mixed layer from a lower well-mixed layer. The region around the point of inflexion is a region of intense stable temperature gradient and consequently, low turbulence levels. Turbulent diffusion through this region is minimal. Further

heating merely increases the temperature of the well-mixed upper layer.

As cooling begins, the wind mixing is augmented by convective mixing caused by static instability and the thermocline (the region containing the point of inflexion) recedes into the deeper layers of the lake. The epilimnion cools until the lake reaches its minimum heat content and near homothermal conditions result.

This report describes the application of a one-dimensional model in predicting the above phenomena. This model was calibrated using data from Cayuga Lake and the calibrated model was applied to Lake Keowee. The purpose of the effort is to develop a predictive ability for long-term thermal behavior of cooling lakes.

SECTION 2

CONCLUSIONS

A one-dimensional model which includes area change with depth, vertical convection, varying diffusivity, thermal discharges, and internal absorption of radiation has been developed. The model was calibrated using Cayuga Lake data base and verified with Lake Keowee data base.

The application to Cayuga Lake indicates excellent performance. A comparison of cylindrical and paraboloid approximations for the lake indicate significant differences in thermocline depth, eddy-diffusivity, and temperatures at mid-depths. This shows that effects of area change with depth are not negligible. The insignificant surface temperature difference is attributable to the fact that equal surface areas were used in both simulations. However, these effects will be more pronounced in real basins where decrease in area with depth is more severe than the linear variation for the paraboloid case.

The long term (nine-year) simulations of temperature profiles, formation and decay of the thermocline for Lake Keowee compare fairly well with measured data. For these simulations, the model did not need recalibration. While the influence of discharge and ambient conditions were satisfactorily modeled, the calculated and measured profiles had much larger differences for Lake Keowee than for the one-year simulation in Cayuga Lake. Two reasons are believed to cause this relatively greater inaccuracy. The first is the complicated discharge patterns in Lake Keowee caused by power plant, hydro and pumped storage operation compared to ambient simulation for Cayuga Lake. The second cause is that for Cayuga Lake; the assumption of horizontal mixing is more meaningful since it is a single basin domain, while Lake Keowee is a double basin domain connected by a canal. The model, however, can be adapted for application to two connected basins.

SECTION 3

RECOMMENDATIONS

The main disadvantage of a one-dimensional thermal model lies in the fact that resolution is sacrificed for computational speed. Three dimensional models are bulky and time consuming but have much better resolution, however, when long term simulations are necessary, a one-dimensional model is recommended.

The model described here can be modified to include the single effects of the various quantities involved in the surface heat transfer phenomenon rather than using the equilibrium temperature concept. This is particularly recommended for the user who is interested in modeling the long term effects of one (for example, evaporation) of the quantities involved in the surface heat transfer processes.

Furthermore, the model can be easily adapted to handle connected multiple domains. This recommendation is discussed in the text.

SECTION 4

THE MATHEMATICAL MODEL

DESCRIPTION

The one-dimensional variable cross-sectional area model used for this study is described in this section. The detailed derivation of the governing equations is described in Appendix A, while the boundary conditions and the important terms occurring in the governing equations are discussed here.

This model which assumes lateral uniformity was developed to predict the vertical temperature profiles for complete annual cycles in a lake. The model includes the effects of variation of the horizontal cross-sectional area with depth. Surface heating due to solar radiation absorbed at the surface layer and the internal heating due to the transmission of the unabsorbed solar radiation to the deeper layers of the lake are taken into account. The exchange of mechanical energy between the lake and the atmosphere is accounted for through the friction velocity and the thermal diffusivity, since these quantities can be related to wind speed. Finally, the effects of power plant discharge and intake are considered.

The full three-dimensional equations of mass and heat balance are:

$$\frac{\partial \rho}{\partial t} = -\bar{\nabla} \cdot \rho \bar{\nabla} \tag{4.1}$$

and

$$\frac{\partial}{\partial t}(\rho C_p T) = \bar{\nabla} \cdot \rho C_p \bar{K} \cdot \nabla \bar{T} - \bar{\nabla} \cdot \rho C_p T \bar{V} + H \tag{4.2}$$

Applying the divergence theorem, and then differentiating and integrating, a set of one-dimensional equations are obtained:

$$A(z) \frac{\partial \rho}{\partial t} = \frac{\partial}{\partial z} A(z) \rho V_z + IA' \tag{4.3}$$

and

$$A(z) \frac{\partial}{\partial t}(\rho C p T) = \frac{\partial}{\partial z}\left[\rho C_p A(z) K_z \frac{\partial T}{\partial z}\right] - \frac{\partial}{\partial z}(\rho C_p A(z) T V_z) + QA' + A(z) H(z) \tag{4.4}$$

where,

z is the vertical coordinate, measured upward from the deepest point of

of the lake. As a subscript it marks the vertical component of a vector.

$A(z)$ is the horizontal cross-section of the lake at height z.

ρ is the density.

t is the time.

V_z is the vertical velocity of flow.

C_p is the heat capacity.

T is the temperature.

K_z is the vertical component of '$\bar{K}$', the heat diffusivity tensor (including turbulent diffusivity).

$H(z)$ is the source of heat per unit volume.

A' is $\frac{dA}{dz}$.

I is the bottom-surface source of mass per unit area.

Q is the bottom-surface source of heat per unit area.

The following variables occur in the governing equations and are defined thus:

Density, ρ, is assumed to vary with temperature in the following form:

$$\rho = 1.02943 + (-2.0 \times 10^{-5})T + (-4.8 \times 10^{-6})T^2 \text{ gm/cc} \qquad (4.5)$$

Equation (4.5) and the discussion of the constants were given by Sengupta and Lick (1974).

Eddy diffusivity, K_z, is a function of both thermal and current structure of a lake. The form used here was deduced by Rossby and Montgomery (1935).

$$K_z = K_{zo}(1 + \sigma_1 R_i)^{-1} \qquad (4.6)$$

where,

K_{zo} is the eddy diffusivity under neutral conditions.

Sundaram et al. (1969) gave an empirical form for the yearly variation of K_{zo}.

$$K_{zo} = 0.21 + 0.052 \sin(\frac{2\pi}{365}t + 2.61) \text{ cm}^1/\text{sec}^2 \qquad (4.7)$$

A sinusoidal variation of K_{zo} with a mean 0.21 cm^1/sec and amplitude of 0.052 cm^2/sec is assumed in Equation (4.7).

The semi-empirical constant $\sigma_1 = 0.1$ is estimated in this study by comparing the values used by Sundaram et al. (1969) and the original value used by Monin and Obukhov (1954).

The third variable appearing in Equation (4.6) is R_i, the Richardson number. This is defined as:

$$R_i = \frac{\alpha_v g z^2}{W^{*2}} \frac{\partial T}{\partial z} \qquad (4.8)$$

where,

α_v is the volumetric coefficient of expansion of water.

α_v is defined as:

$$\alpha_v = 0.0 + 1.538 \times 10^{-5}(T-4) + (-2.037 \times 10^{-7})(T-4)^2 \qquad (4.9)$$

The constants in the above equation were taken from Sundaram et al. (1970). σ_v can also be estimated from Equation (4.5); however, the use of Equation (4.9) leads to a higher accuracy.

g is the acceleration due to gravity.

w* is the friction velocity calculated from known conditions above the lake.

The heat source, H, is that part of the solar radiation transmitted exponentially through the depth of the lake. The relation used in this study has been used by Dake and Harleman (1969) and by Mitry and Ozisik (1976):

$$H(z) = \eta(1-\beta)A(z)\ \phi_o\ EXP(-\eta(z-h)) \qquad (4.10)$$

where,

β = fraction of the solar radiation absorbed at the surface, (0.5).

η = extinction coefficient, (0.75 cm^{-1}).

h = depth of the lake, (m).

ϕ_o = net solar radiation reaching the water surface, ($cal/cm^2/day$).

Equations (4.3) and (4.4) are parabolic and mathematically represent a diffusion process. The solution of these equations requires one initial condition and two boundary conditions.

Initial Conditions

The temperature of the lake at spring homothermy is taken as the initial temperature.

Boundary Conditions

Surface:

$$q_s = \rho C_p K_z \frac{\partial T}{\partial z} \Big| z=h = K_s(T_E - T_s) \qquad (4.11)$$

where,

T_E = equilibrium temperature, (°C).

T_s = surface temperature, (°C).

K_s = surface heat exchange coefficient, (cal/cm^2-s)

T_E Evaluation

Brady et al. (1969) showed empirically that fluctuations in the equilibrium temperature may be conveniently estimated using the approximate relationship:

$$T_E = T_d + H_s/K_s \qquad (4.12)$$

where,

T_d is the dewpoint temperature, estimated from known conditions above the lake.

H_s is the gross rate of short wave solar radiation.

Since the dewpoint temperature tends to remain relatively constant through a single day, Equation (4.12) indicates that the main source of hourly fluctuations in T_E is the solar radiation component. This generally reaches a maximum at solar noon, unless variable cloudiness interferes. At nighttime, T_E approaches the dewpoint temperature, which acts like a relatively invariant datum for periods of 24 hours or less. On an annual basis, however, both T_d and H_s are generally much greater in summer than in winter. The dominant contribution to the amplitude of seasonal fluctuation in T_E is the dewpoint temperature.

K_s Evaluation

The form used by Edinger and Geyer (1967) was also used in this study:

$$K_s = 4.5 + 0.05\, T_s + \beta f(w) + 0.47 f(w) \qquad (4.13)$$

β is found by applying standard curve-fitting techniques to published data pertaining to saturated vapor pressures at various temperatures; a convenient representation given by Edinger and Geyer (1967) is:

$$\beta = 0.35 + 0.015\ T_m + 0.0012\ T_m^2 \quad (\text{mmHg}/^\circ\text{C}) \tag{4.14}$$

$$T_m = \frac{T_s + T_d}{2} \tag{4.15}$$

The evaporative wind speed function f(w) used is also similar to that of Edinger and Geyer (1967).

$$f(w) = 9.2 + 0.46W^2 \quad (W_m^{-2}\text{mmH}_g^{-1}) \tag{4.16}$$

where W is the wind speed (m/s)

Bottom:

The second boundary condition is at the bottom surface of the lake which is assumed to be perfectly insulated.

$$\frac{\partial T}{\partial z}\Big|_{z=0} = 0 \tag{4.17}$$

Numerical Method

Numerical integration of the governing equations require that these equations be replaced by finite difference equations.

In this study, the following notations are used in the finite differencing of the basic equations:

Δz The thickness of a slice (the basin is divided into equal number of slices). This is used as depth increment.

Δt_n The time increment chosen at the n^{th} integration step.

n, n-1 The present and last time at which computations were performed.

j The space subscript. This is used as

$$T_j^n = T(j\Delta z,\ t_n) = T(z,\ t)$$

where z is the vertical coordinate.

Equation (4.4) can now be written in difference form as:

$$\frac{T_j^n - T_j^{n-1}}{\Delta t_n} = \left(\frac{1}{A_j \rho_j}\right)^{n-1} \frac{1}{(\Delta x)^2}\left[(\rho A K_z \Delta T)_{j+\frac{1}{2}}^{n-1} (\rho A K_z \Delta T)_{j-\frac{1}{2}}^{n-1}\right]$$

$$- \left(\frac{1}{A_j \rho_j}\right)^{n-1} \frac{1}{2\Delta z} \left[(\rho A T V_z)_{j+1}^{n-1} - (\rho A T V_z)_{j-1}^{n-1}\right]$$

$$+ \left(\frac{T_j}{\rho_j A_j}\right)^{n-1} \frac{1}{2\Delta z} \left[(\rho A V_z)_{j+1}^{n-1} - (\rho A V_z)_{j-1}^{n-1}\right]$$

$$- \left(\frac{T_j I_j}{\rho_j A_j}\right)^{n-1} \left[2\pi(h-(j\Delta z)\right]^{n-1}$$

$$+ \left[\frac{Q_j}{\rho_j C_p A_j}\right]^{n-1} \left[2\pi(h-(j\Delta z)\right]^{n-1}$$

$$+ \left[\frac{1}{\rho_j C_p}\right]^{n-1} H_j^{n-1}$$

where,

$$(\rho A K_z \Delta T)_{j+\frac{1}{2}}^{n-1} = \rho A K_z\left[(j+\tfrac{1}{2})\Delta z,\ t_{n-1}\right]\left[T_{j+1}^{n-1} - T_j^{n-1}\right]$$

$$(\rho A K_z \Delta T)_{j-\frac{1}{2}}^{n-1} = \rho A K_z\left[(j-\tfrac{1}{2})\Delta z,\ t_{n-1}\right]\left[T_j^{n-1} - T_{j-1}^{n-1}\right]$$

$$K_{z_{j+1}} = K_{zo}\left[1 + \sigma_1\left(-\frac{g z_j}{w^{*2}}\right)^{-1} (\alpha_v)_j z_j \frac{\partial T}{\partial z}\right]$$

$$= K_{zo}\left[(j+\tfrac{1}{2})\Delta z\right]\left\{1 + \sigma_1\left(-\frac{g(j+\frac{1}{2})\Delta z}{w^{*2}}\right)^{-1} \cdot (\alpha_v)_j \left[\tfrac{1}{2}(T_j^{n-1} + T_{j+1}^{n-1})\right](j+\tfrac{1}{2}\Delta z\right\}$$

$$(\alpha_v)_j = A_1 + A_2(T_j - 4) + A_3(T_j - 4)^2$$

$$\rho_{j-\frac{1}{2}} = B_1 + B_2\, T_{j-\frac{1}{2}}^{n-1} + B_3 (T_{j-\frac{1}{2}}^{n-1})^2$$

$$A_{j-\frac{1}{2}} = \frac{\pi b^2}{h}\Big]$$

$$= (j-\tfrac{1}{2})\Delta z\left[\frac{\pi b^2}{h}\right]$$

Terms like ΔT_{j+1} and $\Delta T_{j-\frac{1}{2}}$ can be defined as

$$\Delta T_{j+\frac{1}{2}} = T_{j+1} - T_j$$

$$\Delta T_{j-\frac{1}{2}} = T_j - T_{j-1}$$

The sequence in which calculations are performed is as follows:

The dependent variables, T, K_z, w*, α_v, ρ, T_E, and K_s, are initialized. The area of each slice is calculated. The title of the present year is printed. The values of the variables, K_z, w*, α_v, ρ, T_E, and K_s, are then calculated. The temperatures of the slices are finally calculated. If the temperature profile is unstable, mixing of the unstable portion of the profile is undertaken.

During the next time step, the temperatures are updated, and the dependent variables are calculated again.

The values of the temperature, T, eddy diffusivity, K_z, number of days and the surface heat transfer coefficient, K_s, are printed every time step, every day or normally at the end of each month. At the end of the present year, the new-year title is printed and computations continue as listed above. A detailed description of the programs and flow chart has been published in a user's manual, Lee and Sengupta (1980).

SECTION 5

MODEL CALIBRATION

The model described in the previous section was applied to Cayuga Lake, New York. The main reason was to calibrate the model. Cayuga Lake was chosen for this calibration because of the vast amount of numerical work done on this lake. These include Sundaram and Rehm (1971), Sundaram et al. (1971), Sundaram and Rehm (1972), and Mitry and Ozisik (1976). The model was also verified using Lake Keowee data base; this is described in the next chapter.

CAYUGA LAKE APPLICATION

Cayuga Lake is one of the finger lakes in west central New York. It is the longest, about 40 miles (64 km), of the group, and the second largest, about 66 square miles (171 sq. km), with steep banks cut by inflowing streams. It averages 2 miles (3 km) wide about 500 ft (150 meters) deep, with a surface elevation of 381 ft (115 meters). Tanghannock Creek and its 210-foot (64-meter) cataracts flow into the lake. The lake is drained to the north by the Seneca River, which joins the Oswego River and flows into Lake Ontario. Cayuga Lake is connected by canal with Seneca Lake on the west and Erie Canal on the north. The city of Ithaca lies at the southern end of the lake.

INPUT QUANTITIES

In the numerical integration of the governing equations for Cayuga Lake, the following ralations were used. The numerical values were taken from Sundaram et al. (1971) and Mitry and Ozisik (1976).

Density, ρ, varied as in Equation (4.5), Section 4, of this report.

Eddy diffusivity varied as in Equations (4.6) and (4.7) with $\sigma_1 = 0.1$ and the Richardson number as given in Equation (4.8).

The volumetric coefficient of expansion of water, α_v, used is shown in Equation (4.9).

A sinusoidal relation was assumed for the variation of the friction velocity, w*, with time; normally, w* is defined as

$$w^* = \sqrt{(\tau_s/\rho)} \qquad (5.1)$$

The form used is

$$w^* = A_1 + B_1 \sin(\frac{2\pi t}{365} + C_1) \qquad (5.2)$$

where,

A_1 = Average value of w^*, (3.048 cm/sec).

B_1 = Half the annual variation of w^*, (0.762 cm/sec).

C_1 = Phase angle, (2.61) (chosen in such a way that at time t = 0, w^* = initial value of the friction velocity).

The heat source, H, is taken to vary as in Equation (4.10), with $\beta = 0.5$, $\eta = 0.75$ cm^{-1} and h = 70.0 m ($\cong$200 ft).

The net solar radiation, ϕ_o, reaching the water surface is taken from Mitry and Ozisik (1976):

$$\phi_o = A_2 + B_2 \sin(\frac{2\pi}{365} t + C_2) \qquad (5.3)$$

where,

A_2 = Average value of ϕ_o, (6.14×10^{-3} cal/cm^{2}s).

B_2 = Half the annual variation of ϕ_o, (3.52×10^{-3} cal/cm^{2}s).

C_2 = Phase angle, (0.049) (chosen in the same way as C_1).

The heat flux, Q, in Equation (4.4) is defined as

$$Q = (\rho C_p \Delta T Q_p) / (A(z)) \qquad (5.4)$$

where,

Q_p = Volumetric discharge from the power plant. In this study $Q_p = 1.508 \times 10^8$ cm^3/sec; this value is chosen to correspond to the pumping velocity used by Sundaram et al. (1971), (1/4 ft/day).

$\Delta T = 10°C$ = Assumed temperature change through the condensers of the power plant.

The pumping velocity V_z is defined as

$$V_z = \frac{Q_p}{A(z)} \qquad (5.5)$$

The pumping velocity term effects are felt between the intake and the level at which the heated effluent becomes neutrally buoyant (effective discharge level).

K_s = Assumed constant at 5.65×10^{-4} cal/cm²-s.

For a postulated 3500 MW plant for Cayuga Lake, a 8.79×10^{-4} cal/cm²s of waste heat will have to be rejected.

Surface area of Cayuga Lake is 66 sq. miles (171 sq. km).

The intake to the power plant is fixed at 38.1 m (≅ 125 ft) from the surface of the lake.

Initial temperature is taken as the temperature of the lake at spring homothermy (usually coincides with the minimum surface temperature attained by the lake). For Cayuga Lake, this occurs around March, and the temperature assumed is $T_o = 2.9°C$.

Finally, a sinusoidal variation is assumed for the variation of the equilibrium temperature with time.

$$T_E = A_3 + B_3 \sin(\frac{2\pi}{365} t + C_3) \qquad (5.6)$$

where,

A_3 = Average value of T_E, (11°C).

B_3 = Half the annual variation of T_E, (16°C).

C_3 = Phase angle, chosen in the same way as C_1 or C_2.

The justification for using Equation (5.6) is described in Appendix D of this report.

Two topographies are studied in the application of this model to Cayuga Lake; these are a right circular cylinder and a circular paraboloid approximations for the lake.

Cylindrical Topography

The area (radius, $B = 7.38 \times 10^5$ cm) of the lake is assumed constant throughout the depth. Term A' or $\frac{dA}{dz} = 0$; see Equations (4.3) and (4.4).

Circular Paraboloid Topography

The lake is assumed to be a circular paraboloid with surface radius, $B = 7.38 \times 10^5$ cm. The area at any depth, z (measured from the deepest point of the lake) is given by:

$$A' = \frac{\pi B^2 z}{h} \qquad (5.7)$$

Thus, A' is a constant:

$$A' = \frac{\pi B^2}{h} \qquad (5.8)$$

RESULTS

Computations for a yearly cycle for Cayuga Lake are presented. The verification data base consists of vertical temperature profiles compiled by Henson et al. (1961). The comparison of simulated and observed vertical temperature profiles are shown in Figures 1, 2 and 3. Each figure shows five profiles representing observed (M), discharge (cylindrical domain - CD); discharge (parabolic domain - PD); no-discharge (cylindrical domain - CN); and no-discharge (parabolic domain - PN).

The no-discharge simulations are in good agreement with the data (the data was for no-discharge conditions).

The parabolic case has somewhat better agreement since it represents, qualitatively, the decrease in area with depth. However, the closeness of the simulated results for the two cases is surprising. Most lakes have the rate of decrease in area with depth greater than a paraboloid, which has a linear decrease. Thus, when realistic area changes are used, a greater difference between cylindrical and paraboloid cases can be expected.

The effect of discharge is significant only in the top layers till July. This is because the heated discharge rises to the surface during the first half of the year. For the later months, the discharge temperature is lower than the surface temperature causing the discharge to reach static equilibrium somewhere below the surface. Thus, significant thermal effects of discharge are seen at mid-depths till December. The temperatures are higher at these depths for the paraboloid topography. In general, a temperature difference of the order of 3°C over the no-discharge case, can be seen. At the end of the annual cycle, a residual temperature increase of 1.75°C is detectable.

In the above paragraph, the discharge from the power plant is treated as a plane source which is injected into the domain at a level where the discharge temperature equals the temperature of that level. This level could be called the effective discharge level. The effects of the pumping velocity term, therefore, can only be felt from the intake level to the effective discharge level. A temperature rise of 10°C through the condensers was assumed. This temperature difference justifies the use of density as a function of temperature.

Figures 4 and 5 show the annual stratification cycle. From these figures it is evident that the surface temperature difference between the four cases is less than 2°C over the annual cycle. However, at mid-depths the paraboloid discharge case shows a 5°C difference compared to the no-discharge case; for the cylindrical discharge case this difference is 3°C. Generally, the highest surface temperatures are reached after 150 days, while the highest equilibrium temperature occurs after 120 days.

Thus, there is approximately a 30 day lag in the surface temperature response. The maximum temperatures at mid-depth occur after 240 days for the no-discharge case; for the discharge case, the corresponding time is 210 days. No significant phase lag between cylindrical and paraboloid cases are observed.

Figures 6 and 7 show the eddy diffusivity variation with depth (time in days used as parameter) for the cylindrical and paraboloid cases respectively. It is observed that thermal discharge causes increase in eddy diffusivity in the epilimnion owing to increased mixing. No significant changes are seen in the hypolimnion. There is a temporal increase in the differences between the discharge and no-discharge cases. These observations are true for both domains. However, the diffusivity values are larger for the paraboloid cases. Also, at any given time, the paraboloid case shows deeper thermoclines.

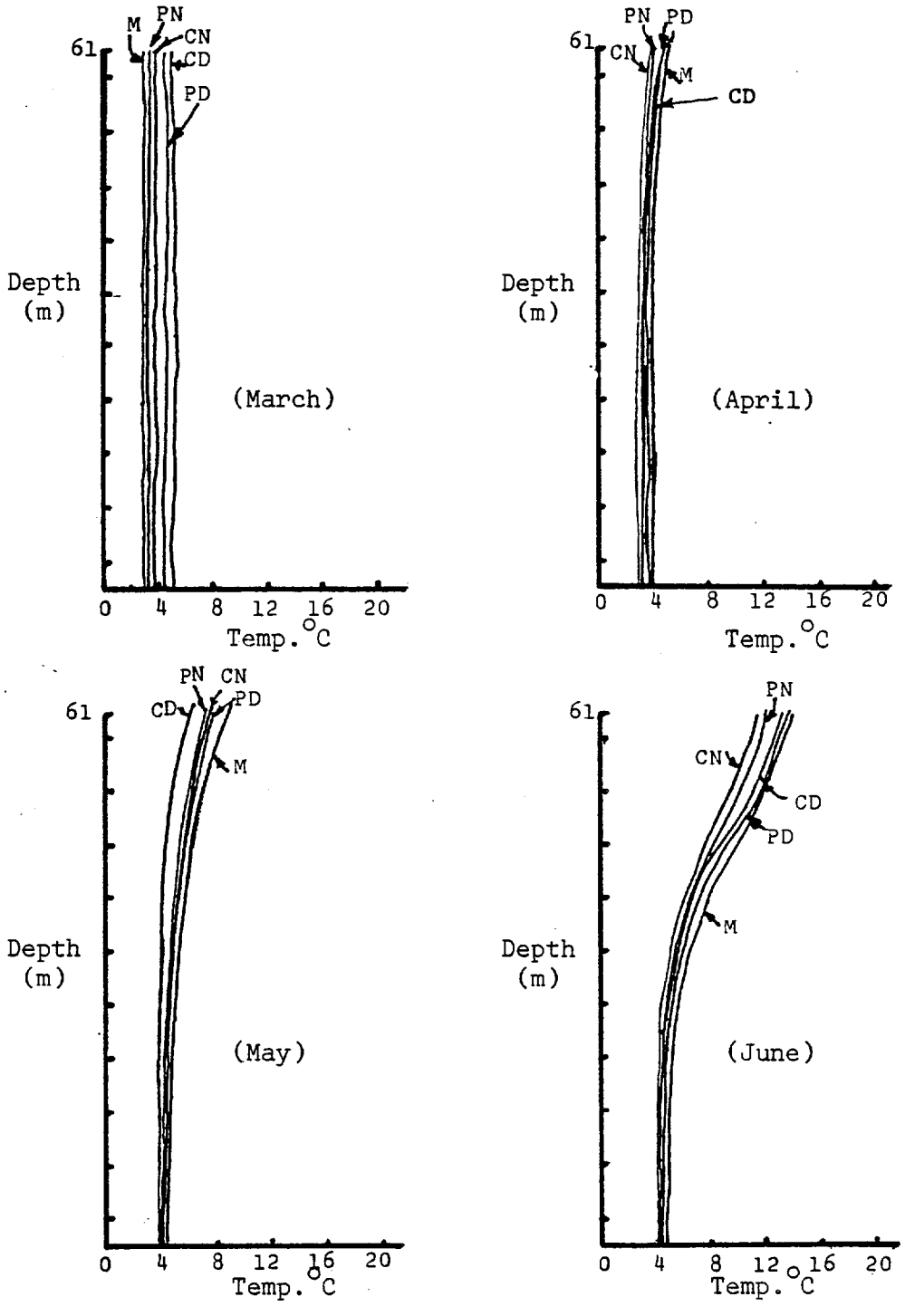

(PN=Paraboloid, No-Discharge; CN=Cylindrical No-Discharge; PD=Paraboloid + Discharge; CD=Cylindrical + Discharge; M=Measured)

Figure 1. Vertical temperature profiles, Cayuga Lake (from 0 to 90 days)

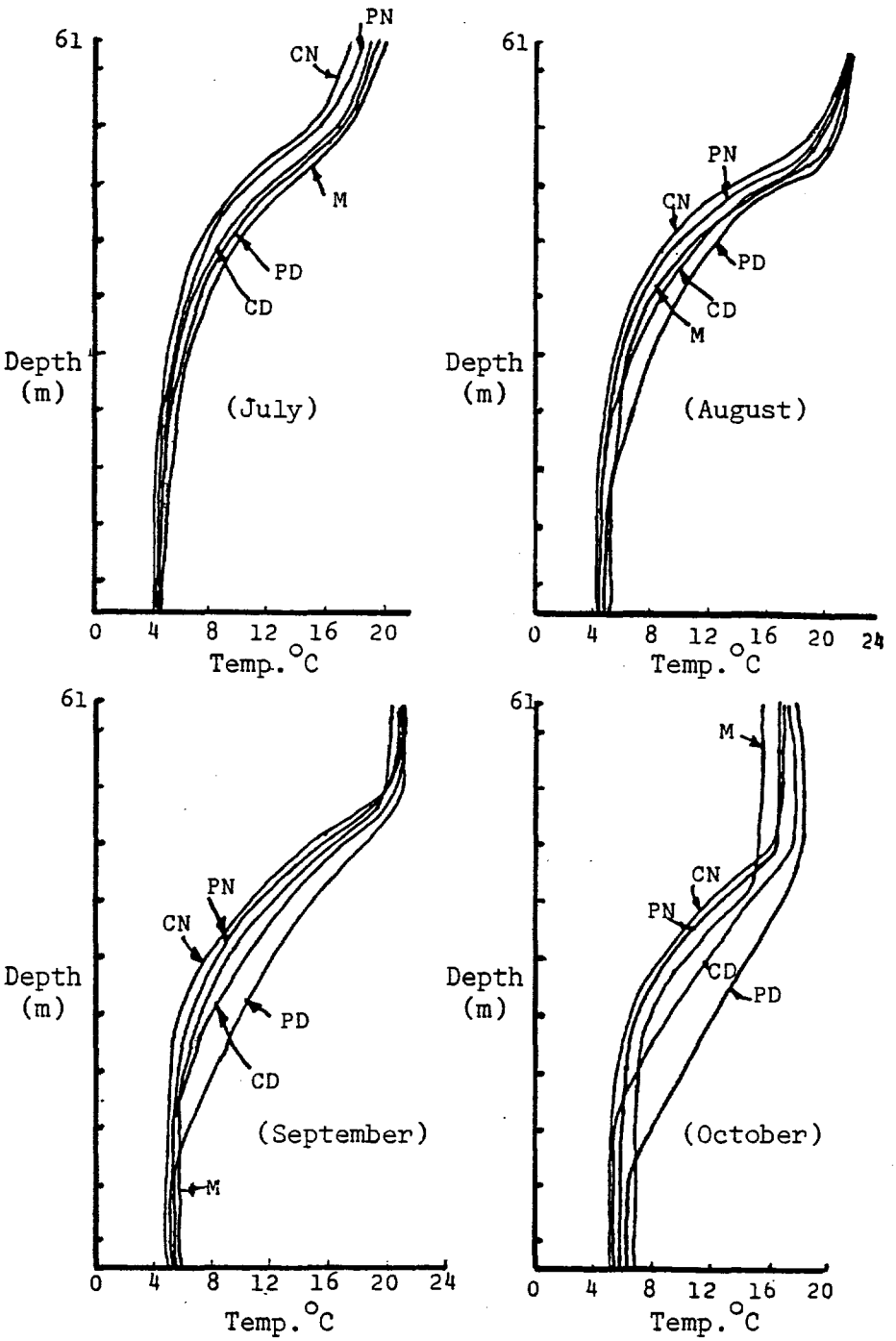

(PN=Paraboloid, No-Discharge; CN=Cylindrical No-Discharge; PD=Paraboloid + Discharge; CD=Cylindrical + Discharge; M=Measured)

Figure 2. Vertical temperature profiles, Cayuga Lake (from 120 to 210 days)

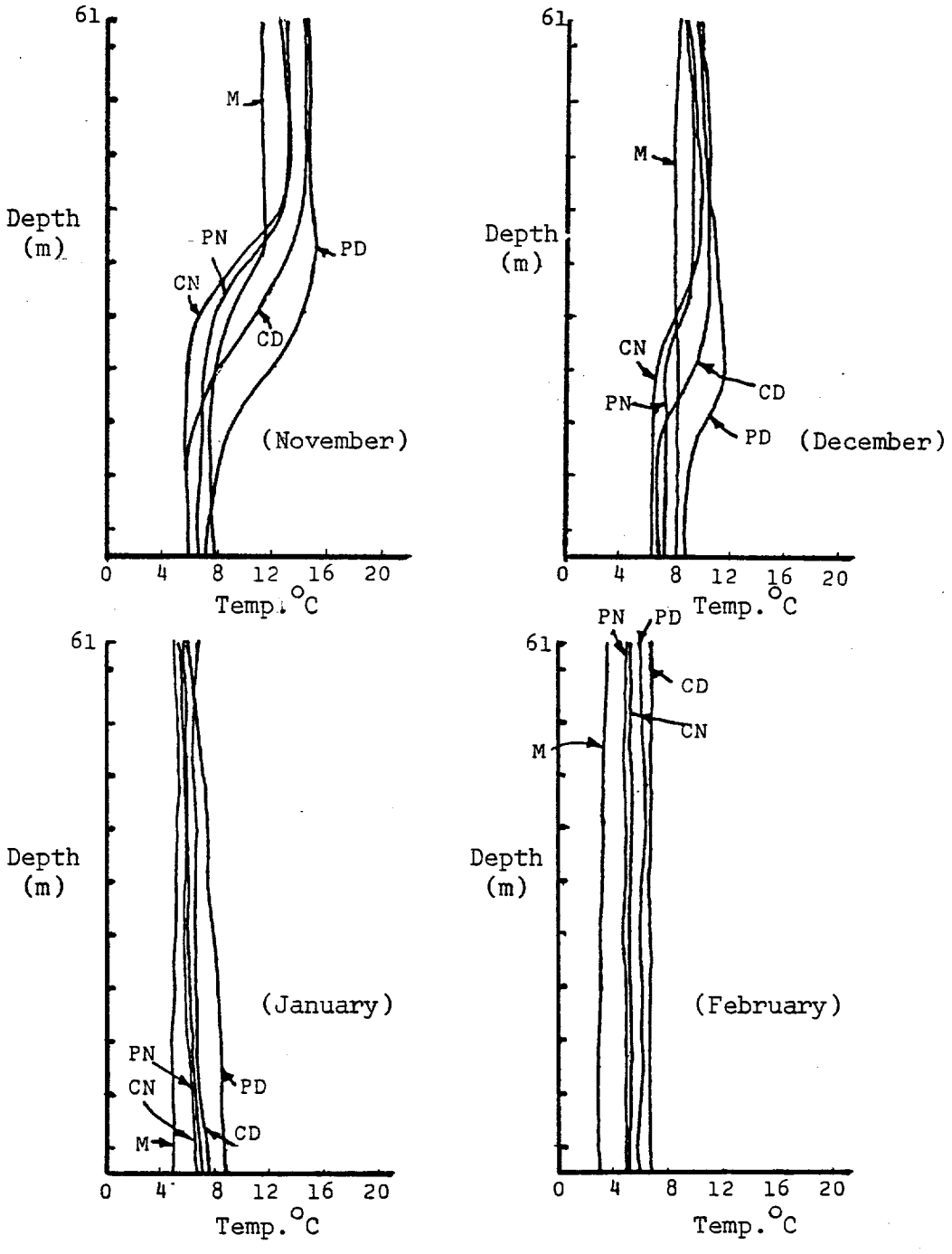

(PN=Paraboloid, No-Discharge; CN=Cylindrical No-Discharge; PD=Paraboloid + Discharge; CD=Cylindrical + Discharge; M=Measured)

Figure 3. Vertical temperature profiles, Cayuga Lake (from 240 to 330 days)

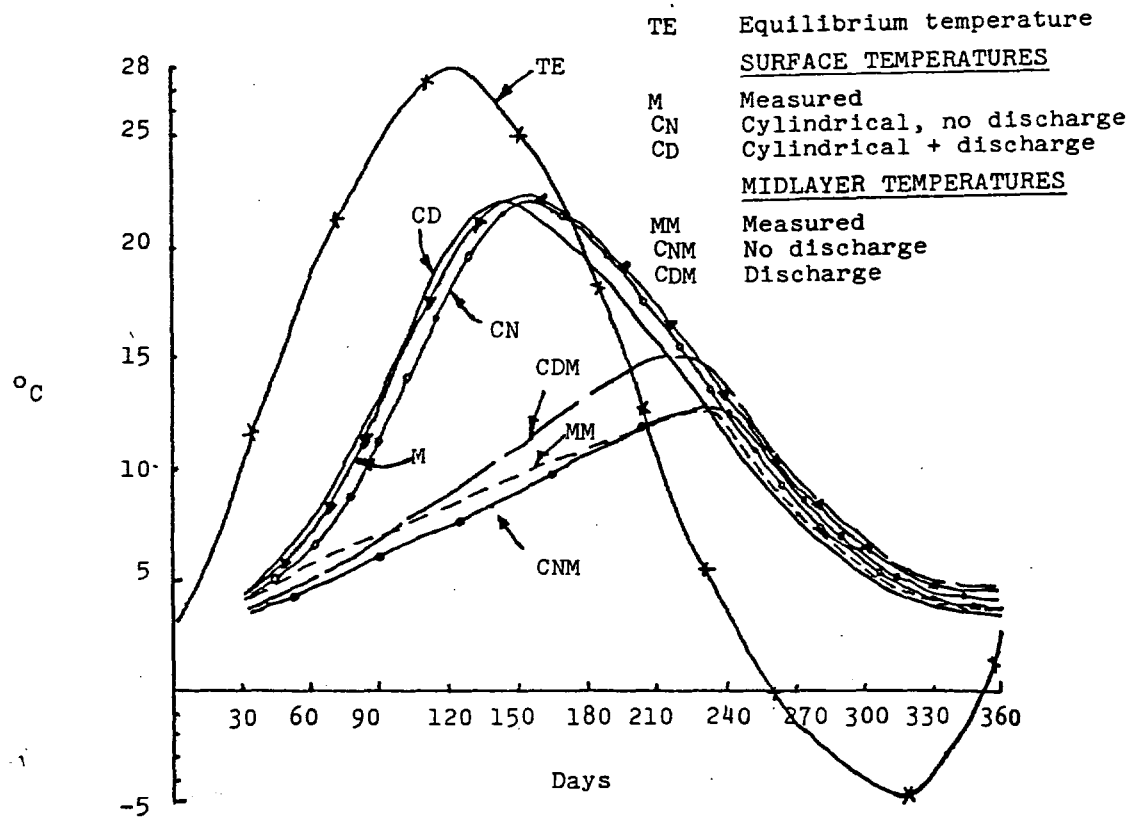

Figure 4. Stratification cycle cylindrical domain, Cayuga Lake

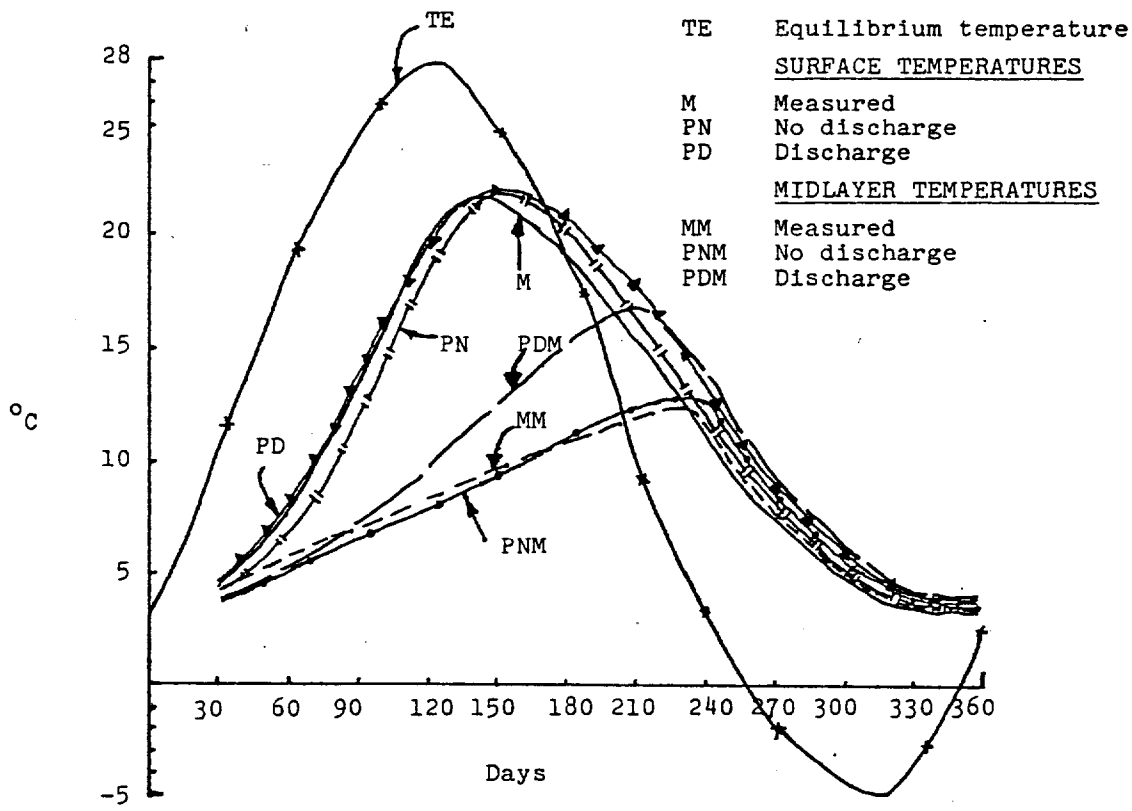

Figure 5. Stratification cycle parabolic domain, Cayuga Lake

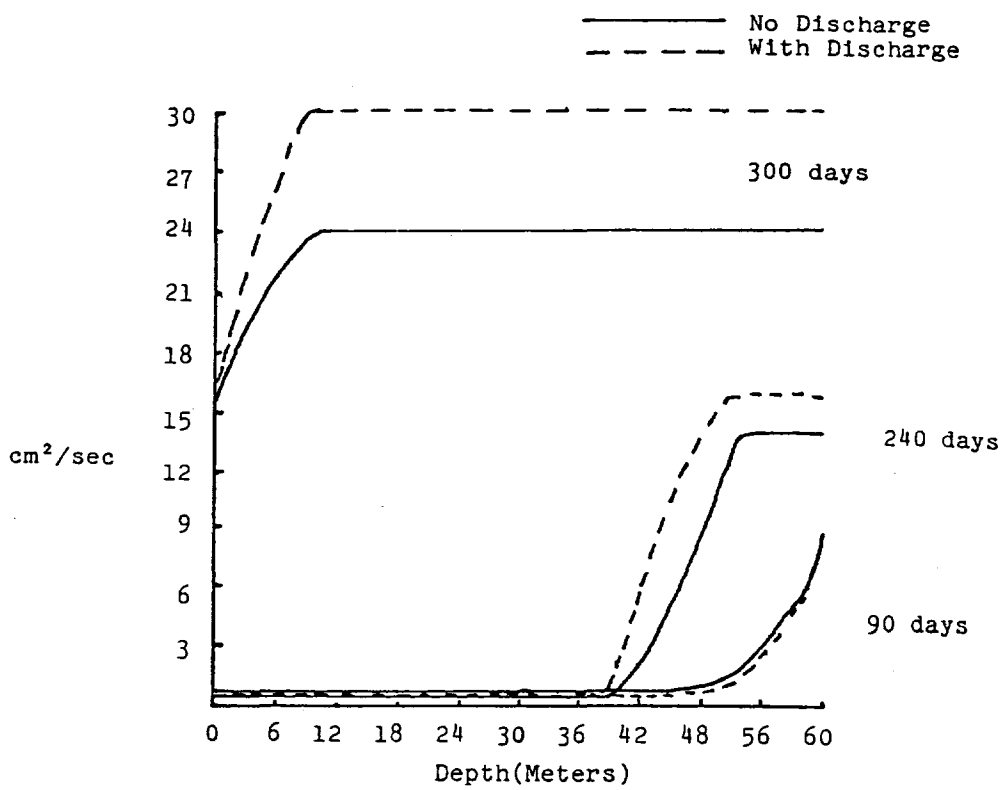

Figure 6. Variation of eddy diffusivity with depth cylindrical domain, Cayuga Lake

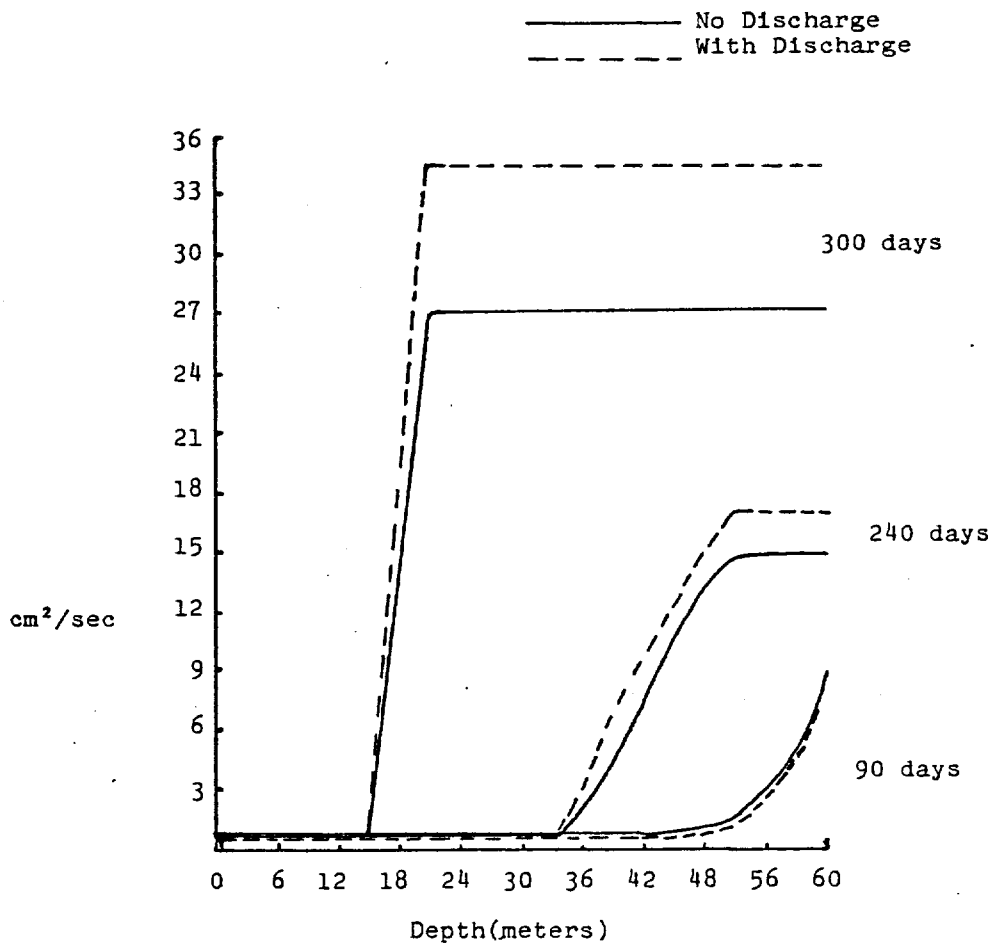

Figure 7. Variation of eddy diffusivity with depth paraboloid domain, Cayuga Lake

SECTION 6

MODEL VERIFICATION

The model calibrated in the last section was applied to Lake Keowee. There were two objectives. The first was to simulate the stratification behavior of Lake Keowee for the period 1971 to 1979, the entire existence of this river-dammed lake, which started receiving power plant heated discharges in 1973. The second objective was to test the accuracy of this model for a situation where horizontal uniformity (see Appendix A) of temperature was somewhat suspected since there are two basins connected by a canal.

LAKE KEOWEE APPLICATION

Lake Keowee is located 40 km west of Greenville, South Carolina. It is the source of cooling water for Oconee Nuclear Power Station (ONS). It was formed from 1968 through 1971 by damming Little and Keowee Rivers. A connecting canal (maximum depth 30.5 m) joins the two main arms of the lake. Flow out of the lake, except for negligible leakage through Little River dam, is through the Keowee Hydro Station. Lake Keowee also exchanges water with Lake Jocassee-pumped storage station. The three-unit steam electric ONS with a net capacity of 2580 Mwe started operating in July 1973. ONS operated at annual gross thermal capacity factors (GTCF) of 11, 28, 69 and 59% in the years 1973 through 1976, respectively, Duke Power Company (1976). From 1977 through 1979 the GTCF varied from 65 to 75 , Duke Power Company (1979).

INPUT QUANTITIES

Since long term effects are the important factors in this sutdy, the input data to the one-dimensional model were mainly monthly averages supplied by Duke Power Company (1976 and 1979). These are:

1. Maximum depth of Lake Keowee = 45 m (≅150 ft).

2. Initial temperature (minimum surface temperature of Lake Keowee) = 7.5°C.

3. ONS condenser cooling water flowrate, Q_p, Table 1.

4. Temperature rise in condenser cooling water, Table 2.

5. Outflow through Keowee Hydro Station, Table 3.

6. Flow through Jocassee-pumpted storage station, Table 4.

7. Wind speed, Table 5 (0.2 meters from surface).

8. Solar radiation reaching the water surface, ϕ_o, Table 6.

9. Dewpoint temperature, Table 7.

RESULTS

Computations were carried out for nine years, 1971 through 1979, using the above monthly-averaged data. The measured temperature profiles referred to in this discussion are horizontal-averaged data collected from seven different locations in Lake Keowee, as shown in Figure 8. This is in approximate agreement with the lateral uniformity assumed in the formulation of this and other one-dimensional models.

Computed (with discharge) and measured temperature profiles for 1971 to 1979 are presented together whenever possible, Figures 9 through 17. A second set of figures, 18 to 26, for the nine simulated years show the computed temperature profiles (with and without discharge). Other figures presented include: a typical variation of eddy diffusivity with depth (time in days as parameter), Figure 27; and a typical temporal variation of the depth of the thermocline, Figure 28. Finally, the variation of the surface heat exchange coefficient with time in years (Figure 29), and the stratification cycle for Lake Keowee (1971-1979), Figure 30, are presented. All the above figures are computer drawn.

For 1971, the year the lake came into existence, Figure 9 shows the computed temperature profiles (solid lines) and the measured temperature profiles (broken lines). The surface temperature comparisons between the measured and computed are excellent except for the start of the heating season when the computed temperatures seem to lag the measured. The maximum lag occurs in April and reduces with the heating season and completely disappears in October when cooling is in full swing. The hypolimnetic temperatures show good agreement with measured data. The mid-layer temperatures compare perfectly for the first half of the year. From August to November, the trend changes and the computed profiles lead the measured. However, the modeling of the formation, maintenance and decay of the thermocline, is good. This can be seen by comparing the shapes of the measured and computed temperature profiles. The comparison improves with increasing years, Figures 10 to 17, and generally follows the same trend as outlined above. The comparison of measured and computed temperature profiles cannot be expected to be more precise for the following reason. The measured values were taken on some specific day (different for some months) during the month while the computed results show the temperature profiles at the end of the month.

To estimate the impact of ONS operations on the thermal dynamics

of Lake Keowee, a set of simulations (with and without discharge) are presented. These are summarized in Figures 18 to 26. Two years are selected for detailed discussion, 1975 and 1978. The earlier year, Figure 22, was a year of very high ONS annual gross thermal capacity factor and the later year, Figure 25, is representative of the situation towards the end of computations. In Figure 22, although the discharge surfaced only during the early and later months of the year, the effect of discharge (broken lines) is clearly evident during most of the months at the subsurface layers (especially below the thermcline). Figure 25 shows the same situation for 1978. This time, however, the discharge surfaced from January through May and then from October through December, at total of three months more than in 1975. The hypolimnetic temperatures were also higher. Finally, by the end of computations, 1979, there was a residual temperature difference of almost 3°C due to discharge. ONS started operations in July 1973, and accordingly, the first three years, Figures 18 to 20, show no differences between discharge and no-discharge simulations.

Figure 27 shows the variation of the eddy diffusivity with depth for 1975, one of the nine years simulated. In this figure, the maximum diffusivity always occurs at the surface for every month. The non-stratified months show a constant diffusivity while the stratified months show very high mixing in the epilimnion and very low mixing in the hypolimnion.

Figure 28 shows the temporal variation of the depth of the thermocline for 1975. This figure is in agreement with one of the generally accepted theories of the formation, maintenance and decay of the thermocline.

Finally, a summary of the stratification cycle for Lake Keowee for the nine years simulated is presented in Figure 30, and the variation of the surface exchange coefficient for the same period is shown in Figures 29 and 30. The maximum surface temperatures occur around 240 days, and the minimum surface temperatures around 60 days for each year. The equilibrium temperature of the lake is superimposed. The maximum equilibrium temperatures occur around 210 days. The surface temperature therefore lags the equilibrium temperature by 30 days. Two curves are shown for the mid-layer temperatures to highlight the effect of ONS operations. The temporal increase of this effect can be seen clearly. The maximum difference occurs during the last quarter of each year. The variation of the surface heat exchange coefficient, as expected, follows the same trend as the variation of the surface temperatures.

TABLE 1. Oconee Nuclear Station Condenser Cooling Water Flowrate (m^3/min)

Month	1973	1974	1975	1976	1977	1978	1979
January	----	3069.3	4612.4	6069.3	5045.8	6176.7	7207.7
February	----	3069.4	3694.9	4440.2	4985.2	6444.6	7319.9
March	----	2976.9	5456.8	4874.3	5113.5	5195.7	7419.5
April	----	2807.3	5570.8	4272.1	6013.6	4811.8	7275.8
May	----	2164.6	6494.3	3970.7	6302.4	4984.2	4189.1
June	----	4171.8	6574.2	5197.6	4385.3	5659.9	5381.2
July	1890.2	5334.6	7104.2	5830.0	5038.6	7058.8	4753.3
August	1910.3	4727.1	7510.1	7248.3	5708.9	7914.9	----
September	2099.5	5961.4	7201.6	6785.4	6964.0	6557.3	----
October	2232.5	4953.4	6993.4	5637.8	6754.7	7407.4	----
November	2170.7	4202.1	7467.1	5809.2	4697.6	6065.1	----
December	3284.6	5225.6	6850.9	4914.8	5854.6	6503.5	----

TABLE 2. Oconee Nuclear Station Condenser Temperature Rise, ΔT (°C)

Month	1973	1974	1975	1976	1977	1978	1979
January	---	4.2	6.3	10.6	12.5	9.0	10.3
February	---	7.4	4.8	7.3	11.4	11.0	10.4
March	---	8.4	8.2	7.1	10.4	13.2	9.6
April	---	8.0	8.3	5.1	11.4	9.7	9.9
May	---	2.7	8.8	5.8	9.4	10.1	8.2
June	---	6.0	8.8	9.3	8.4	8.1	7.1
July	5.3	5.0	8.3	7.4	7.4	7.9	5.0
August	4.6	4.8	7.8	8.5	5.0	7.5	---
September	5.3	5.8	7.4	8.0	5.0	7.6	---
October	7.3	3.5	7.7	7.8	3.8	6.2	---
November	7.7	7.9	8.5	6.7	6.2	8.4	---
December	4.1	5.9	9.4	8.4	7.9	7.2	---

TABLE 3. Monthly Average Flowrates (m^3/sec) - Lake Keowee Hydro Station

Month	1971	1972	1973	1974	1975	1976	1977	1978
January	---	17.5	22.2	71.2	27.0	39.5	35.5	30.1
February	---	32.9	17.2	118.1	50.8	36.2	33.6	22.6
March	---	9.0	33.6	20.7	82.7	42.4	25.4	25.7
April	---	3.0	30.1	16.7	42.5	40.7	50.5	18.7
May	---	21.2	31.6	35.9	63.8	53.3	21.6	52.3
June	---	22.9	55.7	11.8	16.1	53.2	27.5	43.1
July	---	14.3	9.7	43.1	20.3	33.2	20.1	12.2
August	---	15.8	16.1	28.8	39.9	10.8	55.2	28.7
September	22.6	20.2	18.4	17.0	35.1	16.0	16.5	33.1
October	14.9	6.1	3.3	5.1	49.8	39.2	7.5	25.2
November	18.5	30.8	5.6	23.0	47.2	27.2	22.5	13.4
December	8.8	17.3	19.3	12.4	44.1	30.1	20.5	13.4
Annual Average	16.2*	17.6	21.9	33.7	43.3	35.2	27.2	32.1

* Average of September through December.

TABLE 4. Lake Jocassee Hydro Flows (cfs)

Month	1973	1974	1975	1976	1977	1978	1979
January	---	---	---	505	-608	187	---
February	---	---	---	509	206	54	---
March	---	---	---	562	1181	516	---
April	---	---	---	-79	1046	370	---
May	---	---	---	555	27	1762.2	---
June	---	---	---	1032	489	180.2	---
July	---	---	---	112	-831	---	---
August	---	---	-163	-747	-460	---	---
September	---	---	554	39	101	---	---
October	---	---	765	304	152	---	---
November	---	---	615	-251	448	---	---
December	---	---	301	-915	461	---	---

TABLE 5. Lake Keowee, Wind Speed (cm/sec)

Month	1971	1972	1973	1974	1975	1976	1977	1978	1979
January	6.69	6.69	7.22	5.8	6.3	7.4	8.04	7.9	8.6
February	9.3	9.26	7.3	5.8	7.6	8.5	8.4	6.8	7.2
March	9.2	9.20	7.1	7.7	9.6	7.9	7.7	7.6	7.9
April	8.72	8.7	8.44	8.7	7.6	7.6	7.6	7.6	7.6
May	7.5	7.53	6.83	6.8	4.8	7.3	6.2	6.7	6.7
June	5.65	7.95	3.04	6.96	5.82	6.4	6.7	4.7	4.8
July	6.48	6.64	5.32	5.2	5.1	5.9	5.8	5.7	---
August	5.75	6.07	5.1	5.87	5.4	6.7	5.4	5.1	---
September	5.77	5.47	6.8	6.74	7.3	7.13	5.3	5.7	---
October	7.02	7.17	7.1	5.7	7.7	7.21	7.2	6.6	---
November	7.53	7.13	8.14	7.2	6.9	7.27	7.5	5.8	---
December	8.3	6.8	5.6	6.9	7.2	8.2	7.2	7.3	---

TABLE 6. Lake Keowee Gross Solar Radiation (Langleys)

Month	1971	1972	1973	1974	1975	1976	1977	1978	1979
January	167.0	176.0	162.7	191.4	191.4	209.8	205.5	227.0	208.0
February	264.4	257.6	279.5	226.9	226.9	310.9	317.6	308.0	251.0
March	264.4	352.5	348.5	326.1	326.1	338.6	328.5	408.0	373.0
April	457.0	448.0	449.3	397.7	397.7	496.9	427.3	429.0	479.0
May	480.5	433.6	449.5	436.0	436.0	448.4	473.0	513.0	513.0
June	478.0	564.3	507.7	559.3	559.3	480.2	543.3	598.0	---
July	409.0	493.8	496.9	459.5	459.5	288.3	551.8	568.0	---
August	428.2	453.5	391.6	480.0	480.0	480.4	423.9	461.0	---
September	329.0	386.3	338.4	339.2	339.2	345.1	350.7	385.0	---
October	261.3	298.1	341.7	302.5	302.5	287.5	286.6	369.0	---
November	247.7	220.9	247.6	231.1	231.1	237.5	196.2	232.0	---
December	147.7	148.0	154.0	181.9	181.9	195.0	178.2	191.0	---

TABLE 7. Lake Keowee Dewpoint Temperature (°C)

Month	1971	1972	1973	1974	1975	1976	1977	1978	1979
January	3.0	1.67	1.0	8.2	3.0	-1.0	-6.6	-2.8	-3.33
February	0.9	-2.22	-1.0	0.0	3.5	3.2	-2.78	-5.0	0.0
March	6.3	1.11	10.0	6.3	2.2	3.9	6.0	1.2	5.0
April	7.5	6.6	7.7	10.7	7.2	11.2	10.2	9.6	9.2
May	17.2	11.11	14.3	17.2	17.5	14.0	15.4	14.0	14.0
June	18.8	13.13	20.25	17.8	19.0	18.3	18.0	19.4	19.4
July	20.0	18.77	22.2	21.0	21.3	19.8	20.2	20.8	20.7
August	19.44	22.22	21.7	21.0	21.0	18.0	20.7	20.8	21.0
September	18.33	18.8	20.8	17.5	16.2	15.4	18.7	15.5	15.7
October	13.88	11.5	13.5	10.2	12.4	8.2	9.2	9.3	10.0
November	2.88	5.9	7.2	6.0	7.9	1.0	7.0	9.0	10.3
December	5.5	4.0	3.2	3.8	2.0	-1.5	0.4	0.4	0.9

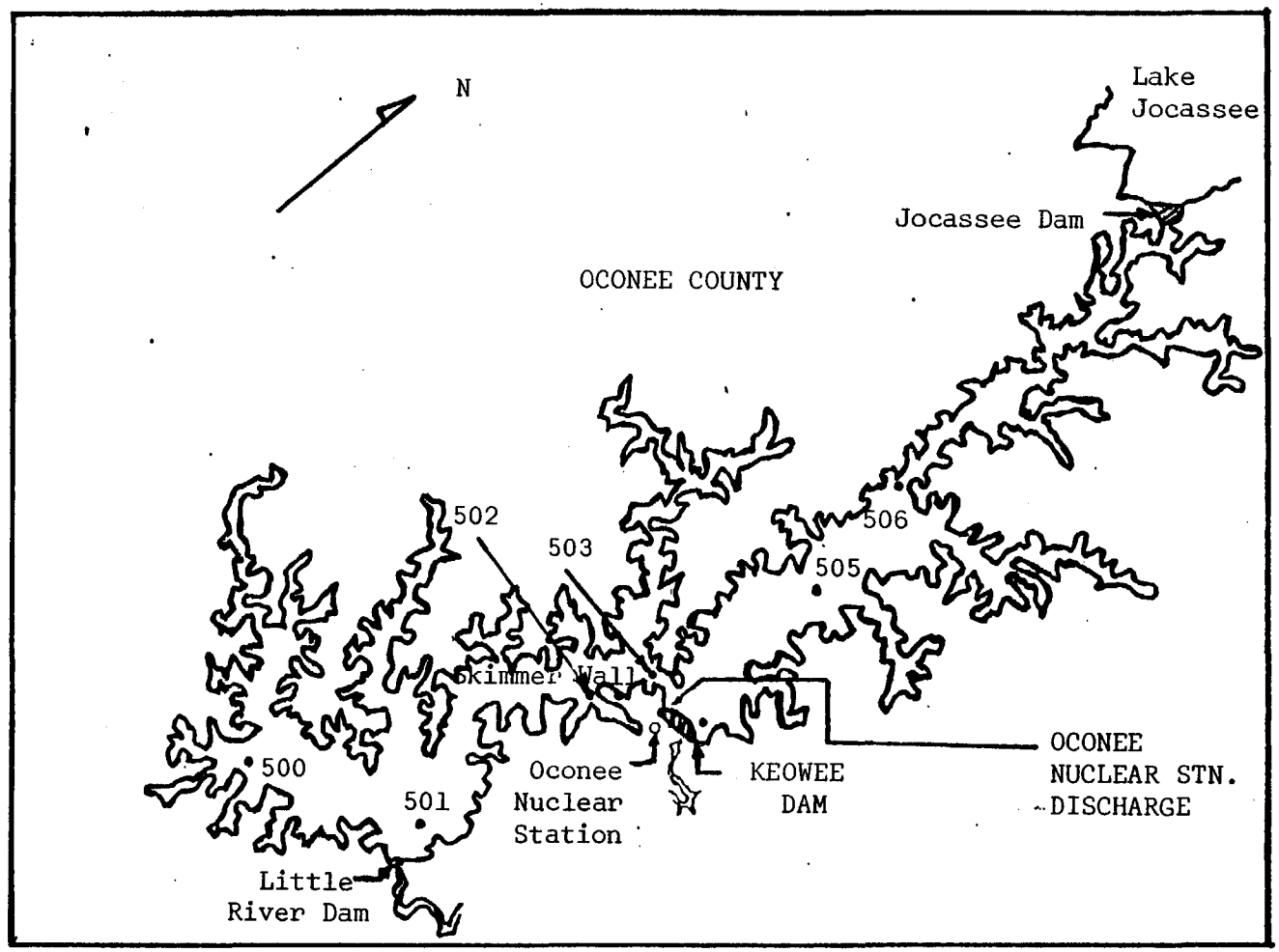

Figure 8. Map of Lake Keowee

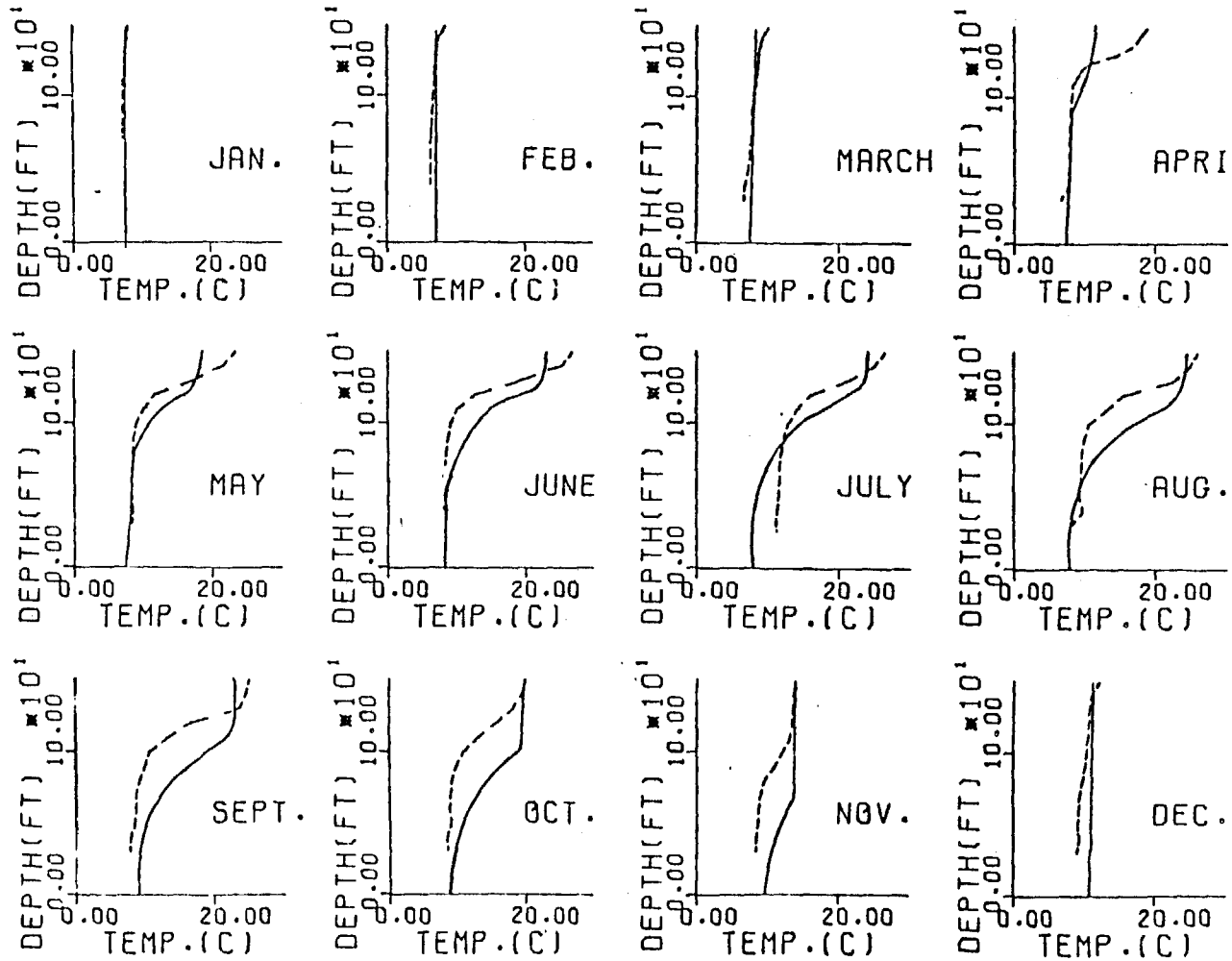

Figure 9. Measured (broken lines) and predicted temperature profiles, Lake Keowee, 1971

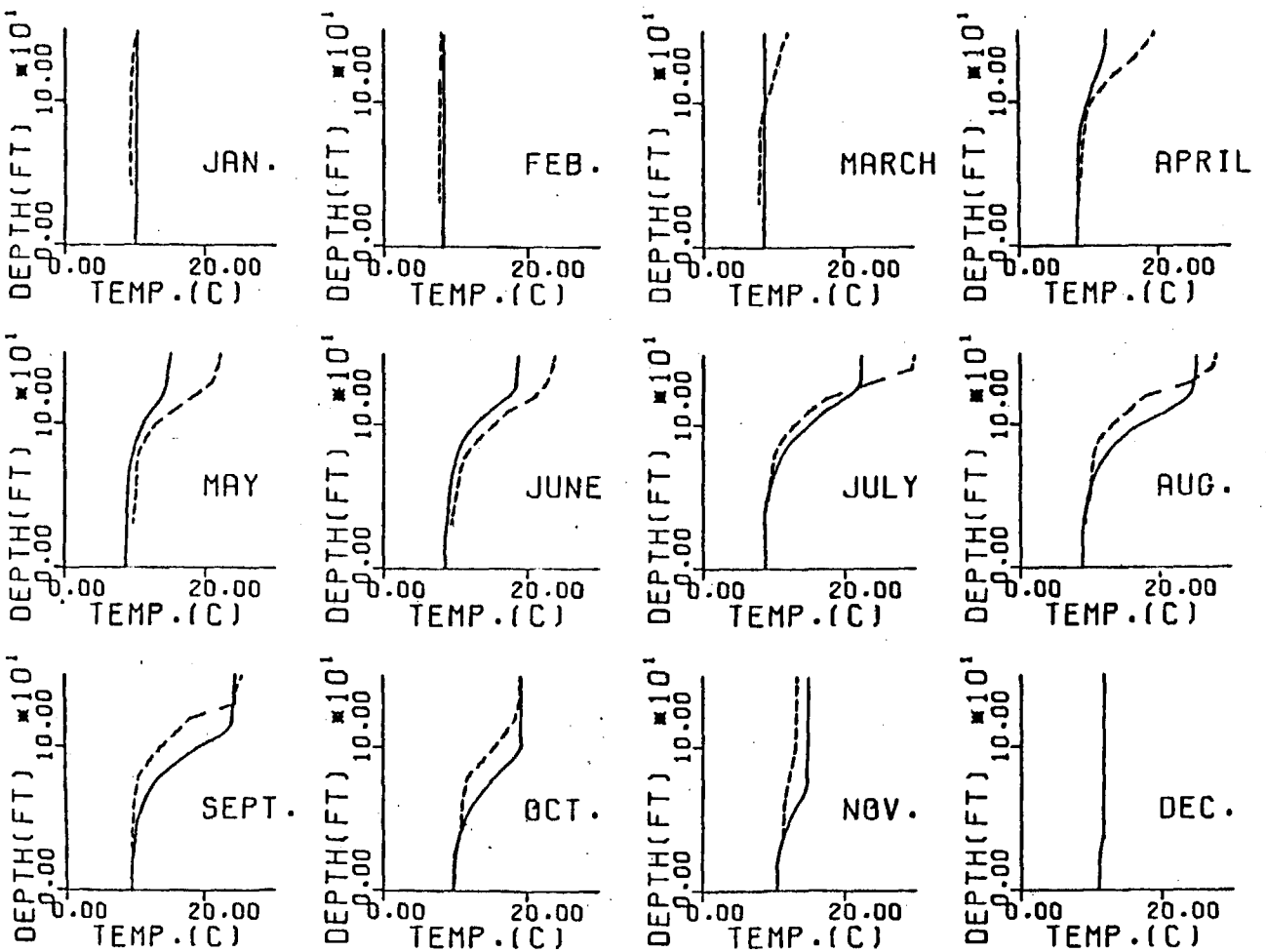

Figure 10. Measured (broken lines) and predicted temperature profiles, Lake Keowee, 1972

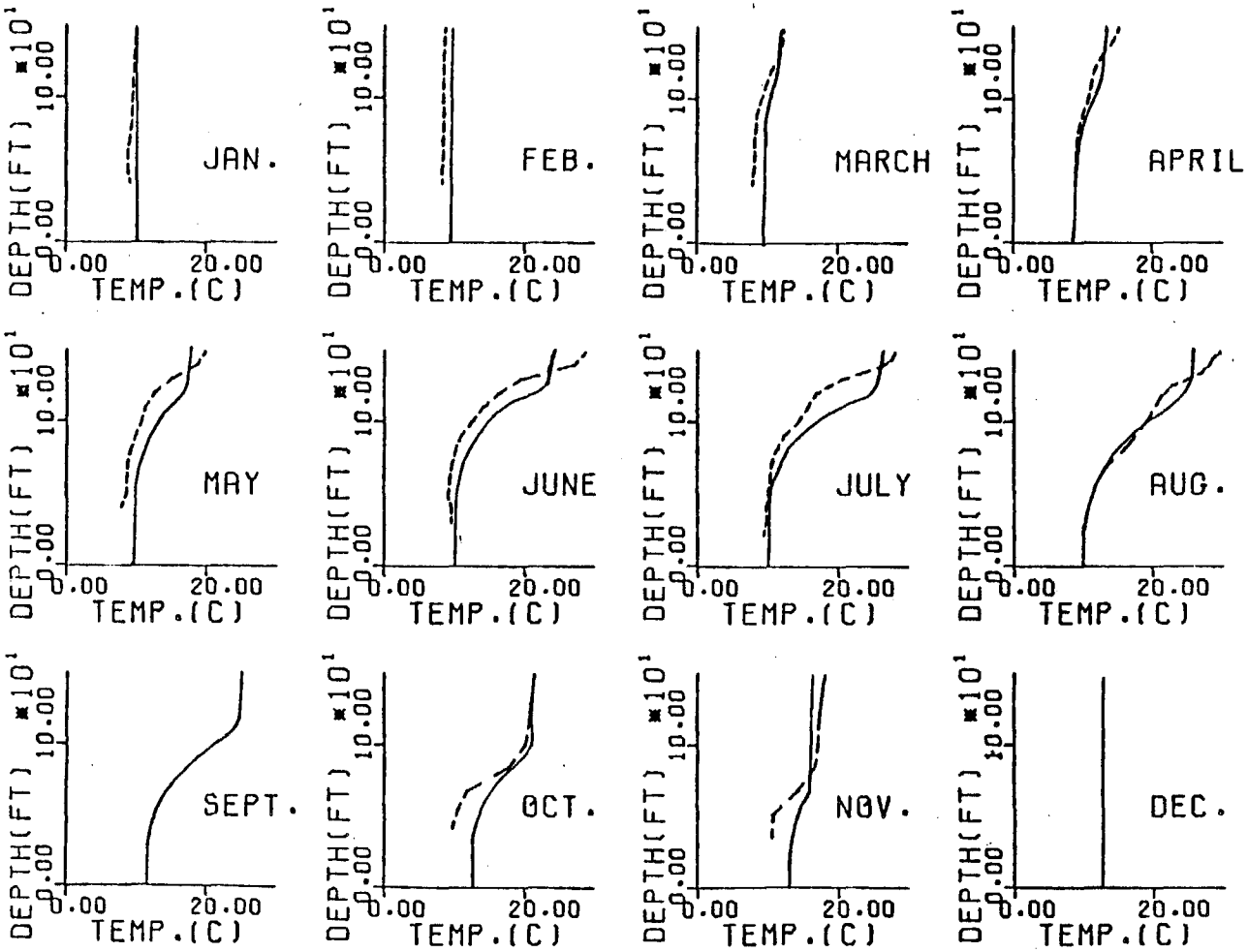

Figure 11. Measured (broken lines) and predicted temperature profiles, Lake Keowee, 1973

JAN.
FEB.
MARCH
APRIL

DEPTH(FT) ×10¹
10.00
0.00
0.00
20.00
TEMP.(C)
JAN.
FEB.
APRIL
MAY
JUNE
JULY
AUG.

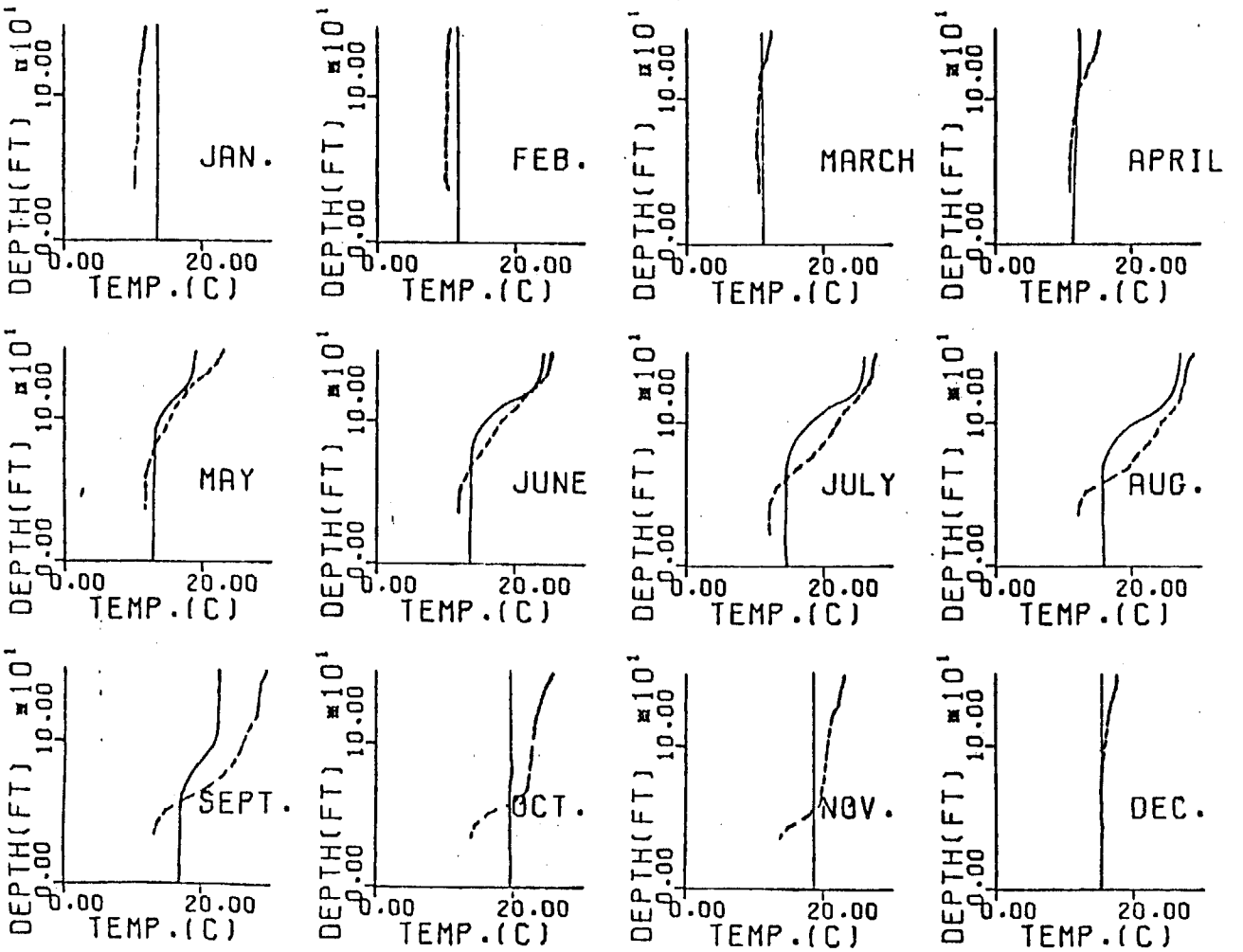

Figure 13. Measured (broken lines) and predicted temperature profiles, Lake Keowee, 1975

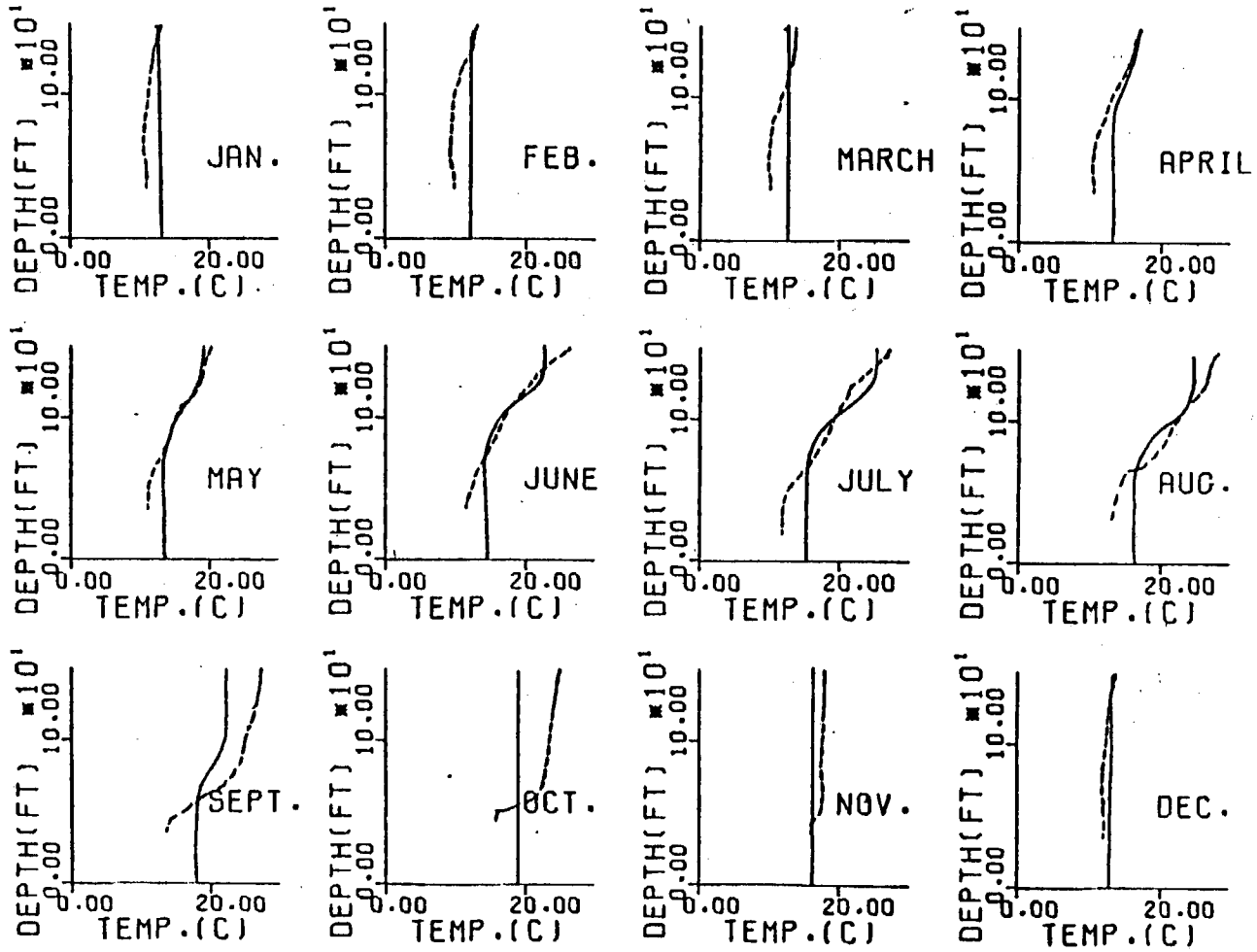

Figure 14. Measured (broken lines) and predicted temperature profiles, Lake Keowee, 1976

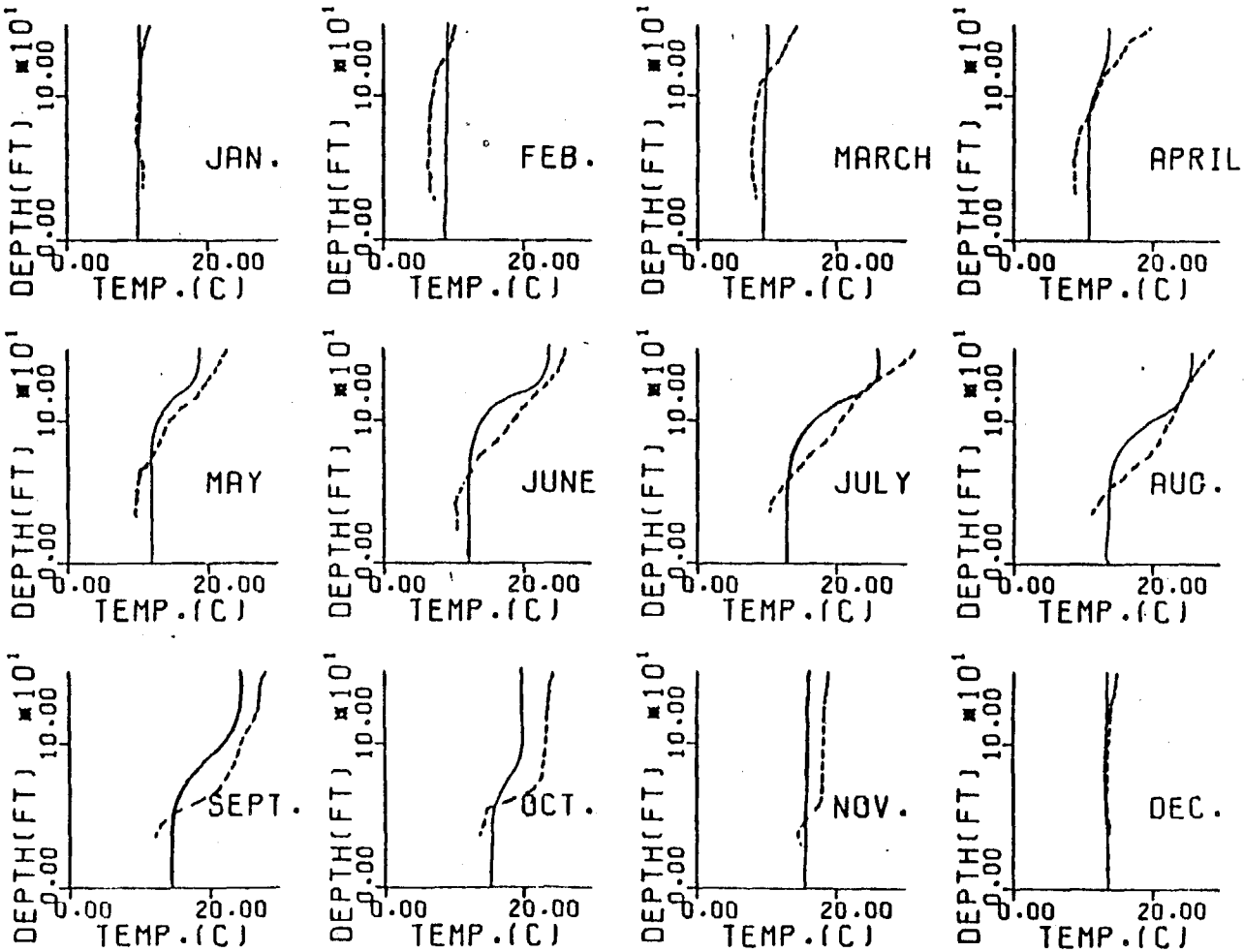

Figure 15. Measured (broken lines) and predicted temperature profiles, Lake Keowee, 1977

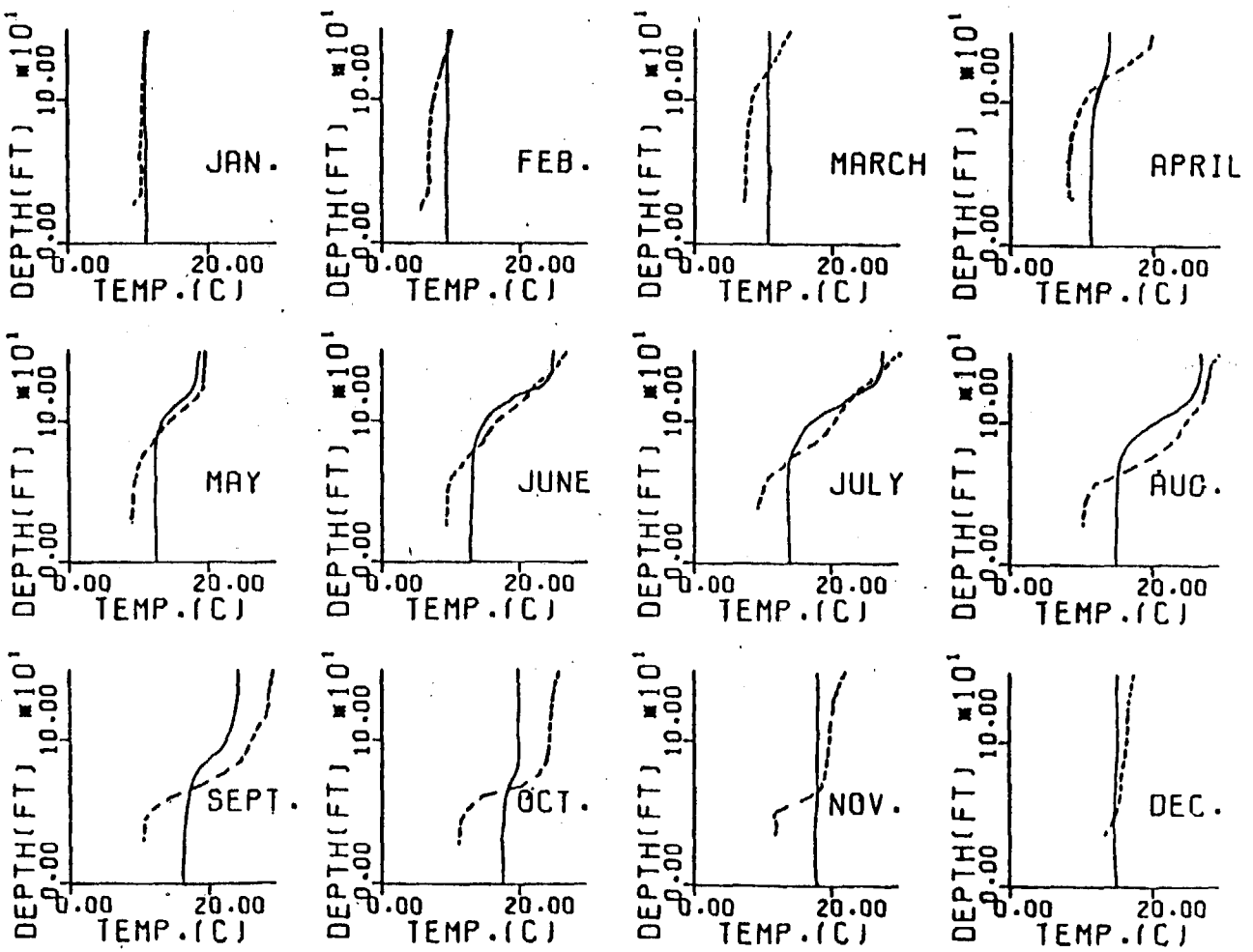

Figure 16. Measured (broken lines) and predicted temperature profiles, Lake Keowee, 1978

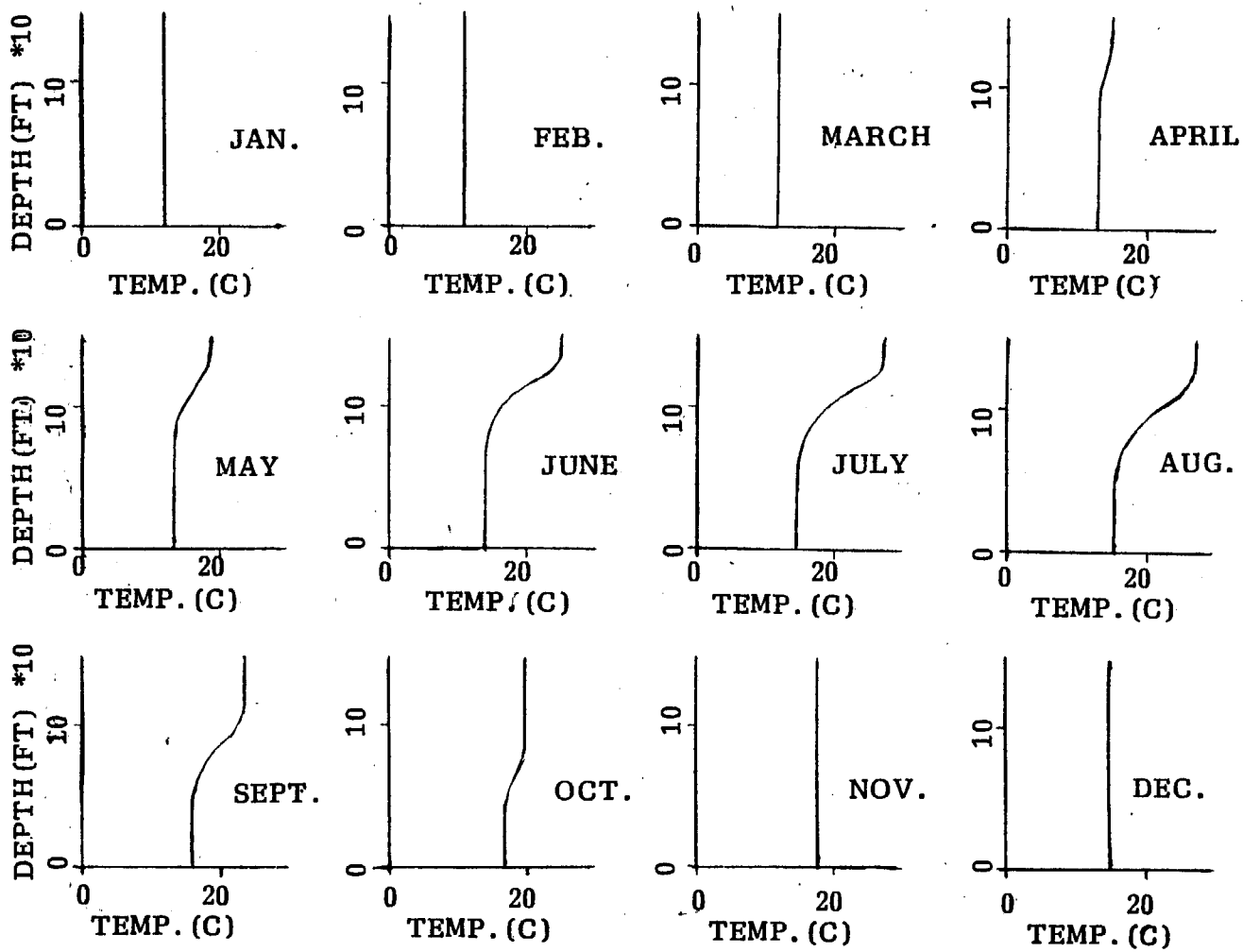

Figure 17. Predicted discharge temperature profiles, Lake Keowee, 1979

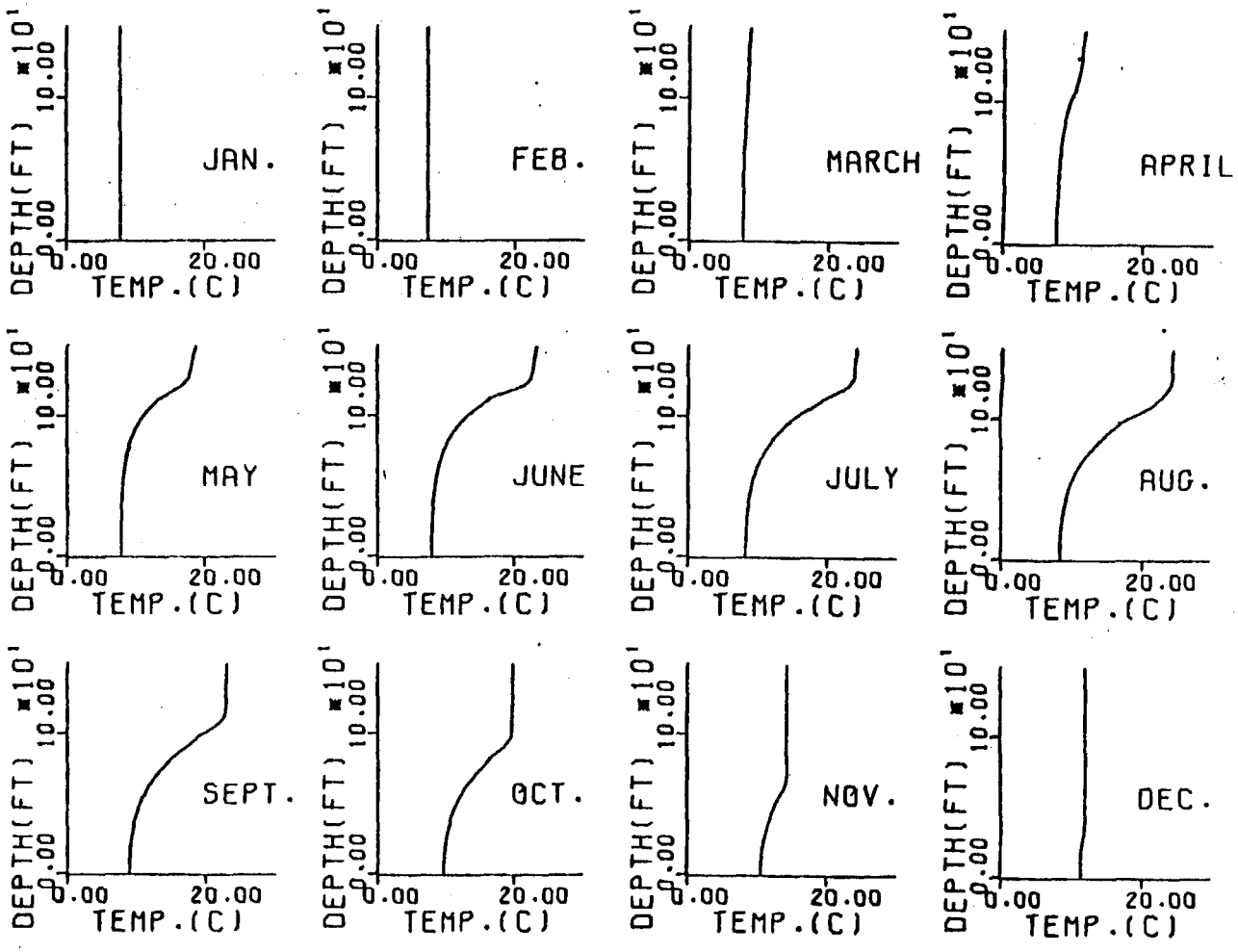

Figure 18. Predicted no-discharge temperature profiles, Lake Keowee, 1971

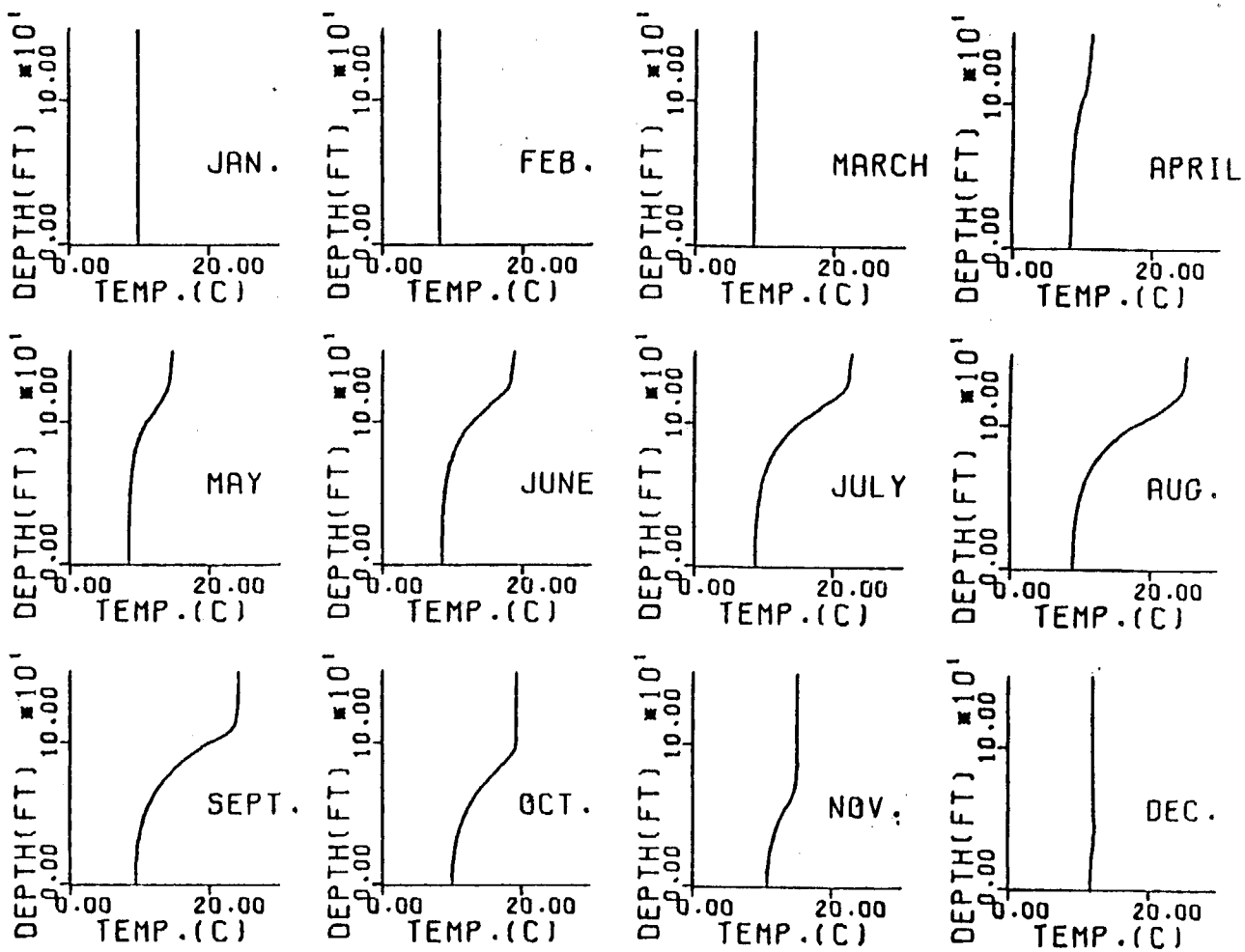

Figure 19. Predicted no-discharge temperature profiles, Lake Keowee, 1972

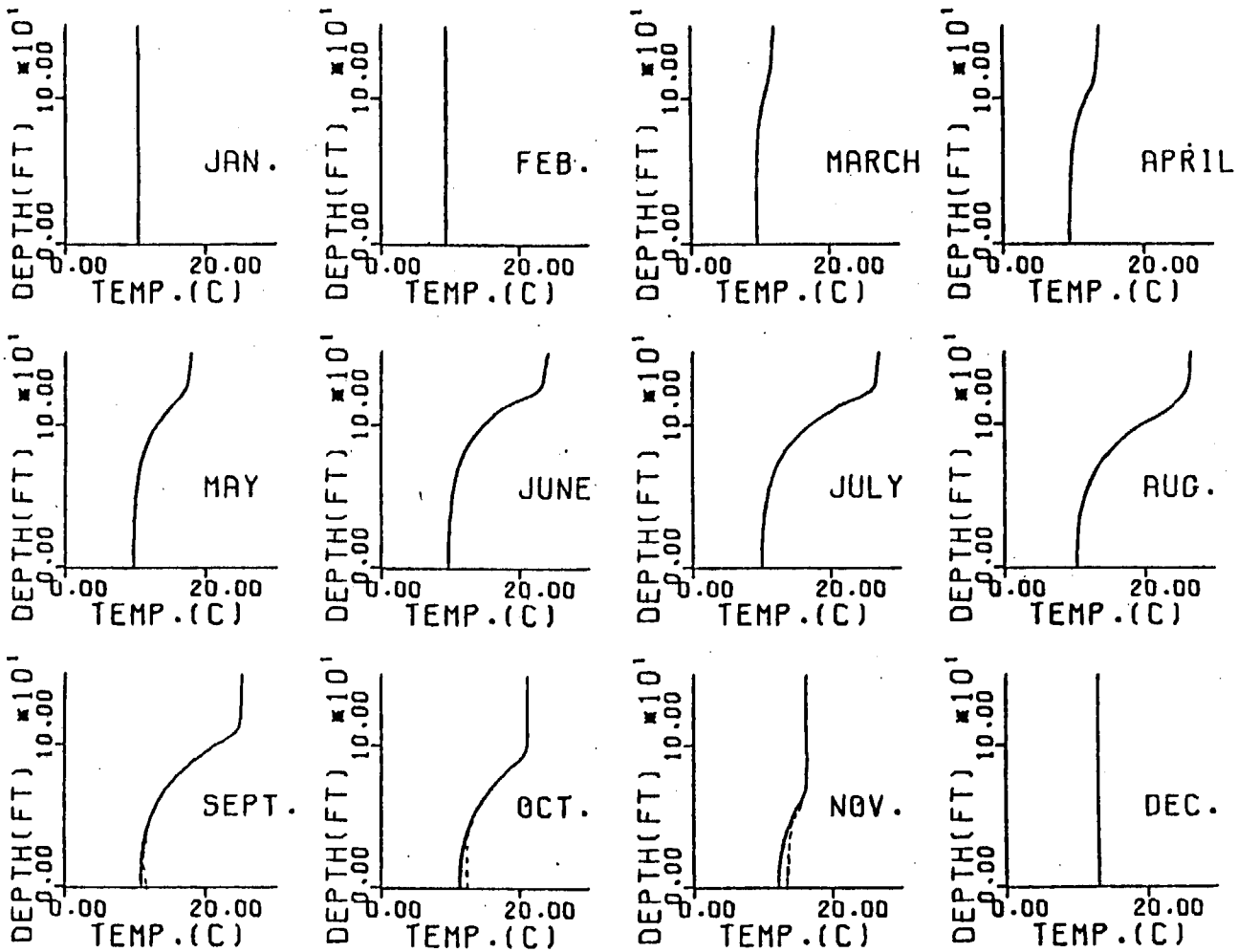

Figure 20. Predicted discharge (borken lines) and no-discharge temperature profiles, Lake Keowee, 1973

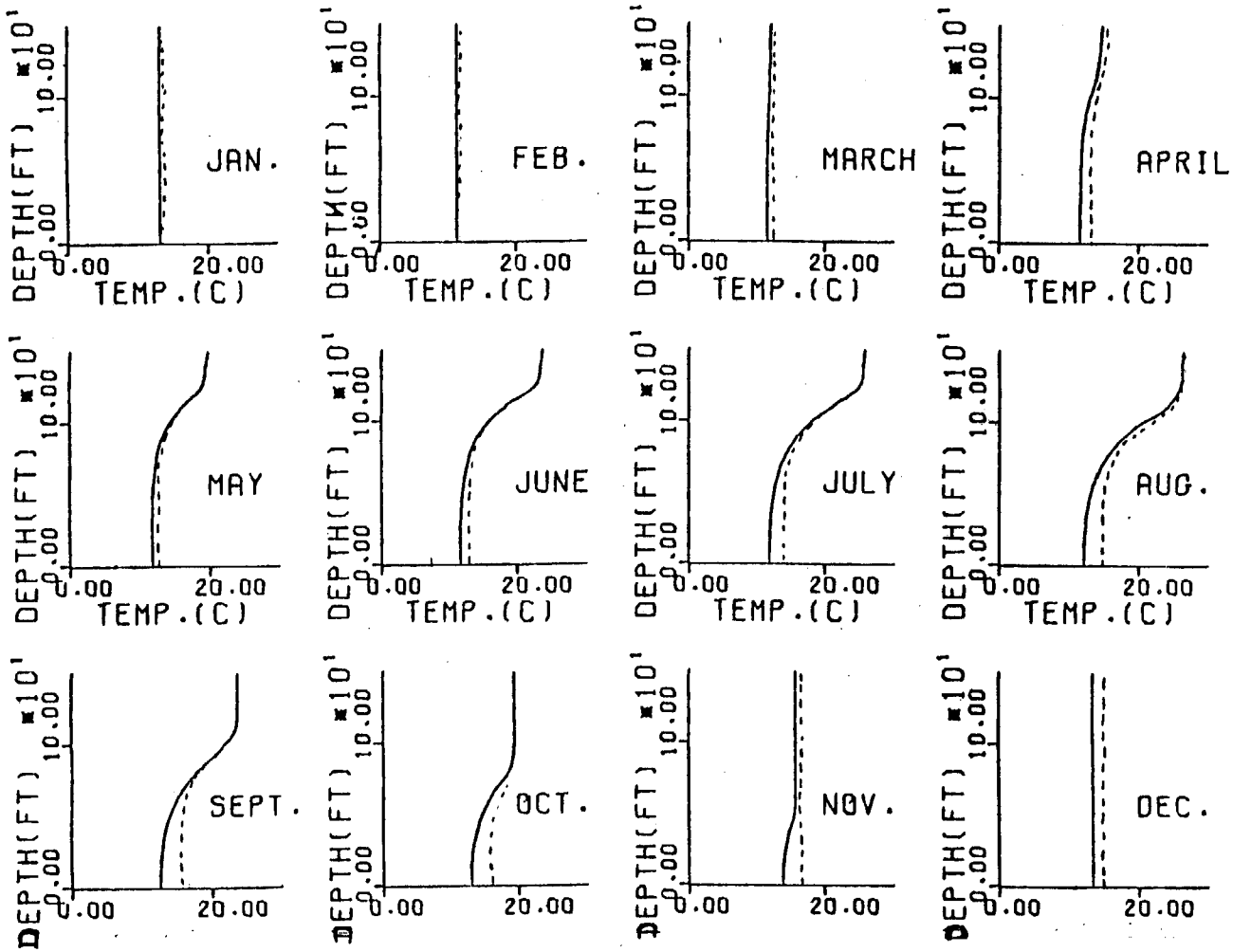

Figure 21. Predicted discharge (broken lines) and no-discharge temperature profiles, Lake Keowee, 1974

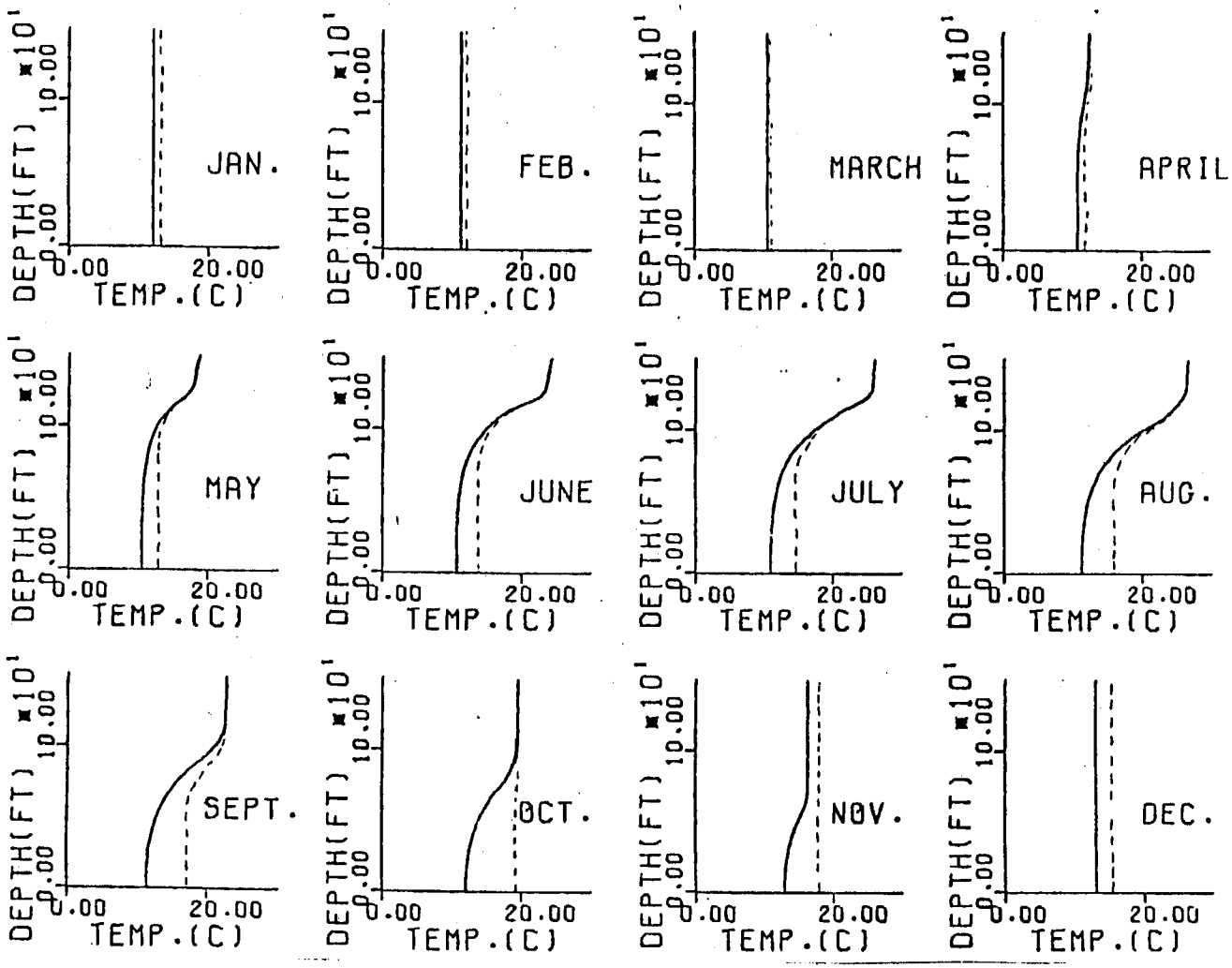

Figure 22. Predicted discharge (borken lines) and no-discharge temperature profiles, Lake Keowee, 1975

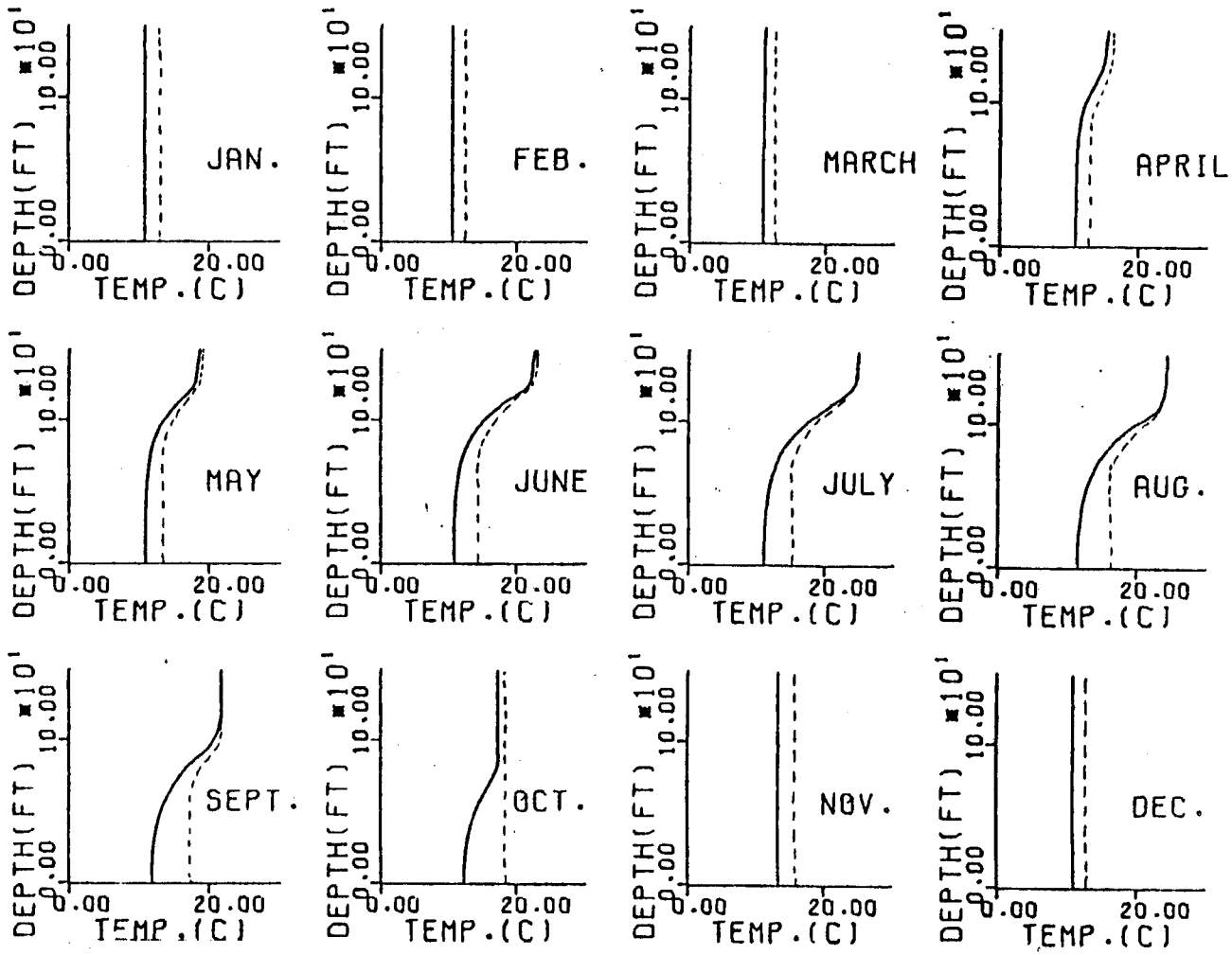

Figure 23. Predicted discharge (borken lines) and no-discharge temperature profiles, Lake Keowee, 1976

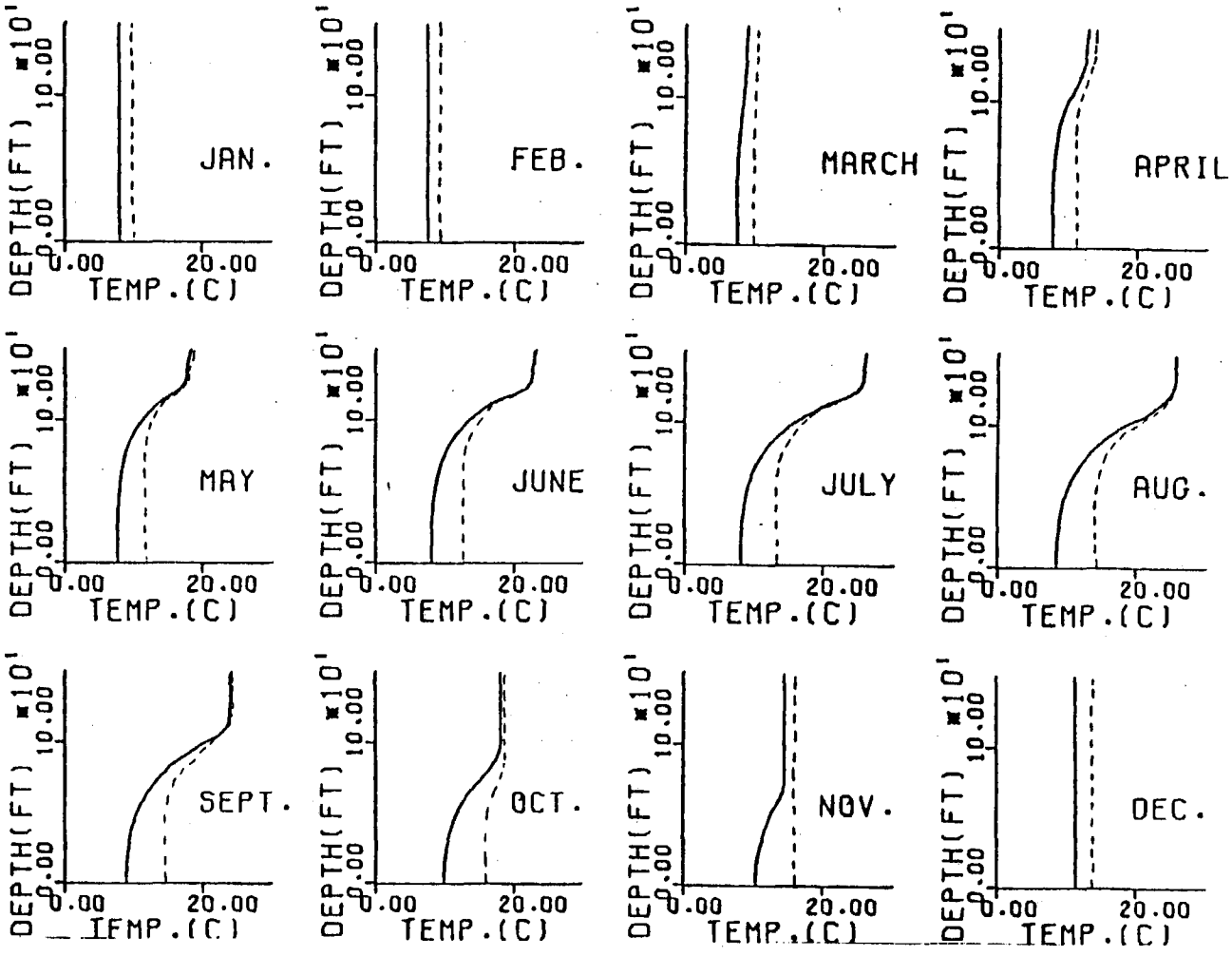

Figure 24. Predicted discharge (broken lines) and no-discharge temperature profiles, Lake Keowee, 1977

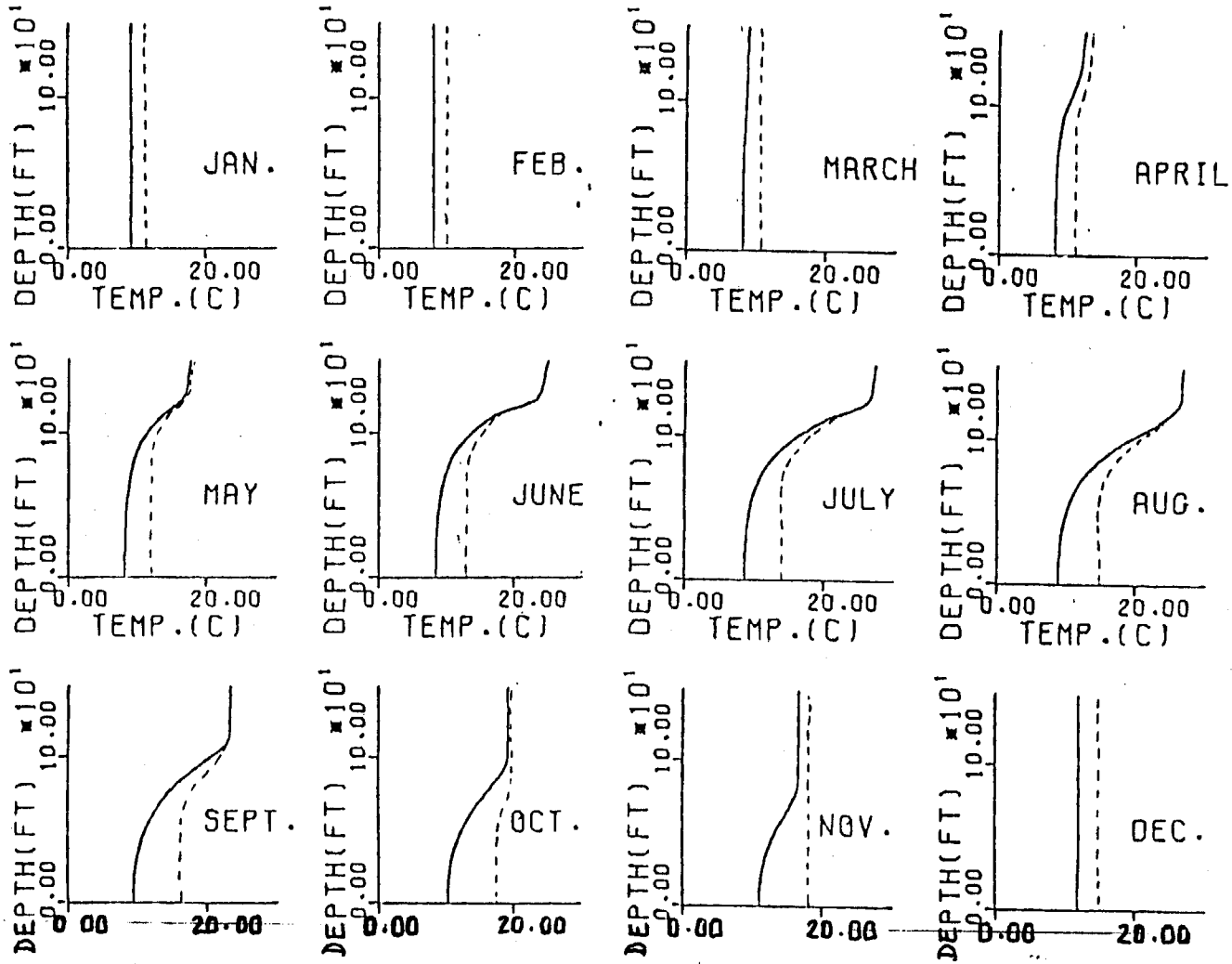

Figure 25. Predicted discharge (broken lines) and no-discharge temperature profiles, Lake Keowee, 1978

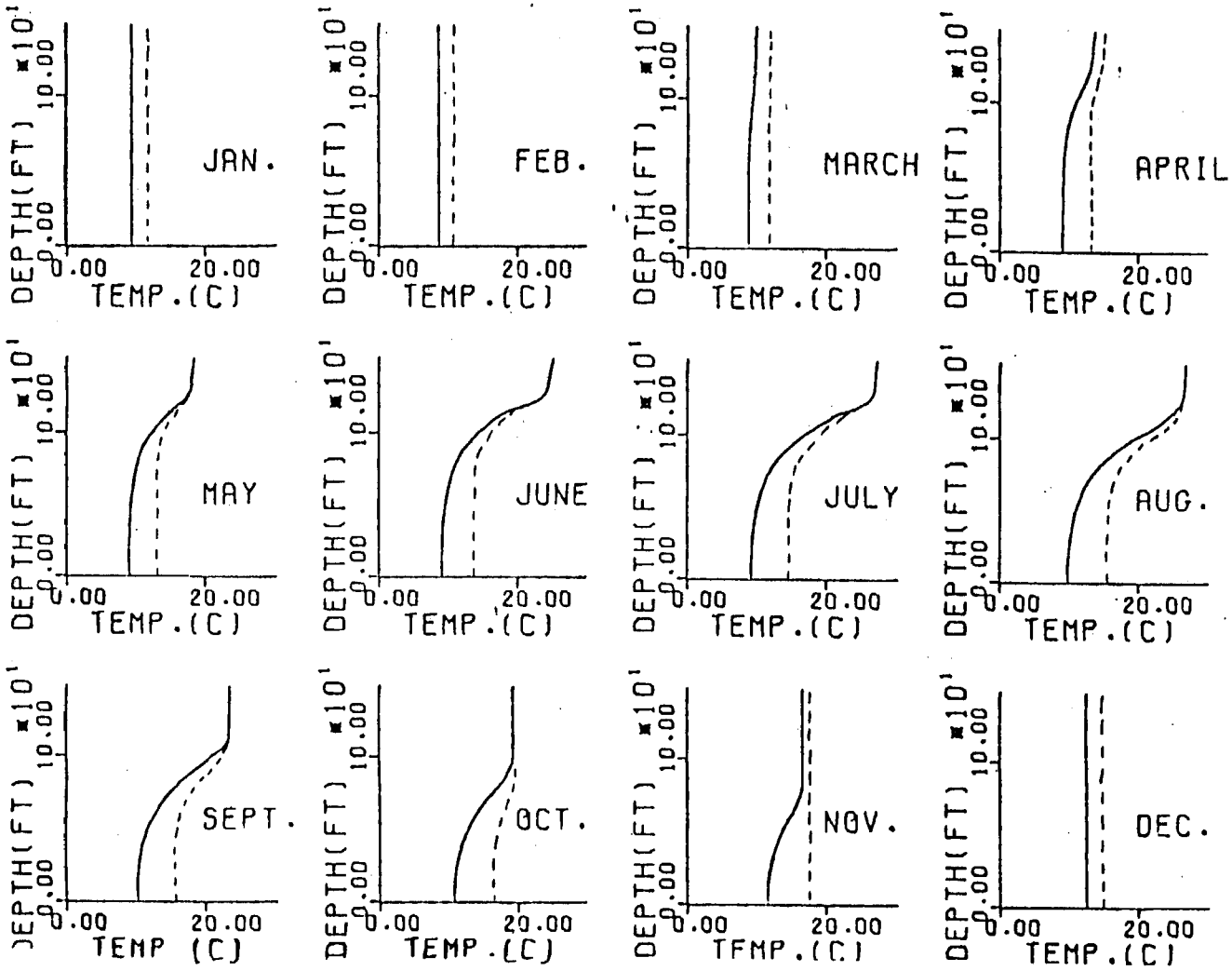

Figure 26. Predicted discharge (broken lines) and no-discharge temperature profiles, Lake Keowee, 1979

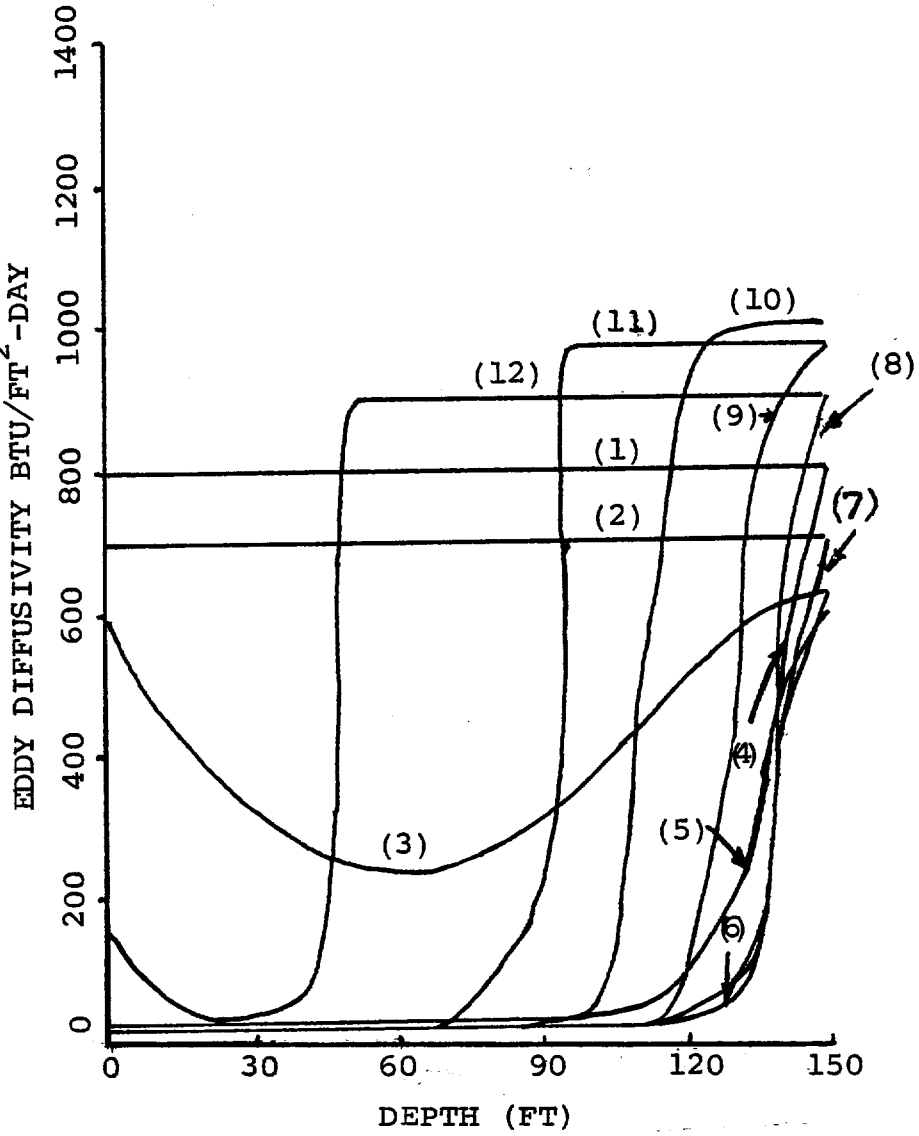

Figure 27. Variation of eddy diffusivity with depth, Lake Keowee, 1975

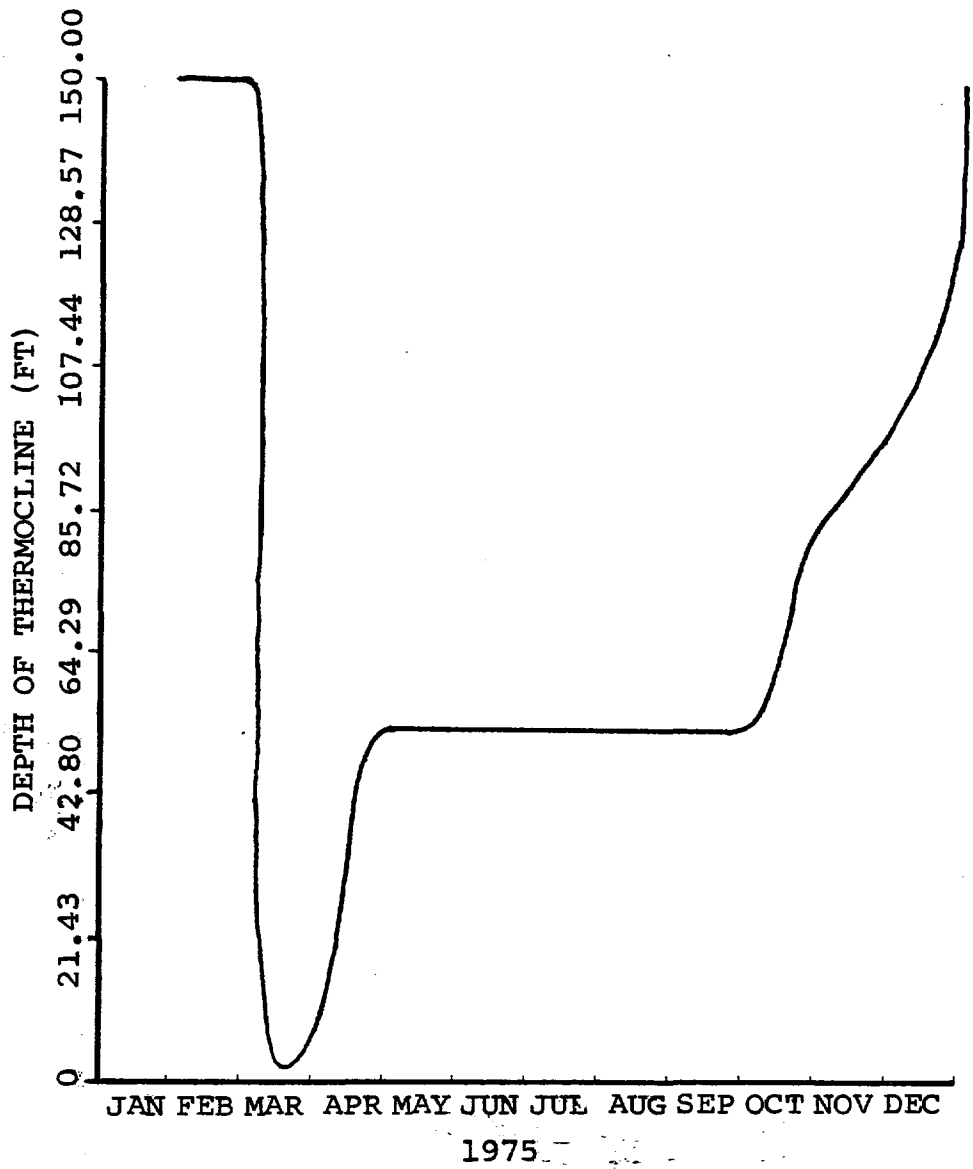

Figure 28. Monthly variation of the depth of the thermocline, Lake Keowee, 1975

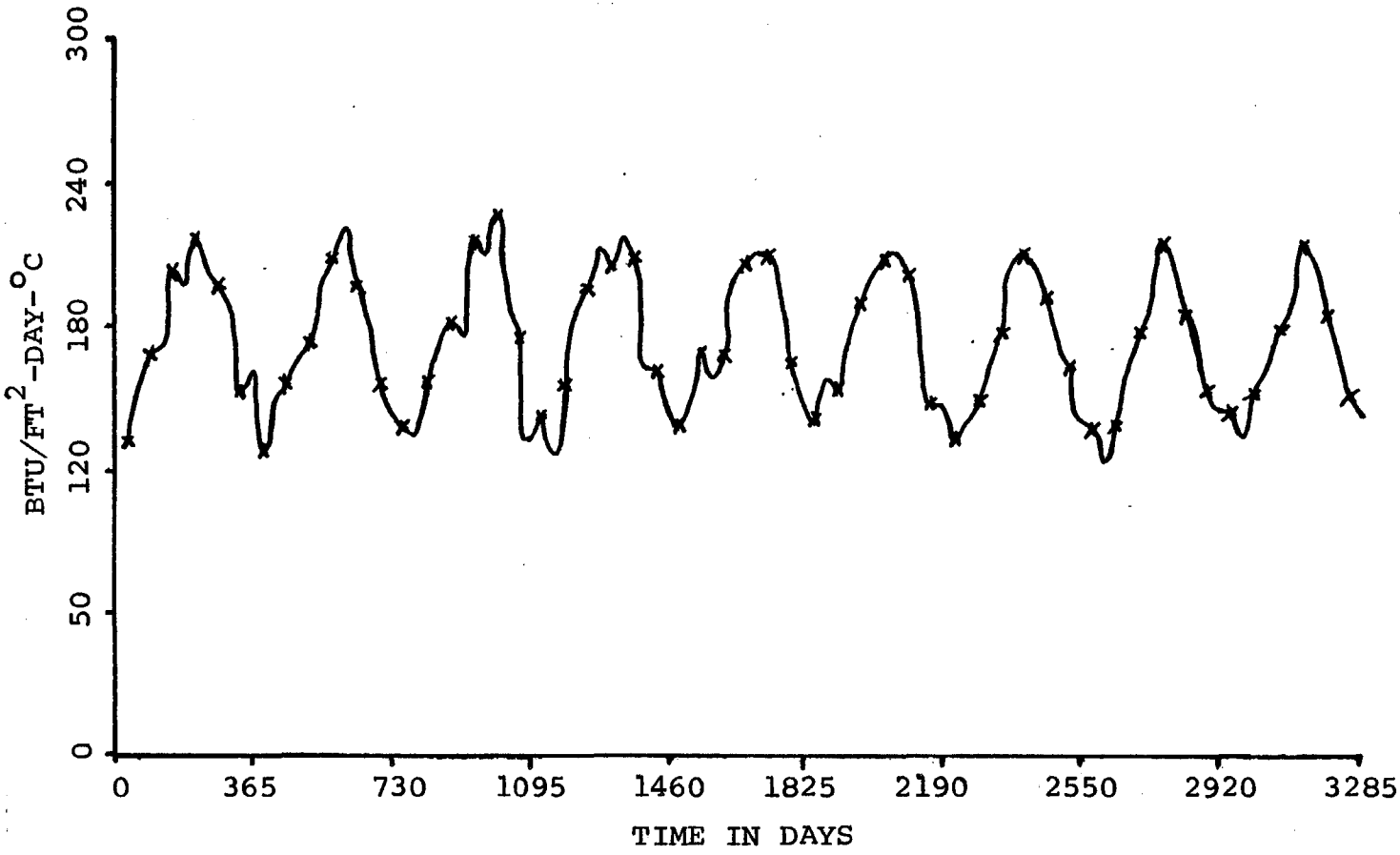

Figure 29. Temporal variation of the surface exchange coefficient, Lake Keowee, 1971-1979

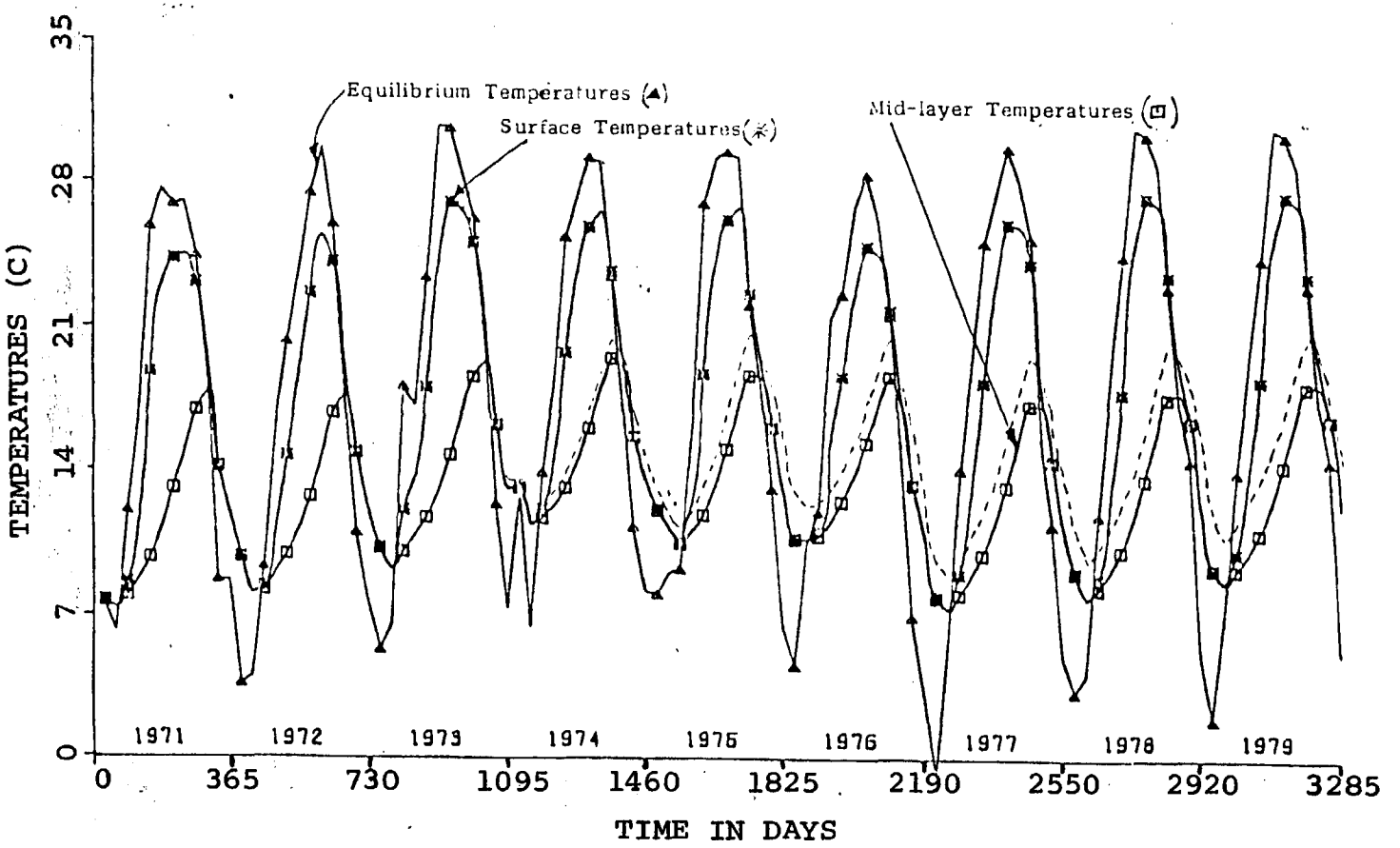

Solid Lines (No-discharge)
Broken Lines (Discharge-midlayer Temperatures)

Figure 30. Stratification cycle, Lake Keowee, 1971-1979

REFERENCES

Dake, J. M. K and D. R. F. Harelman. Thermal Stratification in Lakes: Anaytical and Laboratory Studies. Water Resources Research, Vol. 5, No. 2. pp 484-495. April 1969.

Duke Power Company. Unpublished Materials. 1971-1979.

Dutton, J. A. and R. A. Bryson. 1962. Heat Flux in Lake Mendota Limnol Ocenanog. 7, 80.

Edinger, J. E. and J. C. Geyer. Heat Exchange in the Environment. Sanitary Eng. and Water Resources Report. 1967.

Henson, E. B., Bradshaw, A. S. and D. C. Chandler. The Physical Limnology of Cayuga Lake, New York. Memoir 378, 1961. Agricultural Research Station, Cornell University, Ithaca, New York.

Kraus, E. B. and J. S. Turner. A One-dimensional Model for the Seasonal Thermocline II. The General Theory and Its Consequences. Tellus, Vo. 19, No. 1. pp 98-105. 1967.

Lerman A. and M. Stiller. 1969. Vertical Eddy Diffusivity in Lake Tiberias. Verh. International Verein. Limnol. 17, 323.

Monin, A. S. and A. M. Obukhov. Basic Regularity in Turbulent Mixing in the Surface Layer of the Atmosphere. USSR Acad. Sci. Works of Geophys. Met., No. 24, 163. 1954.

Mitry, A. M. and M. N. Ozisik. A One-dimensional Model for Seasonal Variation of Temperature Distribution in Stratified Lakes. International J. Heat Mass Transfer, Vol. 19. pp 201-205. 1976.

Oconee Nuclear Station Environmental Summary Report. Duke Power Company, 1971-1976, Vol. 1. November 1977.

Rossby, C. C. and B. R. Montgomery. The Layer of Frictional Influence in Wind Ocean Currents. Papers in Physical Oceanography, Vol. 3, No. 3. p 101. 1935.

Sengupta, S., Lee, S. S. and E. Nwadike. A One-dimensional Variable Cross-section Model for the Seasonal Thermocline. Proceedings of the 2nd Conference on Waste Heat Management and Utilization. p IX-A-3. 1978.

Sengupta, S. and W. Lick. A Numerical Model for Wind-driven Circulation and Heat Transfer in Lakes and Ponds. FTAS/TR-74-98.

Sundaram, T. R., Easterbrook, C. C., Piech, K. R. and G. Rudinger. An Investigation of the Physical Effects of Thermal Discharges into Cayuga Lake. Report VT-2616-0-2. Cornell Aeronautical Laboratory, Buffalo, New York. November 1969.

Sundaram, T. R. and R. G. Rehm. Formulation and Maintenance of Thermoclines in Stratified Lakes Including the Effects of Power Plant Discharge. AIAA Paper No. 70-238. 1970.

Sundaram, T. R., Rehm, R. G., Rudinger, G. and G. E. Merritt. A Study of Some Problems on the Physical Aspects of Thermal Pollution. VT-2790-1-1. Cornell Aeronautical Laboratory, Buffalo, New York. 1971.

Sundaram, T. R. and R. G. Rehm. Formation and Maintenance of Thermoclines in Temperate Lakes. AIAA Journal, Vol. 9, No. 7. pp 1322-1329. 1971.

Sundaram, T. R. and R. G. Rehm. Effects of Thermal Discharges on the Stratification Cycles of Lakes. AIAA Journal, Vol. 10, No. 2. pp 204-210. 1972.

Sweers, H. E. 1969. Two Methods of Describing the "Average" Vertical Temperature Distribution of a Lake. J. Fish. Res. Bd., Canada 25. 1911.

APPENDICES

APPENDIX A

DERIVATION OF THE MATHEMATICAL MODEL

DERIVATION OF THE VARIABLE CROSS-SECTIONAL AREA MODEL

Assuming lateral uniformity (horizontally uniform lake), the isotherms coincide with the isopycnals. The equations for such a model are obtained from the basic balance equations of mass and heat:

$$\frac{\partial \rho}{\partial t} = -\bar{\nabla} \cdot \rho \bar{v} \qquad (A.1)$$

$$\frac{\partial}{\partial t}(\rho C_p T) = \bar{\nabla} \cdot \rho C_p \bar{K} \cdot \bar{\nabla} \cdot \rho C_p T \bar{V} + H \qquad (A.2)$$

where,

ρ = density.

t = time.

V = velocity of flow.

C_p = heat capacity.

T = temperature.

K = heat diffusivity tensor (including turbulent diffusivity).

H = source of heat per unit volume.

Most models have started with the above equations and neglected all the terms involving the two horizontal components (or dimensions). The neglect of the horizontal divergence in such simple models is not always justified. There are at least two reasons for the existence of horizontal divergence in real lakes.

1. The variation of horizontal cross-sectional area of the lake with depth.

2. The existence of sources of heat and matter efflux on the bottom of the lake at depths above the deepest point.

The need to include these in the diffusion equations of lakes was already felt; Lerman and Stiller (1969), Dutton and Bryson (1962) and Tzur (1973). Only Tzur (1973) formulated corrected diffusion equations.

Another complication in applying a 1-D model to a lake is caused by seiches and internal waves. When these are present, the height of an isopycnal loses its meaning. According to Sweers (1968), averaging simultaneous temperature profiles at different points of a lake or taking profiles during a short interval of time in one or more points can lead to distortion of the shape of the thermocline. He recommends averaging the depths of isotherms instead. In a lake of constant depth this is probably the best available approximation but fails for a lake of varying depth.

The effects of area change with depth are included by the following treatments of Equations (A.1) and (A.2). Integrating Equation (A.1) over the volume of water below height h measured from the deepest point in the lake yields

$$\int_{\forall} \frac{\partial \rho}{\partial t} d\forall = \int_{\forall} \bar{\nabla} \cdot \rho \bar{V} d\forall$$

Using Gauss theorem on the right hand side yields

$$\int_{\forall} \frac{\partial \rho}{\partial t} d\forall = -\rho \int_{S} \hat{n} \cdot \bar{V} dS \qquad (A.3)$$

where S is a surface completely surrounding the volume $\forall$, hence

$$dS = dC + dA$$

where C is the surface area of the part of the bottom of the lake that is bounded by the contour at height z. As a subscript, z marks the vertical component of a vector.

Using $d\forall = A dz$ in Equation (A.3) yields

$$\int_{o}^{h} \frac{\partial \rho}{\partial t} A dz = -\rho \int_{C} \hat{n} \cdot \bar{V} dC - \rho \int_{A} \hat{n} \cdot \bar{V} dA$$

i.e.

$$\int_{o}^{h} \frac{\partial \rho}{\partial t} A dz = -\int_{o}^{h} \rho V_n dC - \rho V_z A(h) \qquad (A.4)$$

Integrating Equation (A.2) over the volume of water below height h measured from the deepest point in the lake yeilds

$$\int_V \frac{\partial}{\partial t}\rho C_p T dV = \int_V (\bar{\nabla}\cdot\rho C_p \bar{K}\cdot\bar{\nabla}T)dV - \int_V \bar{\nabla}\cdot\rho C_p T\bar{V}dV + \int_V H dV$$

Applying the divergence theorem to the first two terms on the right yields

$$\int_o^h A(z)\frac{\partial}{\partial t}\rho C_p T dz = \int \hat{n}\cdot(\rho C_p \bar{K}\cdot\nabla T)dS - \int(\hat{n}\cdot\rho C_p T\bar{V})dS + \int_o^h A(z)H(z)dz$$

Using $dS = dA + dC$ yields

$$\int_o^h A(z)\frac{\partial}{\partial t}\rho C_p T dz = \int_o^h (\rho C_p \bar{K}\cdot\bar{\nabla}T)_z dA + \int_o^h (\rho C_p \bar{K}\cdot\bar{\nabla}T)_n dC - \int_o^h (\rho C_p T\bar{V})_z dA - \int_o^h (\rho C_p T\bar{V})_n dC + \int_o^h A(z)H(z)dz$$

i.e.

$$\int_o^h A(z)\frac{\partial}{\partial t}\rho C_p T dz = \rho C_p A(h)[\bar{K}\cdot\bar{\nabla}T]_z + \int_o^h \rho_c C_c [\bar{K}\cdot\bar{\nabla}T]_n dC - \rho C_p A(h)TV_z - \int_o^h \rho_c C_c T_c V_n dC + \int_o^h A(z)H(z)dz \qquad (A.5)$$

where,

z = the vertical coordinate measured upward from the deepest point of the lake. As a subscript, it marks the vertical component of a vector.

C = the surface area of the part of the bottom of the lake that is bounded by the contour at height z.

n = subscript that marks the component of a vector that is perpendicular to the lake-bottom positive upwards.

A(z) = the horizontal cross-section of the lake at height z.

As all the properties of the lake are constant over the horizontal isopycnals, the integration over the isopycnals becomes simple multiplication by their areas.

Differentiating Equations (A.4) and (A.5) with respect to the height, a set of 1-D equations are obtained from Equation (A.4):

$$A\frac{\partial \rho}{\partial t} = -\frac{\partial}{\partial z}A\rho V_z - \rho_c V_n \frac{\partial C}{\partial z} \qquad (A.6)$$

The last term in the above equation is the mass addition term (source term) from Equation (A.5):

$$A\frac{\partial}{\partial t}\rho C_p T = \frac{\partial}{\partial z}\rho C_p A(K\cdot\bar{\nabla}T)_z - \frac{\partial}{\partial z}\rho C_p A T V_z$$

$$+ [\rho_c C_c(\bar{K}\cdot\bar{\nabla}T)_n - \rho_c C_c T_c V_n]\frac{dC}{dz} + AH \qquad (A.7)$$

In the above equation,

$\rho_c C_c(\bar{K}\cdot\bar{\nabla}T)_n \equiv$ Conduction

Heat addition terms

$\rho_c C_c T_c V_n \equiv$ Convection

Because the horizontal gradients vanish, Equation (A.7) can be simplified further by noting that

$$(\bar{K}\cdot\bar{\nabla}T)_z = K_z\frac{\partial T}{\partial z} \qquad (A.8)$$

Following a similar treatment used by Y. Tzur (1973), the slope of the bottom of lakes is usually small; it rarely exceeds a gradient of 0.1, Assuming this and considering an elemental area shown below,

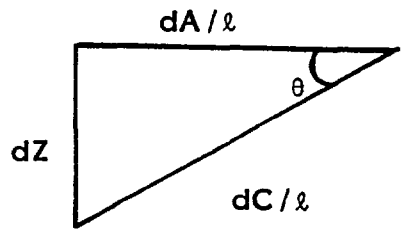

$\tan\ \theta = \ell\frac{dz}{dA} \equiv$ gradient of the lake bottom

$$\text{Cos}\ \theta = \text{Cos}[\tan^{-1}\ \ell\frac{dz}{dA}] \qquad \text{(A.9)}$$

also

$$\text{Cos}\ \theta = \frac{dA}{dC} \qquad \text{(A.10)}$$

From Equation (A.9) and (A.10)

$$\frac{dA}{dC} = \text{Cos}[\tan^{-1}\ \ell\frac{dz}{dA}] \qquad \text{(A.11)}$$

$$= \text{Cos}[\text{arctan (gradient)}]$$

$$= \eta \cong \text{average of Cos arctan gradient of the bottom surface at that depth.}$$

From Equation (A.11)

$$dA = \eta dC$$

or

$$\frac{dA}{dz} = \eta\frac{dC}{dz}$$

i.e.

$$\frac{dC}{dz} = \frac{1}{\eta}\frac{dA}{dz}$$

Since Cos arctan (0.1) = 0.995, $\eta \cong \frac{1}{\eta} = 1.$

Alternatively, η can be incorporated into the surface sources (equation (A.7)).

The 1-D equations can now be written in more concise and convenient forms:

$$A\frac{\partial \rho}{\partial t} = -\frac{\partial}{\partial z} A\rho V_z + IA' \qquad \text{(A.12)}$$

and

$$A\frac{\partial}{\partial t}(\rho C_p T) = \frac{\partial}{\partial z}(\rho C_p A K_z \frac{\partial T}{\partial z}) - \frac{\partial}{\partial z}(\rho C_p A T V_z) + QA' + AH \qquad \text{(A.13)}$$

where,

$A' = \frac{dA}{dz}$

I = bottom-surface source of mass per unit area.

Q = bottom-surface source of heat per unit area.

Boundary Contitions

Surface:

Equilibrium Temperature Concept

The bulk temperature of a vertically-mixed body of water under natural conditions, Tn, tends to increase or decrease with time, according to whether the sum, ΣH, of its heat inputs (net solar and atmospheric radiation, thermal discharge and heat outputs; back-radiation, evaporation, and condensation) is positive or negative:

$$\frac{dT_n}{dt} = \Sigma H / \rho C_p h \qquad (A.14)$$

Following a similar procedure used by Edinger and Geyer (1967), Equation (A.14) can be transformed (without linearizing the temperature dependence of the components of ΣH) to yield

$$\frac{dT_n}{dt} = K_s (T_E - T_n) / \rho C_p h \qquad (A.15)$$

where,

K_s = surface exchange coefficient that depends on the water temperature and wind speed

T_E = equilibrium temperature, defined as the hypothetical water surface temperature at which the net rate of surface heat exchange would be zero.

Equation (A.15) expresses this definition of T_E for the particular case of a vertically-mixed water body ($\frac{dT_n}{dt} = 0$ when $T_n = T_E$). Edinger and Geyer (1967) show that the two parameters are intrinsically coupled together via water temperature and meteorological conditions. For this reason iterative techniques are often used when applying Equation (A.15) in a predictive role and because the rate of convergence is extremely rapid. The first step often yields satisfactory results.

Brady et al. (1969) have shown empirically that fluctuations in the equilibrium temperature may be conveniently estimated using the approximate relationship:

$$T_E = T_d + H_s / K_s \qquad (A.16)$$

where,

T_d = dewpoint temperature.

H_s = gross rate of shortwave solar radiation.

Since the dewpoint temperature tends to remain relatively constant through a single day, Equation (A.16) indicates that the main source of hourly fluctuations in T_E is the solar radiation components. This generally reaches a maximum at solar noon, unless variable cloudiness interferes. At nighttime T_E approaches the dewpoint temperature which acts like a relatively invariant datum for periods of 24 hours or less. On an annual basis, however, both T_d H_s are generally much greater in summer than in winter. The dominant contribution to the amplitude of seasonal fluctuation in T_E is the dewpoint temperature.

Exchange Coefficient Evaluation

The same form used by Edinger et al. (1967) was used:

$$K_s = 4.5 + 0.05\ T_s + \beta f(w) + 0.47\ f(w) \qquad (A.17)$$

where,

T_s = surface temperature.

β is found by applying standard curve-fitting techniques to published data pertaining to saturated vapor pressures at various temperatures; a convenient representation given by Edinger and Geyer (1967) is

$$\beta = 0.35 + 0.015\ T_m + 0.0012\ T_m^2 (mmHg/C) \qquad (A.18)$$

where,

$$T_m = \frac{T_s + T_d}{2} \qquad (A.19)$$

The evaporative windspeed function f(w) used is also similar to that of Edinger and Geyer (1967):

$$f(w) = 9.2 + 0.46\ W^2 (Wm^{-2}mmHg^{-1}) \qquad (A.20)$$

where,

W = wind speed (m/S).

The first boundary condition is at the surface and can now be stated as:

$$q_s = \rho C_p K_z \frac{\partial T}{\partial z}\Big|_{z=h} = K_s (T_E - T_s) \qquad (A.21)$$

Bottom:

The second boundary condition is at the bottom of the lake which is assumed to be perfectly insulated

$$\frac{\partial T}{\partial z}\Big|_{z=0} = 0 \qquad \text{(A.22)}$$

and the initial condition is the temperature of the lake at spring homothermy.

$$T_{initial} = T_o \qquad \text{(A.23)}$$

APPENDIX B

MEASURED TEMPERATURE PROFILES
(Individual Stations)

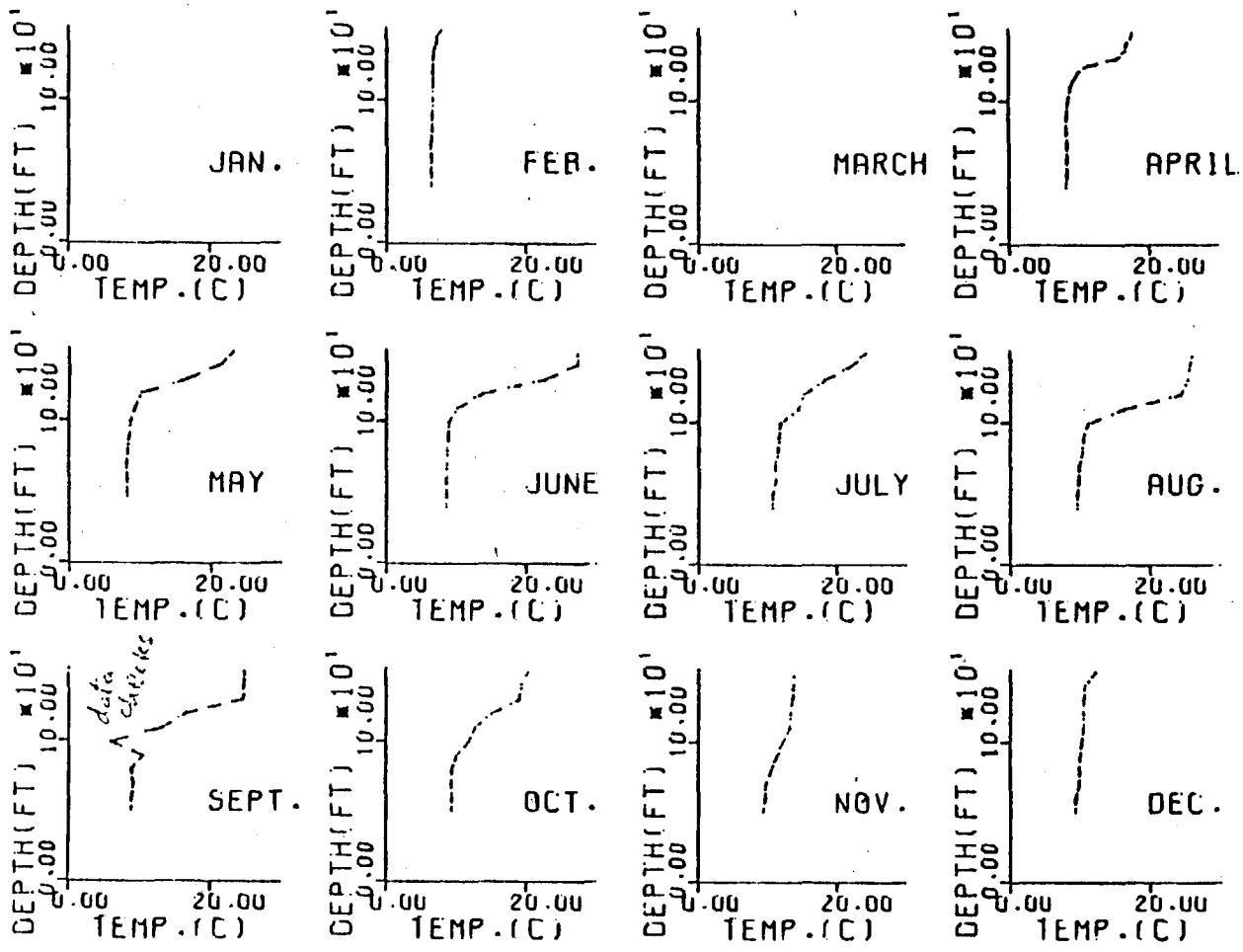

Figure B-1. Lake Keowee measured temperature profiles, 1971 - Station 500

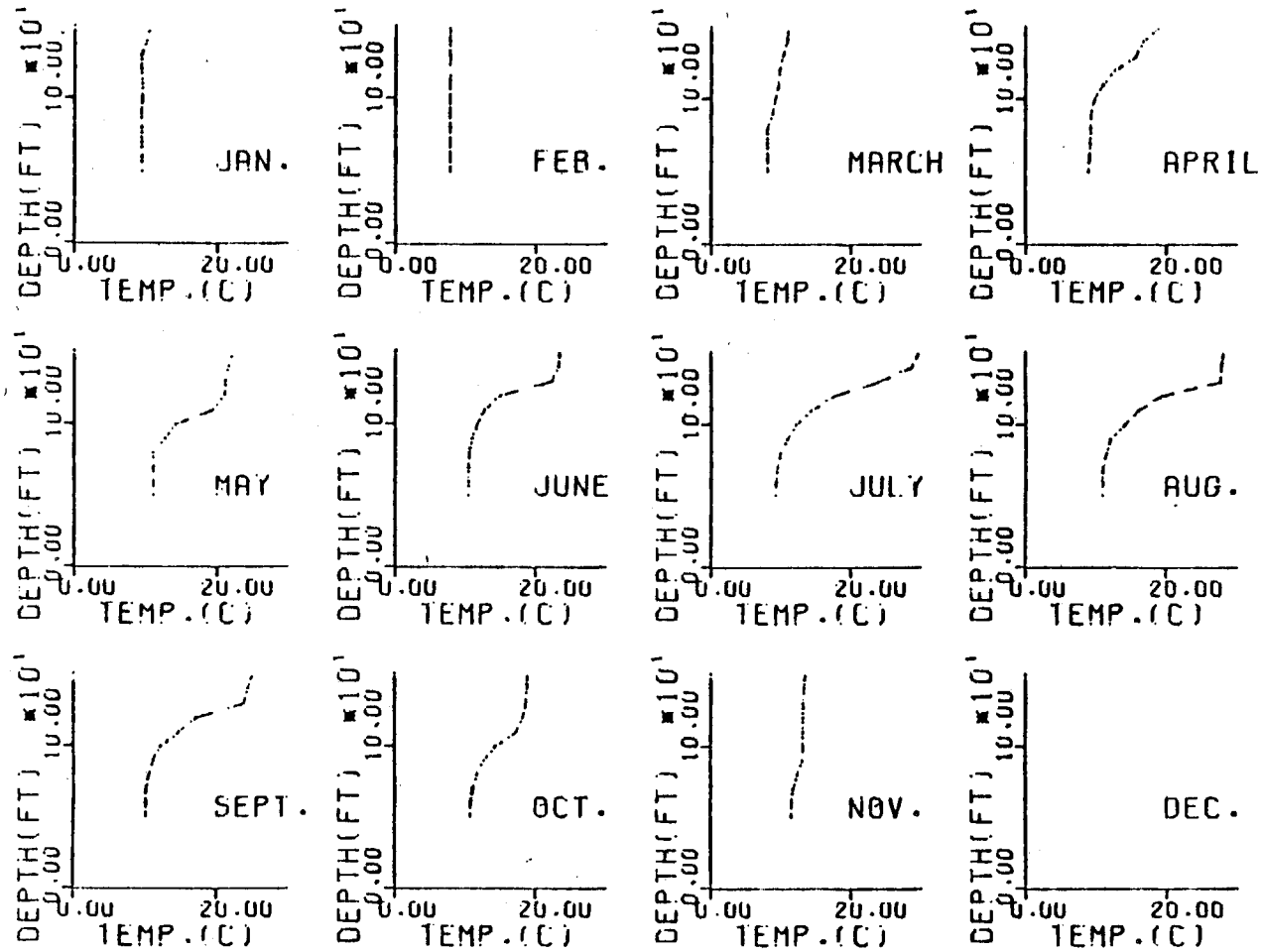

Figure B-2. Lake Keowee measured temperature profiles, 1972 - Station 500

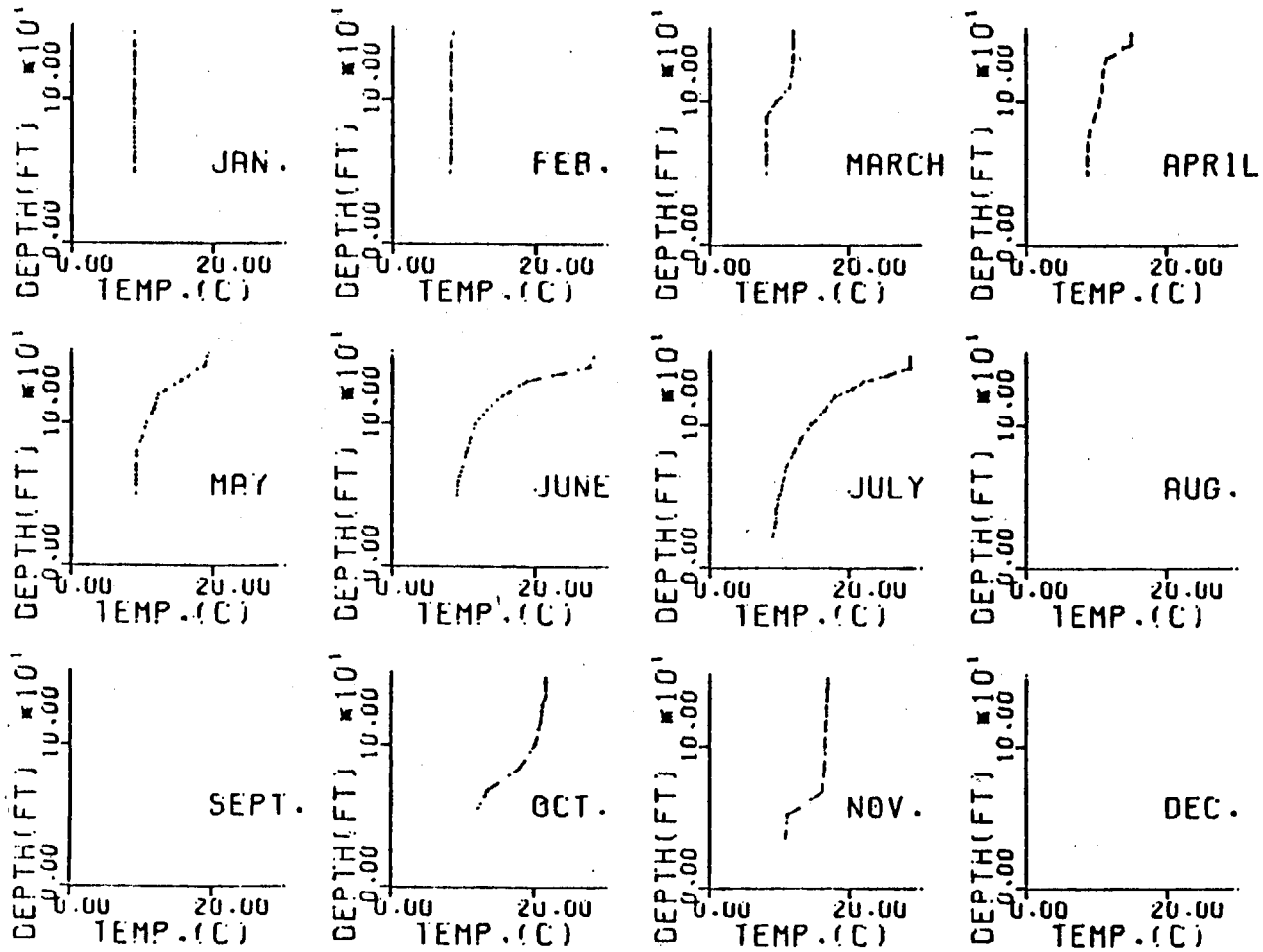

Figure B-3. Lake Keowee measured temperature profiles, 1973 - Station 500

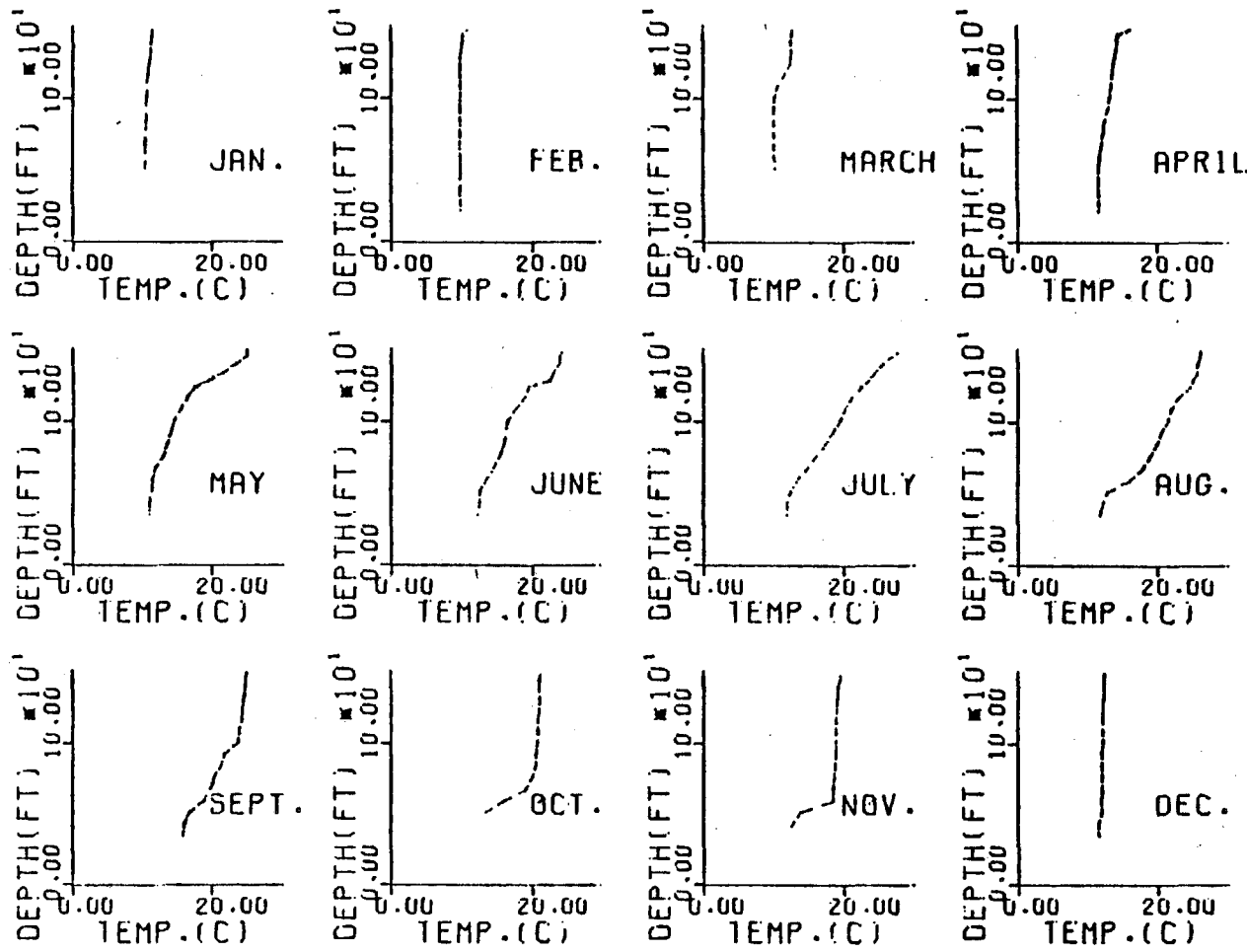

Figure B-4. Lake Keowee measured temperature profiles, 1974 - Station 500

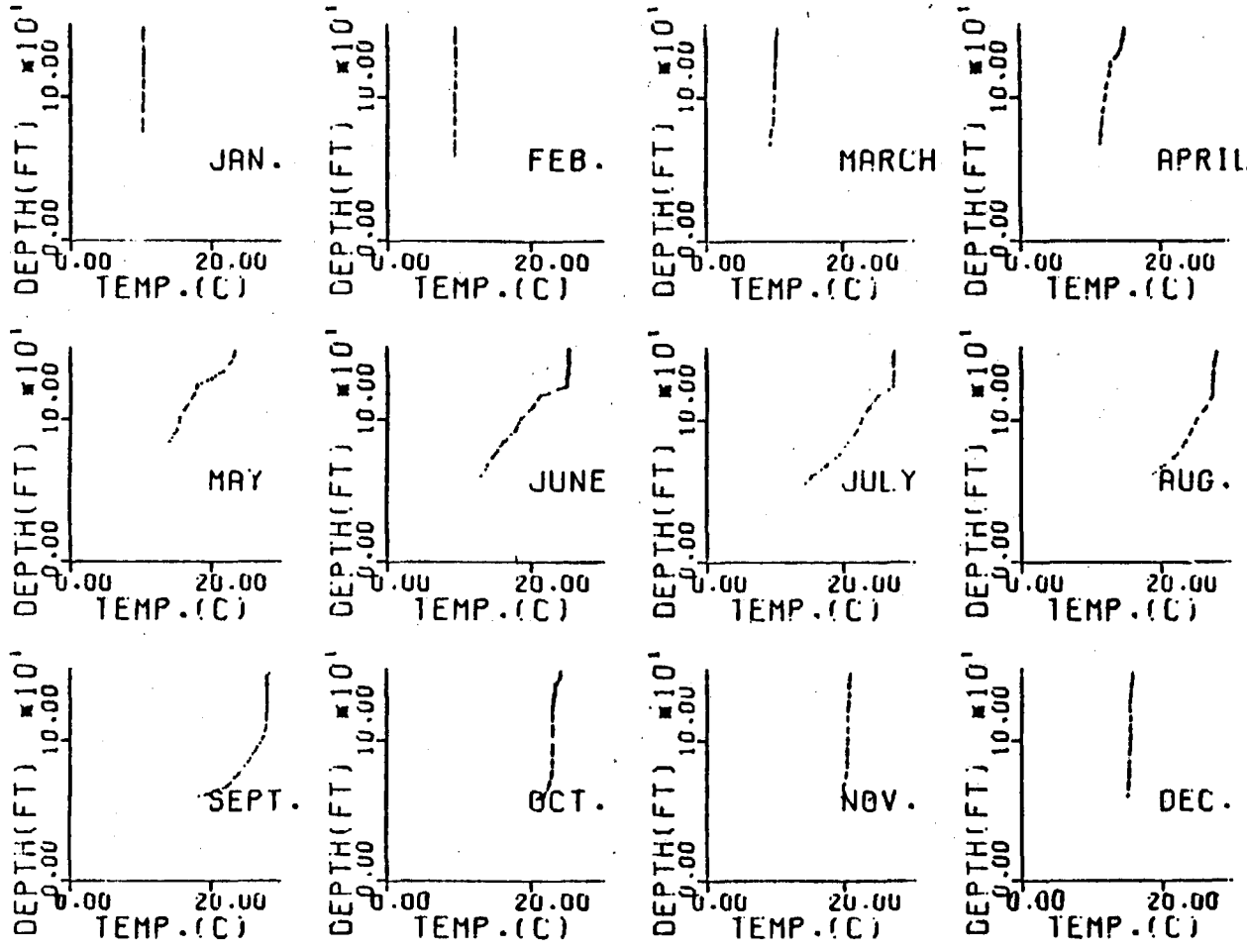

Figure B-5. Lake Keowee measured temperature profiles, 1975 - Station 500

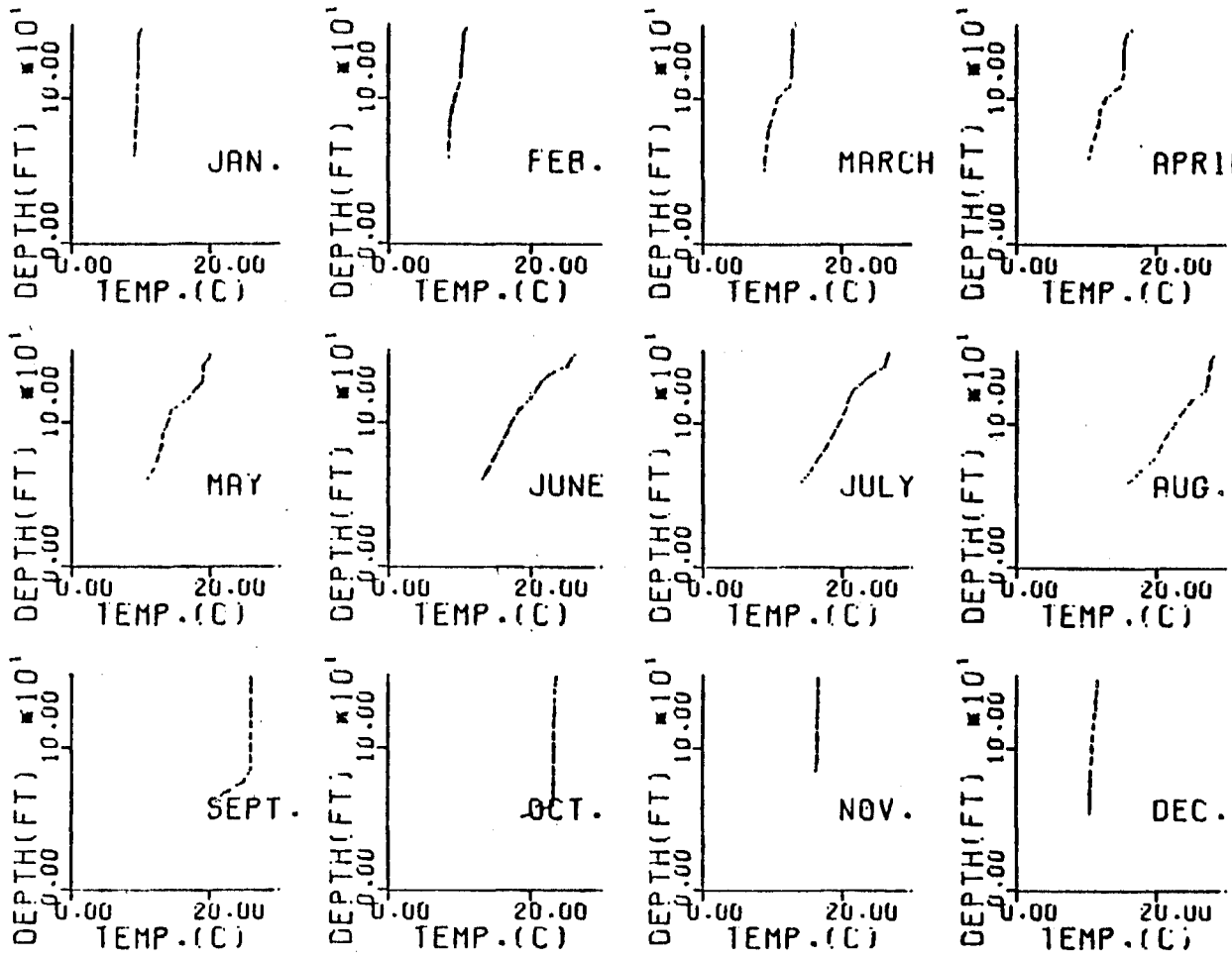

Figure B-6. Lake Keowee measured temperature profiles, 1977 - Station 500

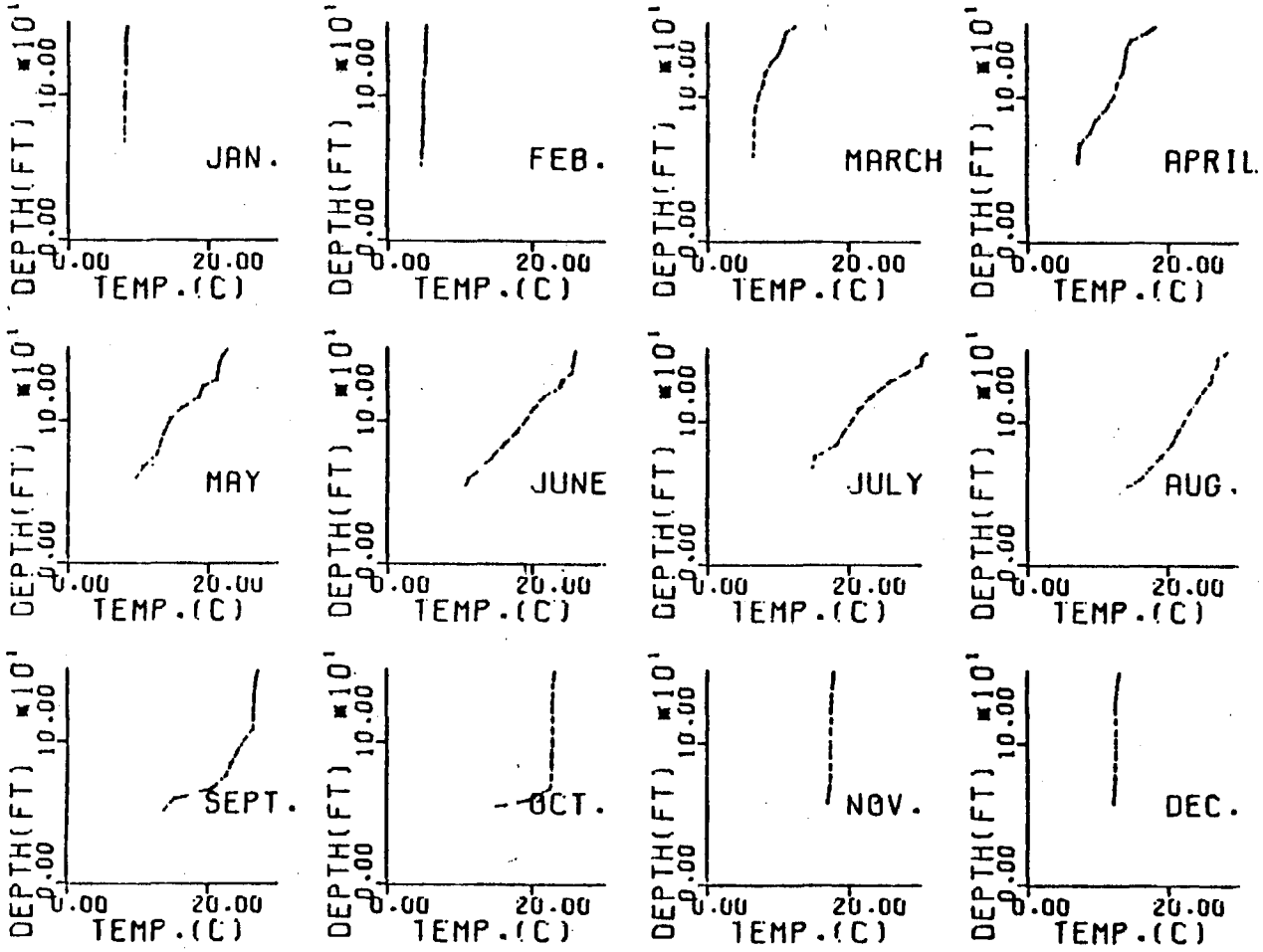

Figure B-7. Lake Keowee measured temperature profiles, 1977 - Station 500

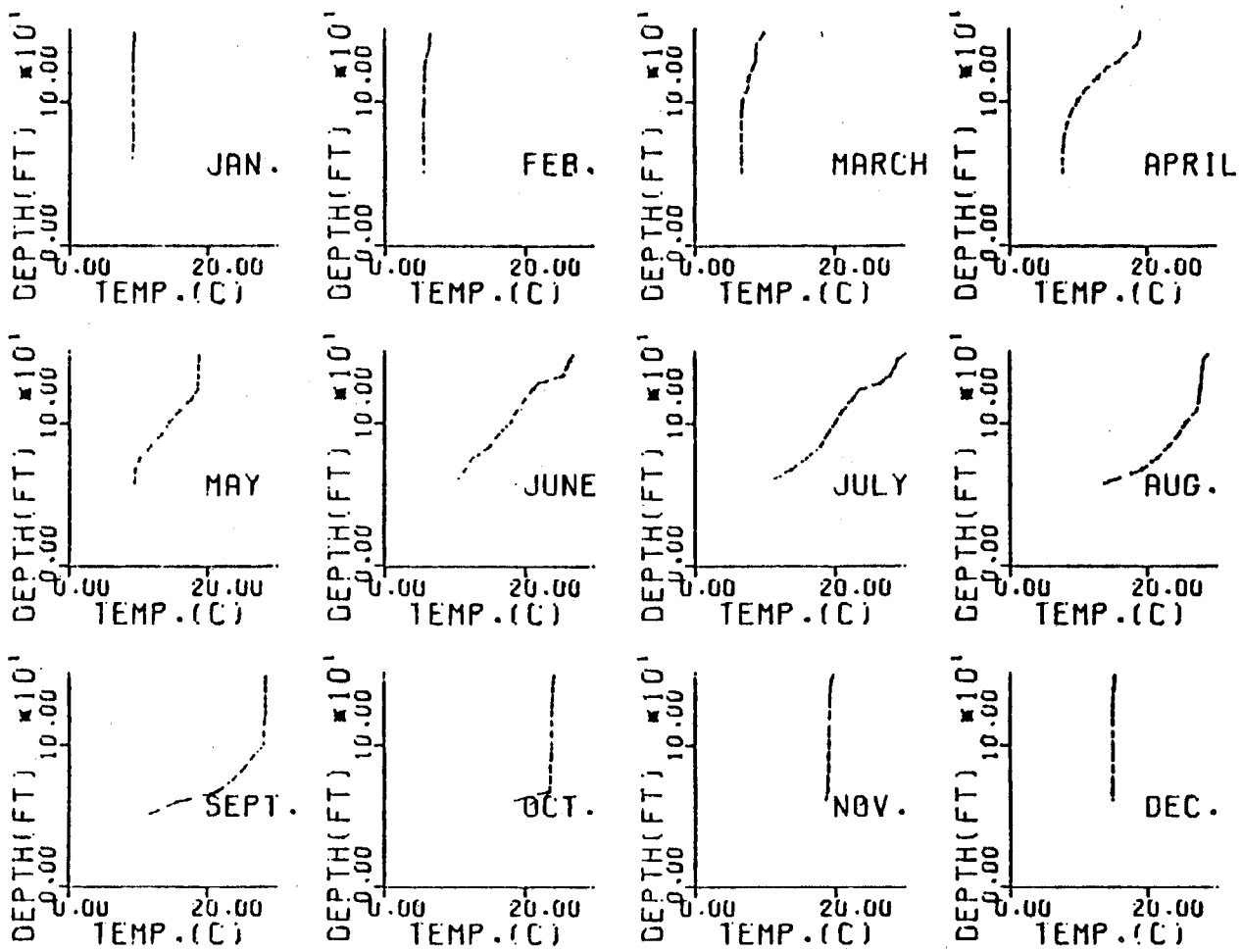

Figure B-8. Lake Keowee measured temperature profiles, 1978 - Station 500

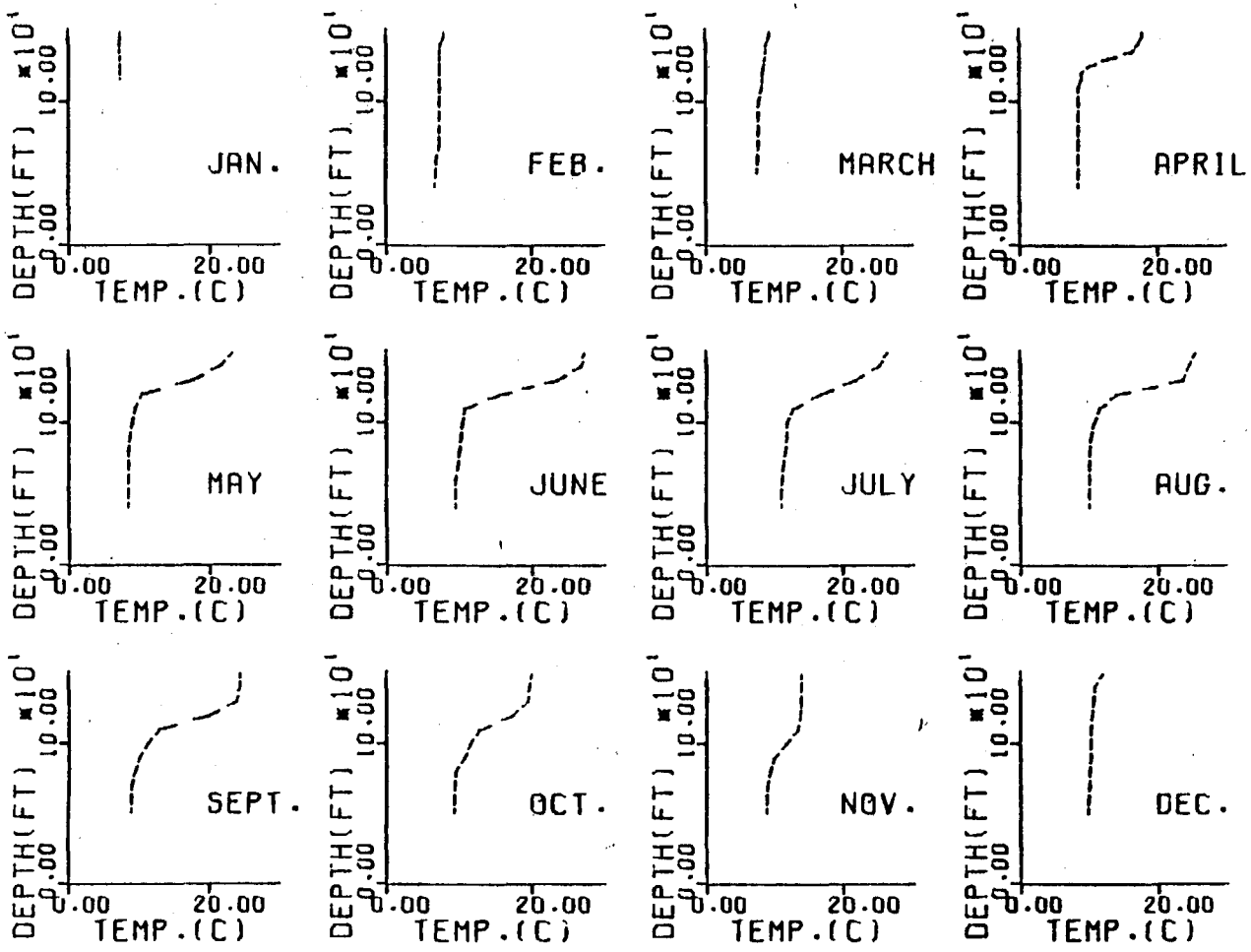

Figure B-9. Lake Keowee measured temperature profiles, 1971 - Station 501

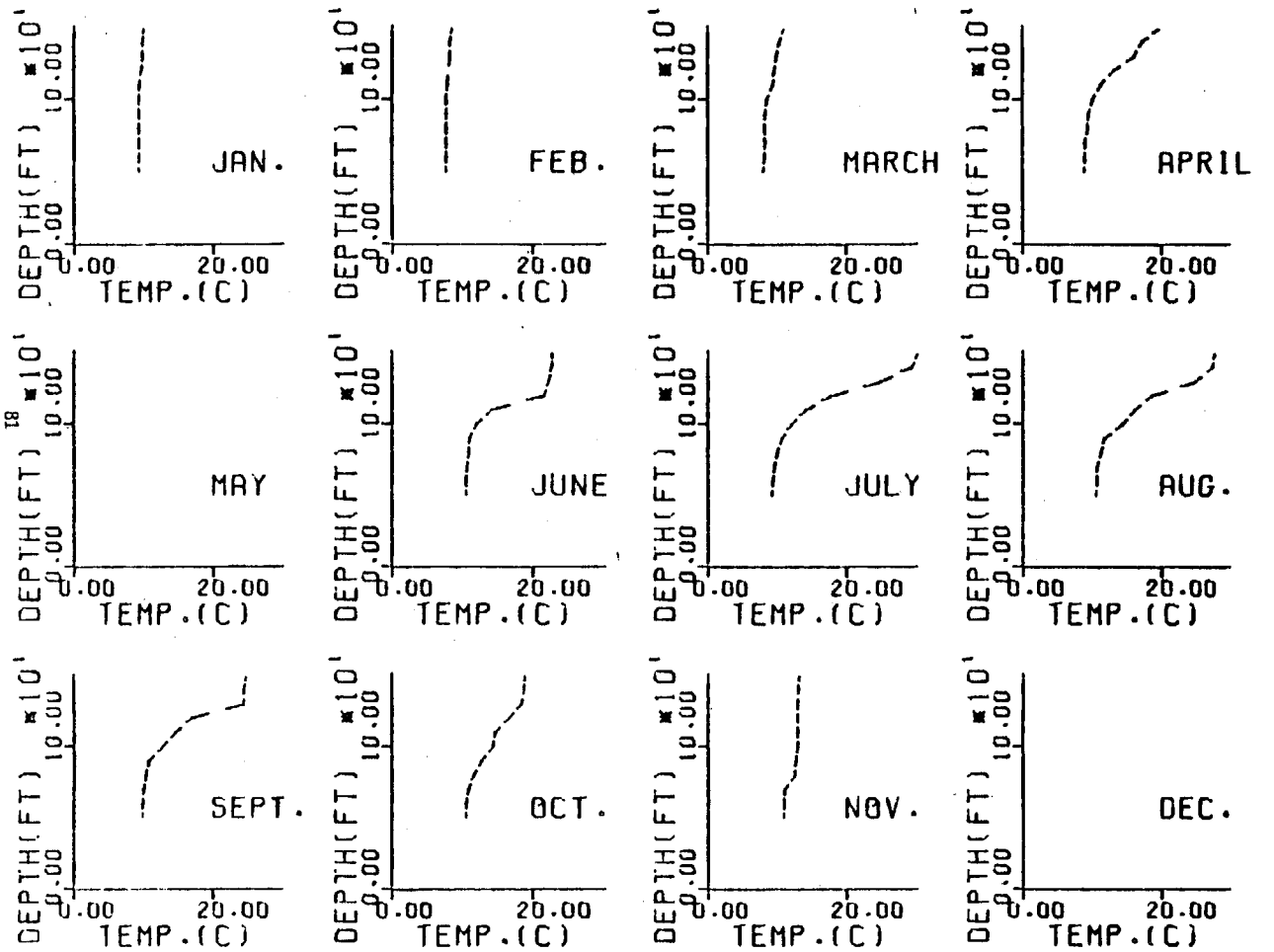

Figure B-10. Lake Keowee measured temperature profiles, 1972 - Station 501

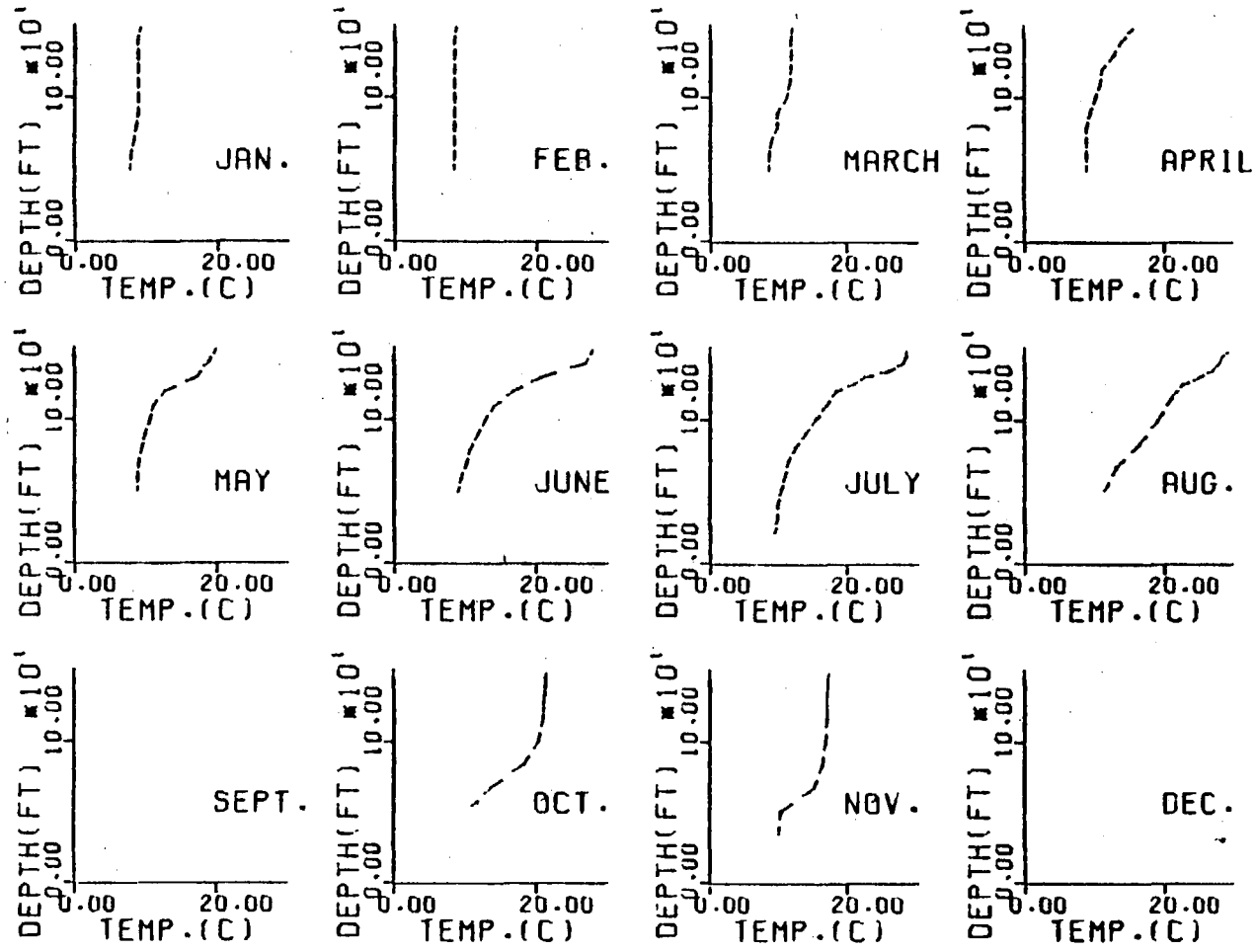

Figure B-11. Lake Keowee measured temperature profiles, 1973 - Station 501

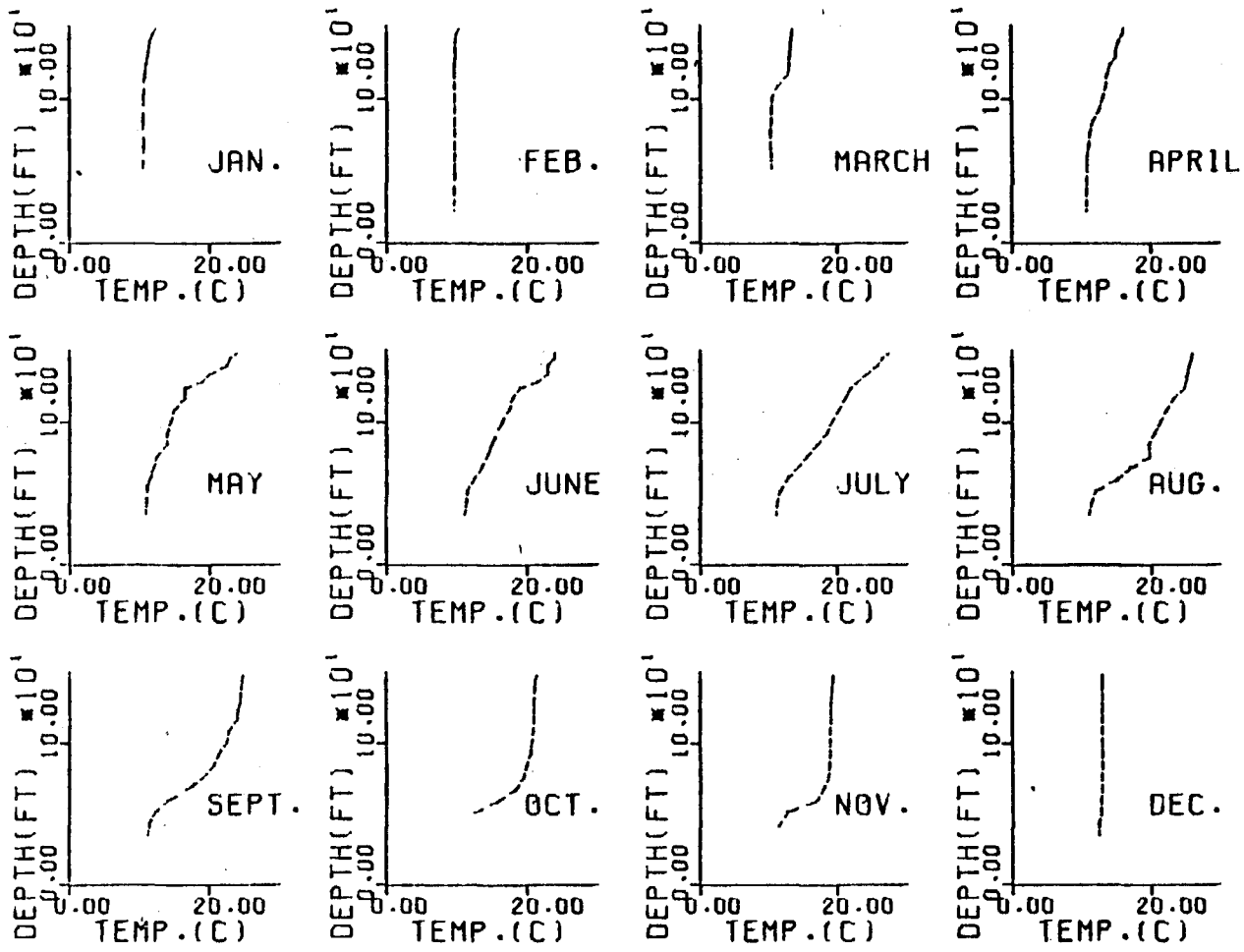

Figure B-12. Lake Keowee measured temperature profiles, 1974 - Station 501

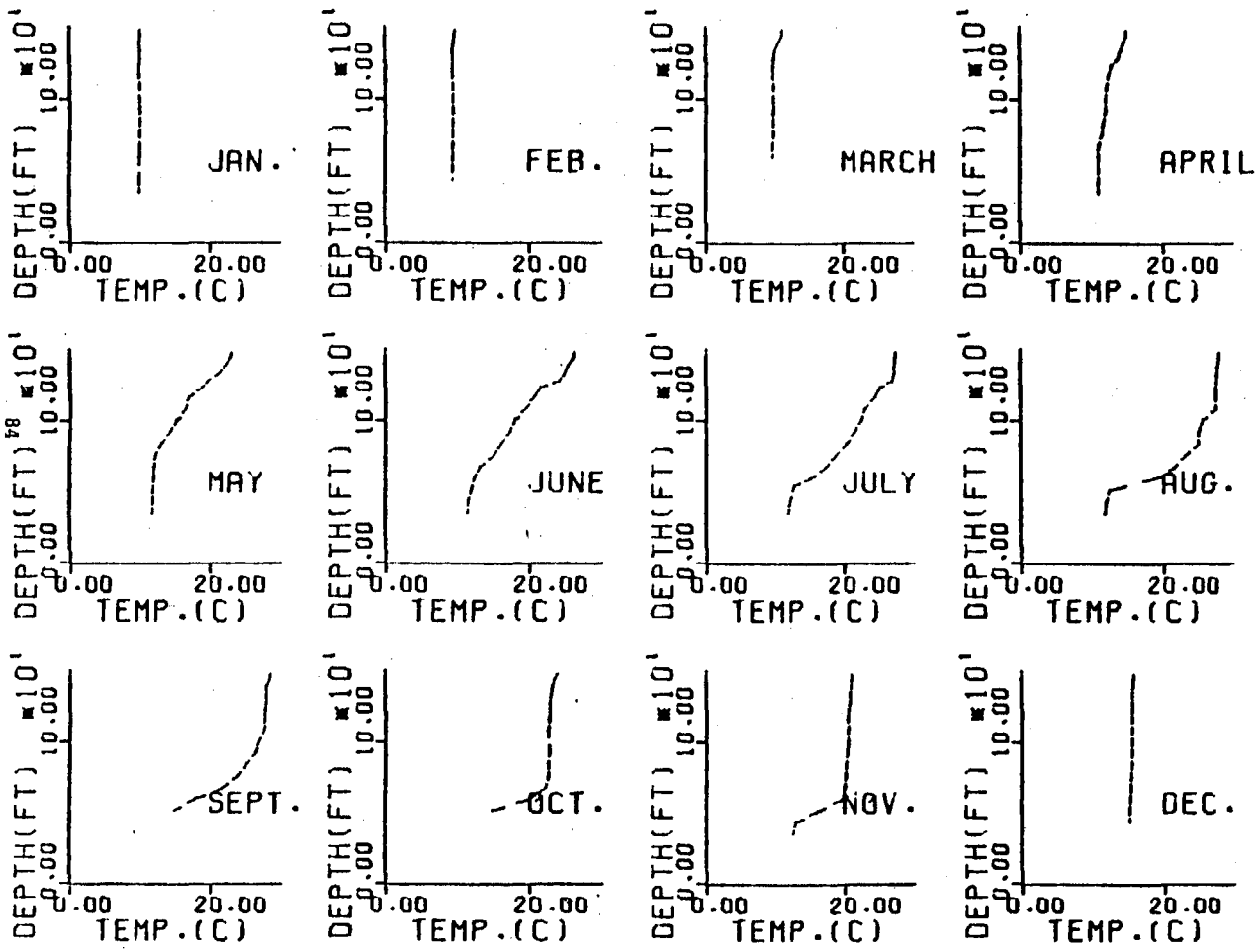

Figure B-13. Lake Keowee measured temperature profiles, 1975 - Station 501

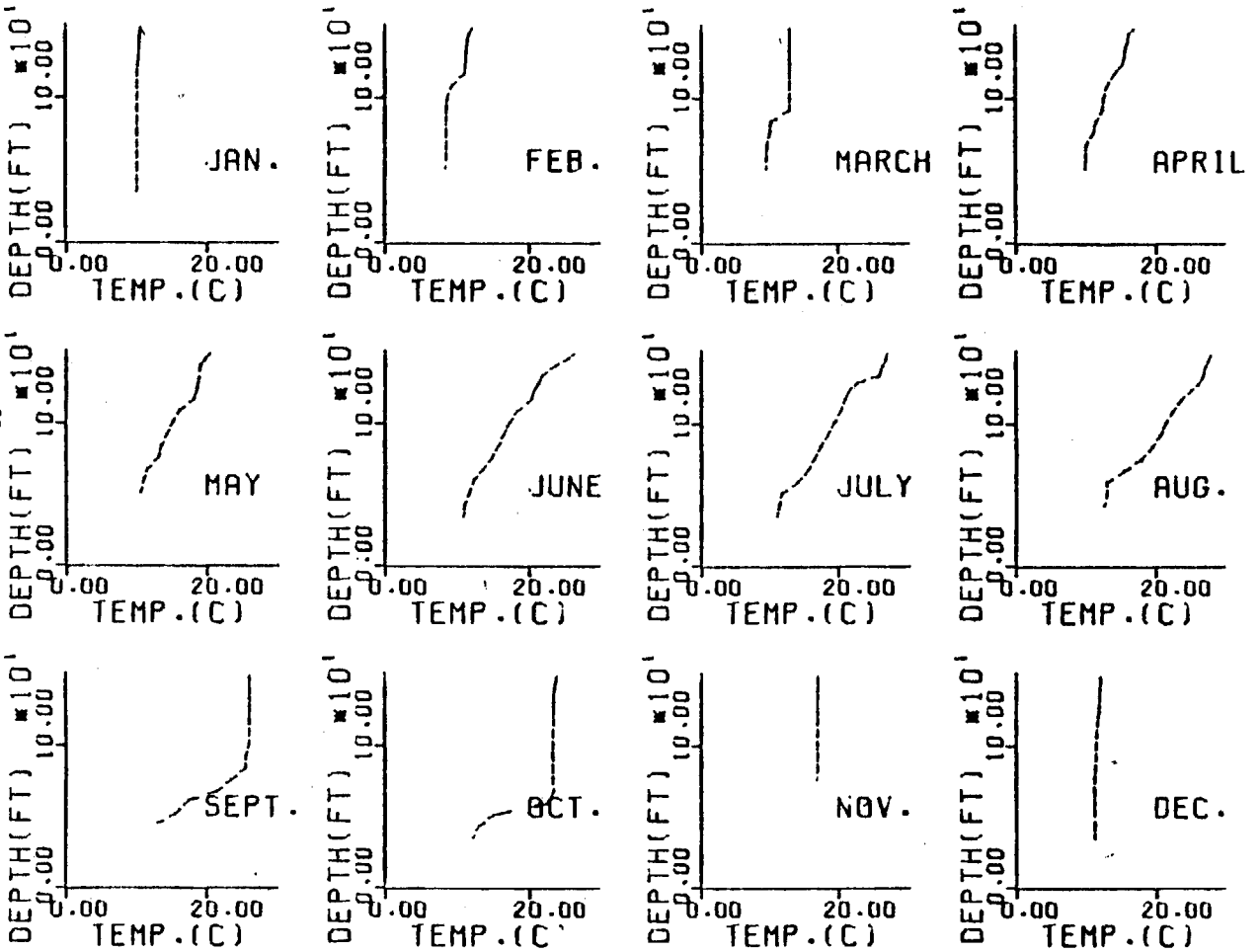

Figure B-14. Lake Keowee measured temperature profiles, 1976 - Station 501

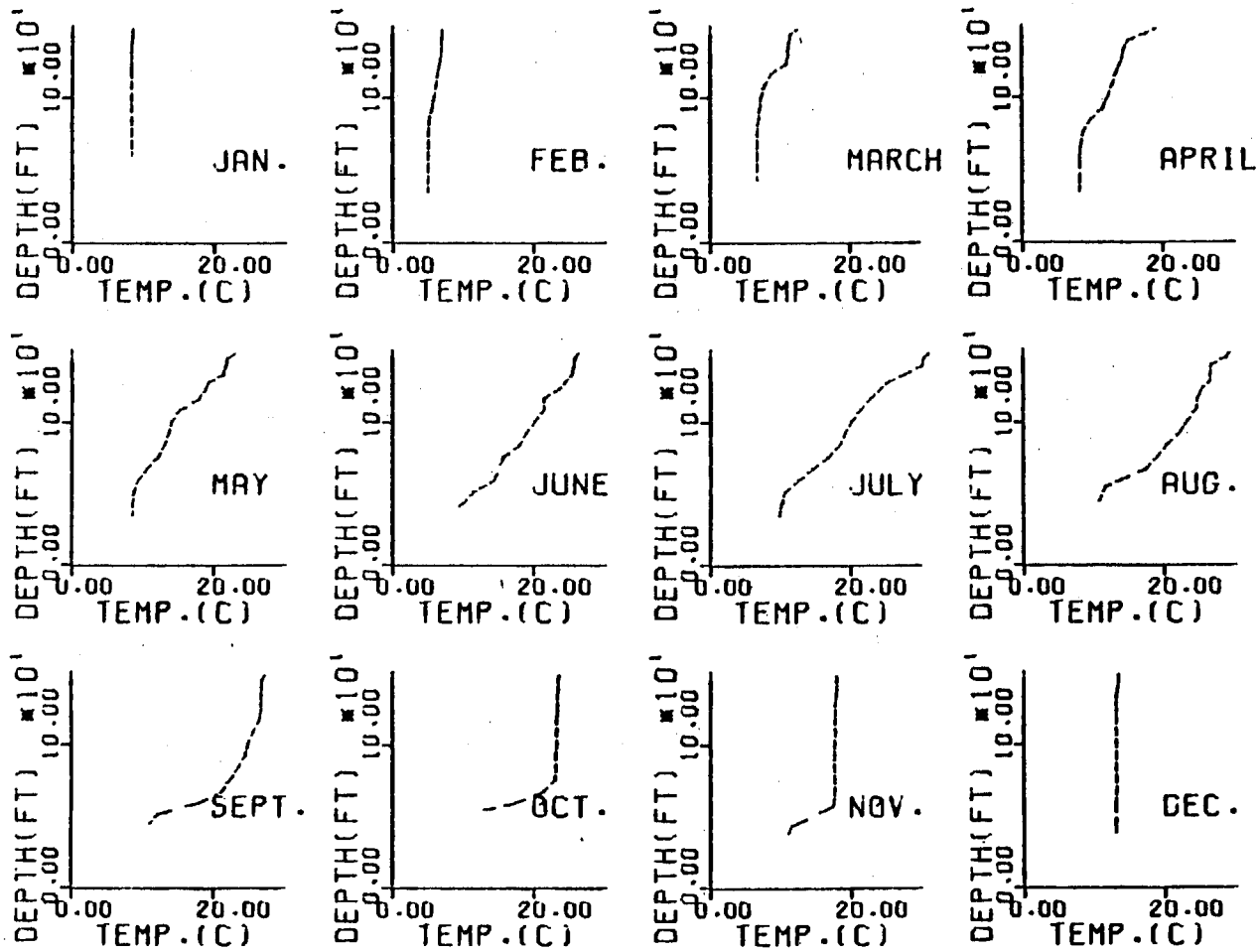

Figure B-15. Lake Keowee measured temperature profiles, 1977 - Station 501

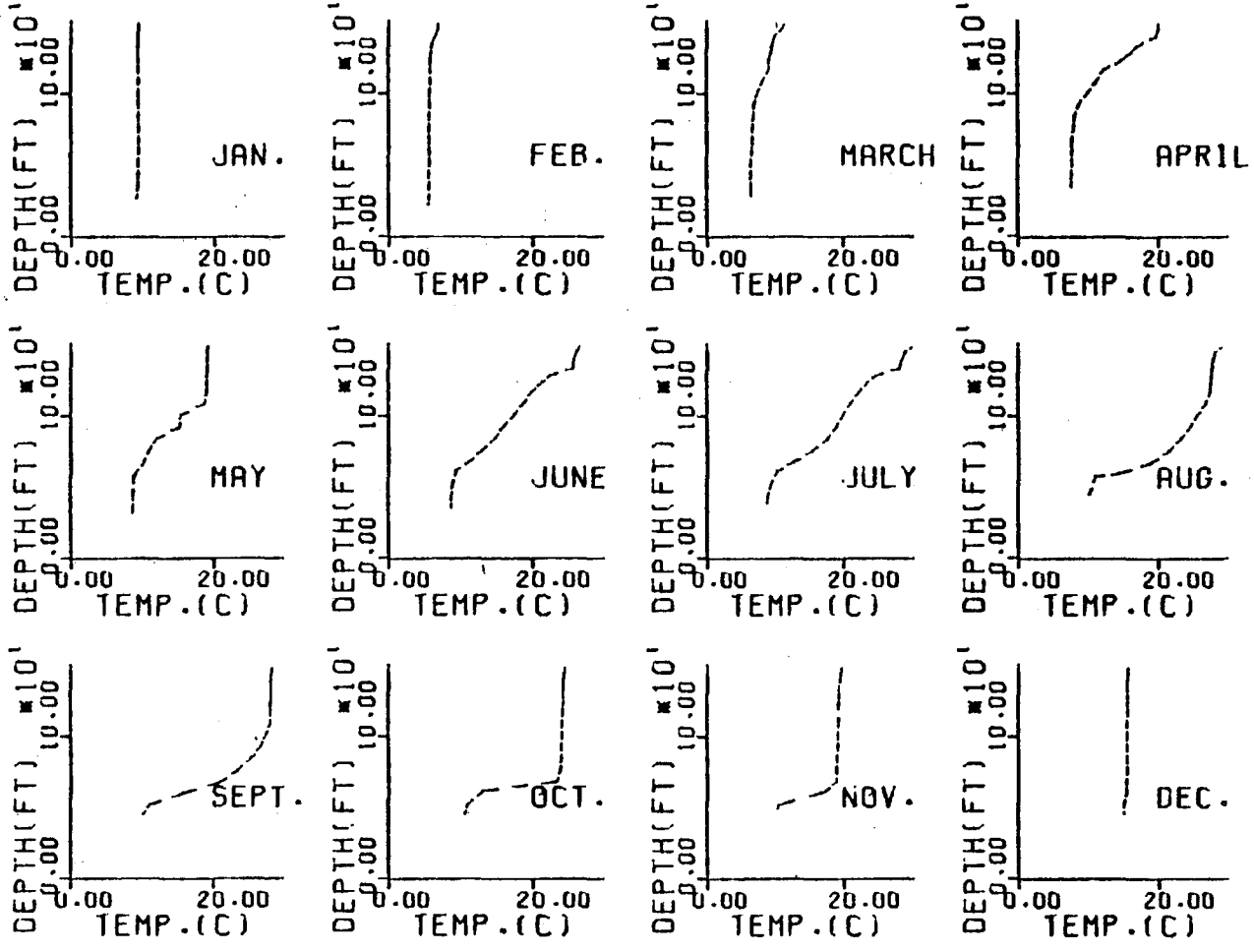

Figure B-16. Lake Keowee measured temperature profiles, 1978 - Station 501

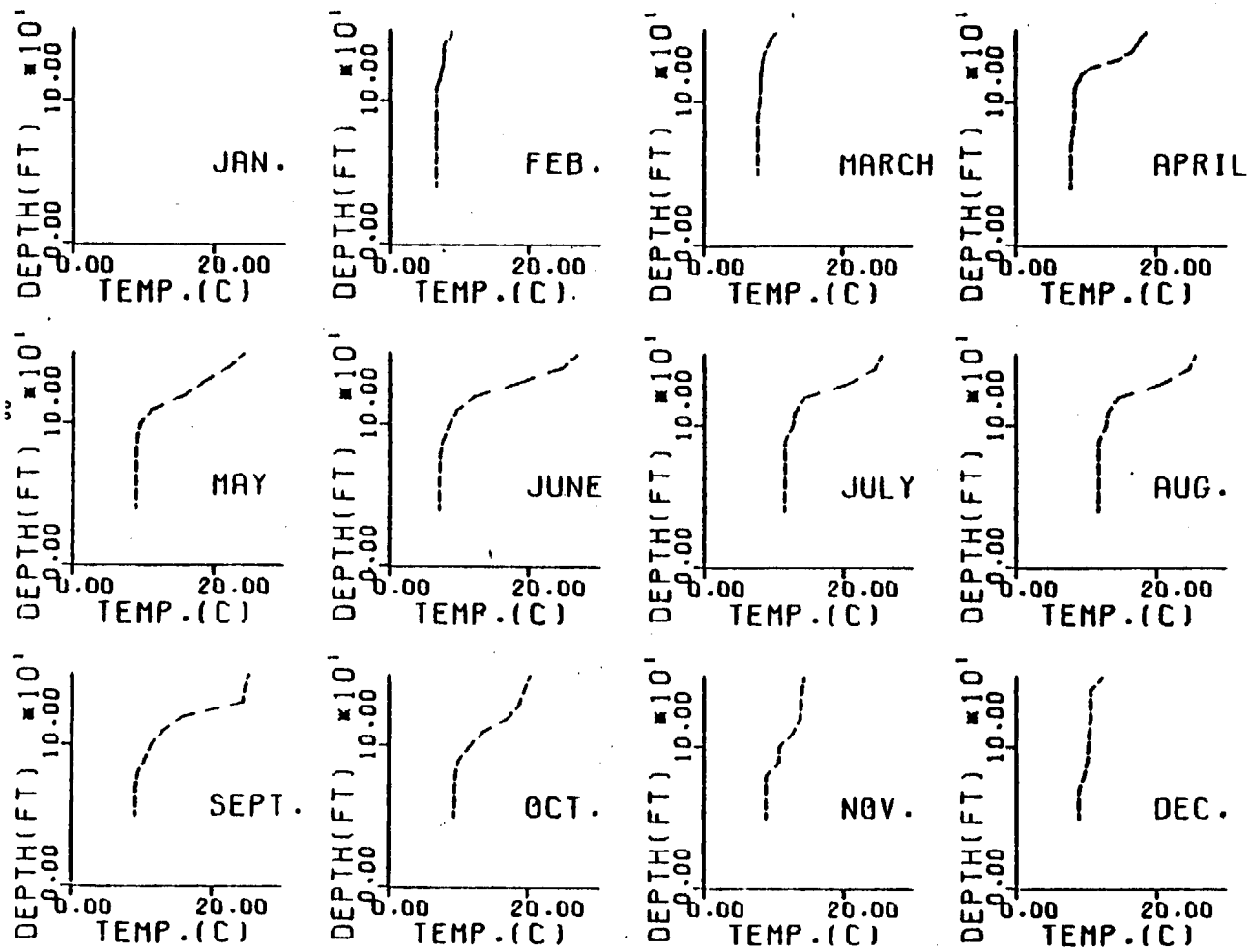

Figure 17. Measured temperature profiles. Lake Keowee, Station 502, 1971

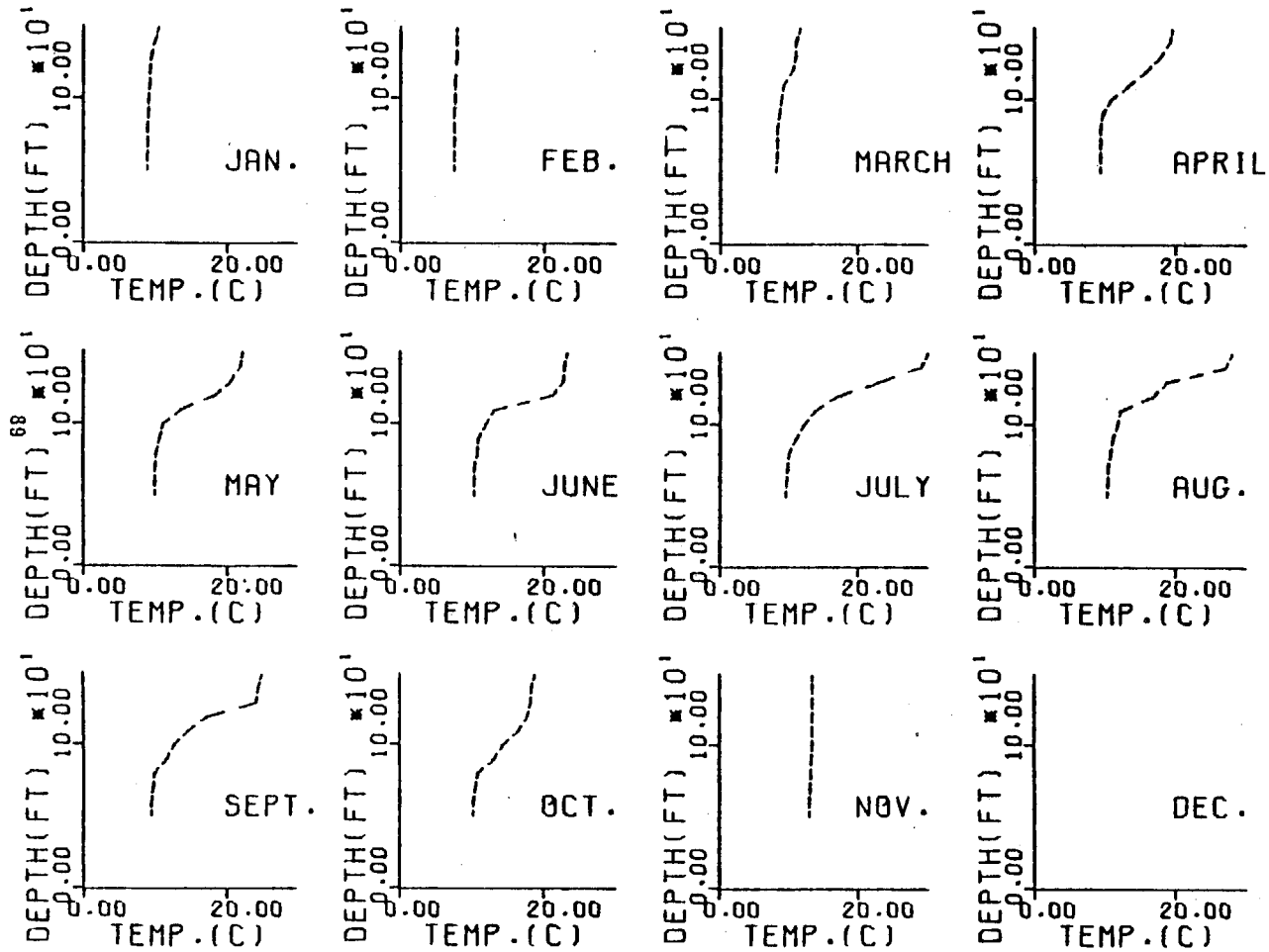

Figure B-18. Lake Keowee measured temperature profiles, 1972 - Station 502

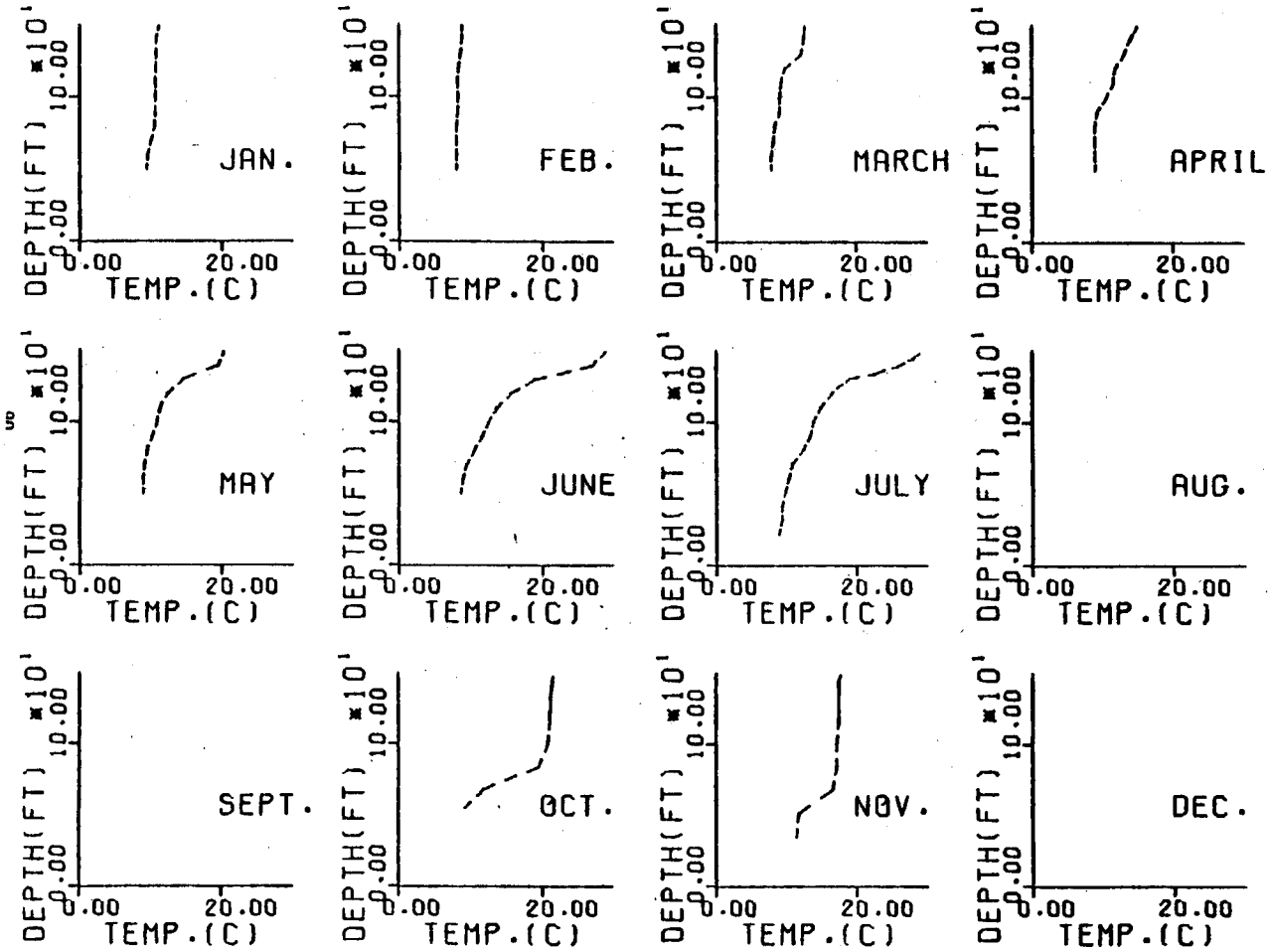

Figure B-19. Lake Keowee measured temperature profiles, 1973 - Station 502

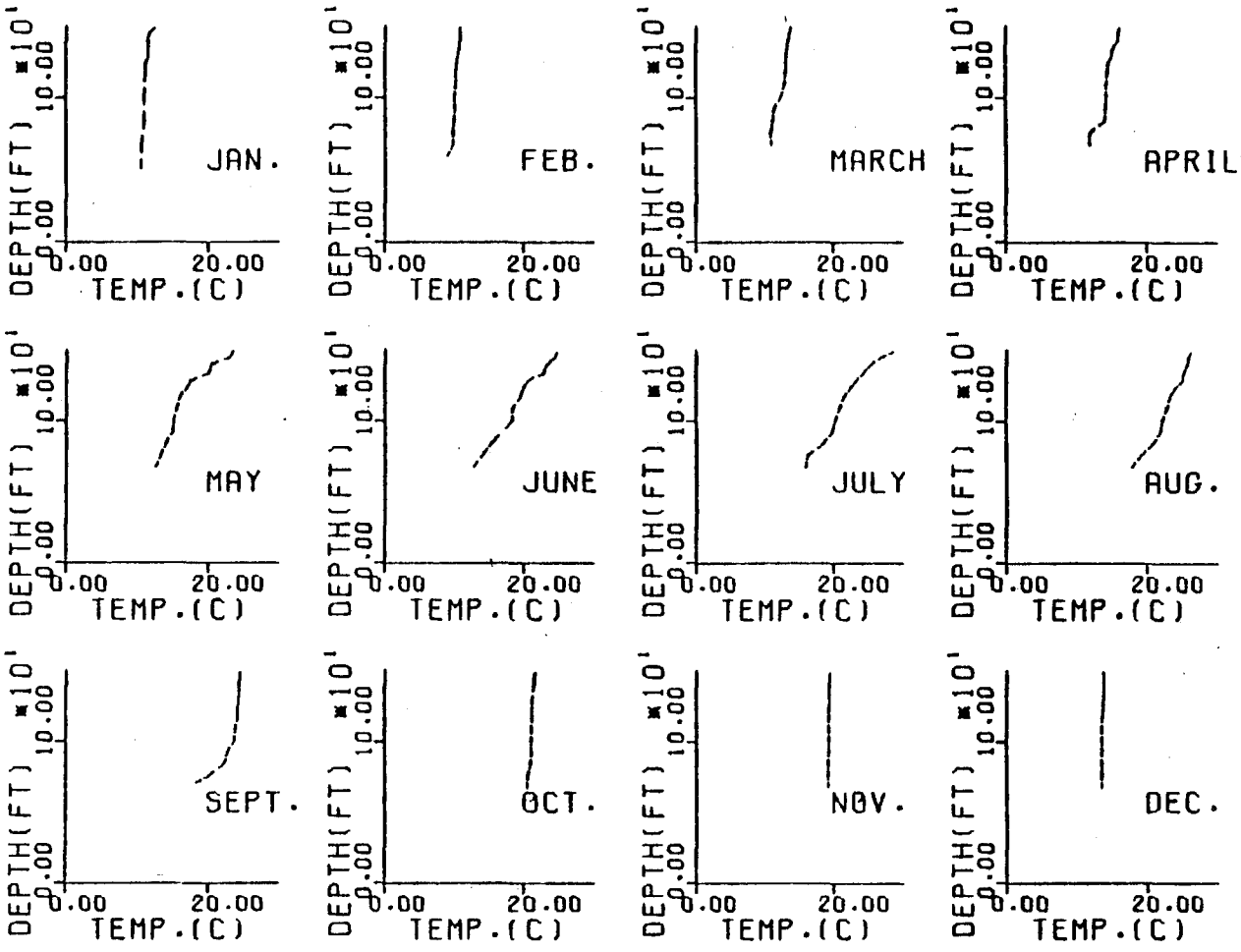

Figure B-20. Lake Keowee measured temperature profiles, 1974 - Station 502

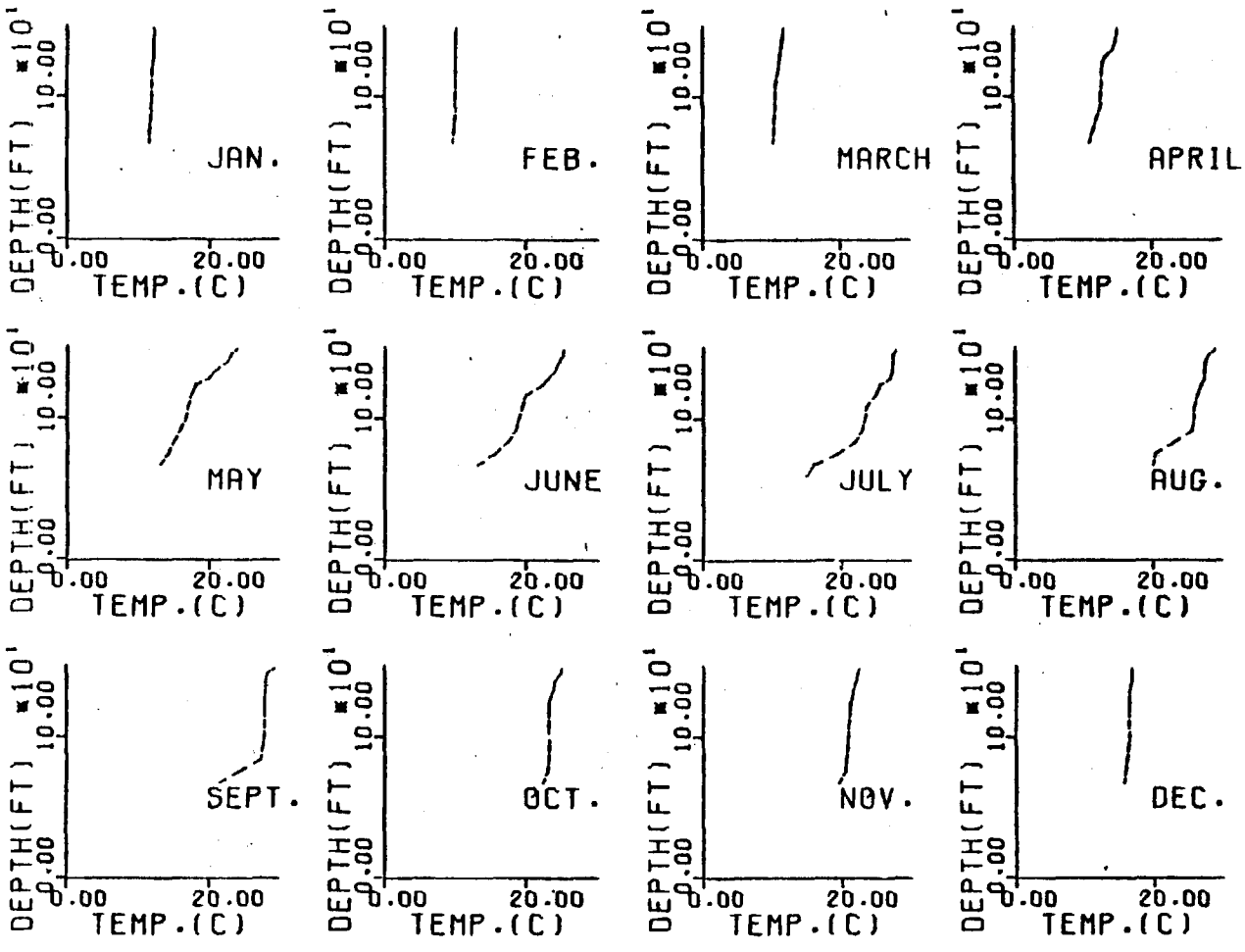

Figure B-21. Lake Keowee measured temperature profiles, 1975 - Station 502

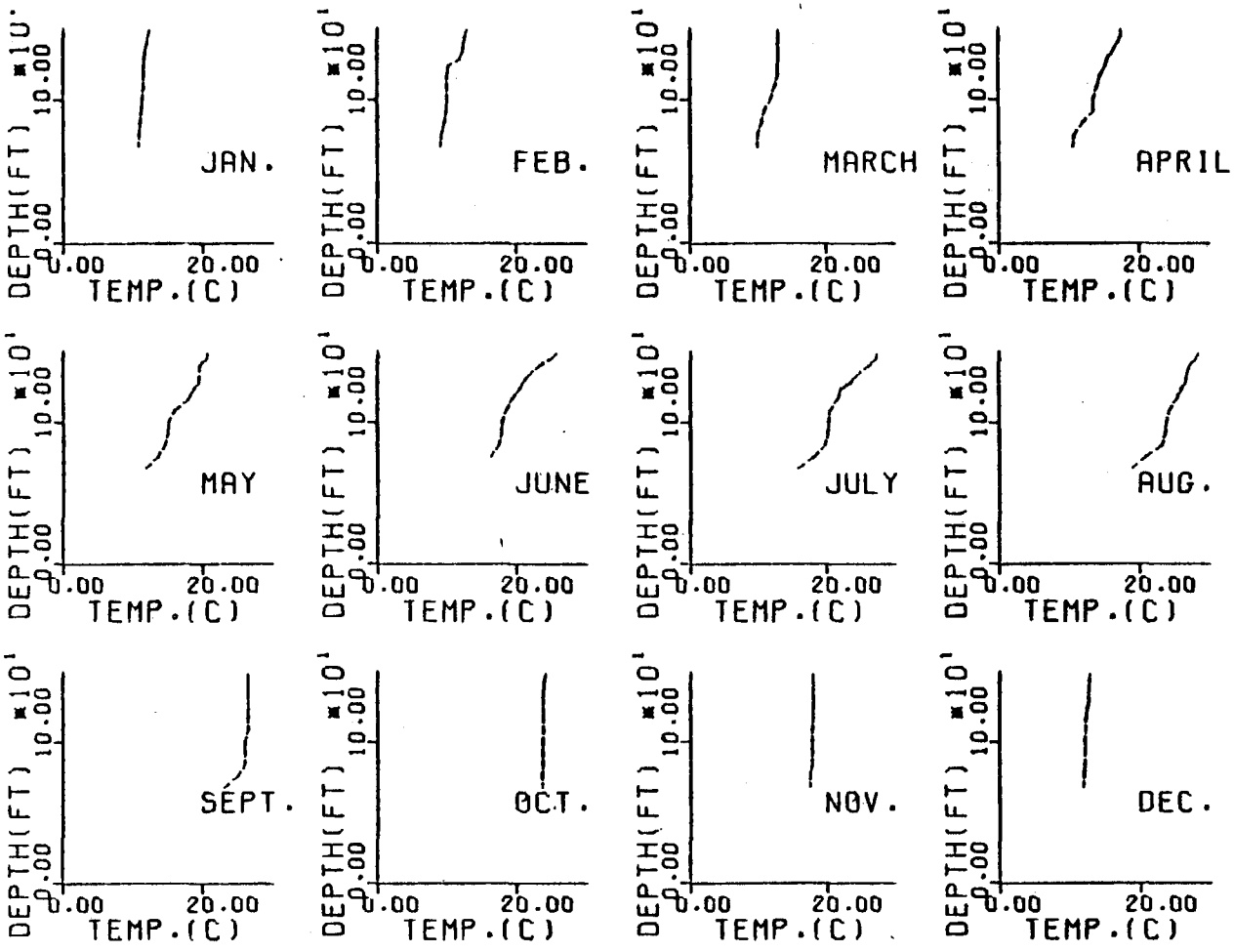

Figure B-22. Lake Keowee measured temperature profiles, 1976 - Station 502

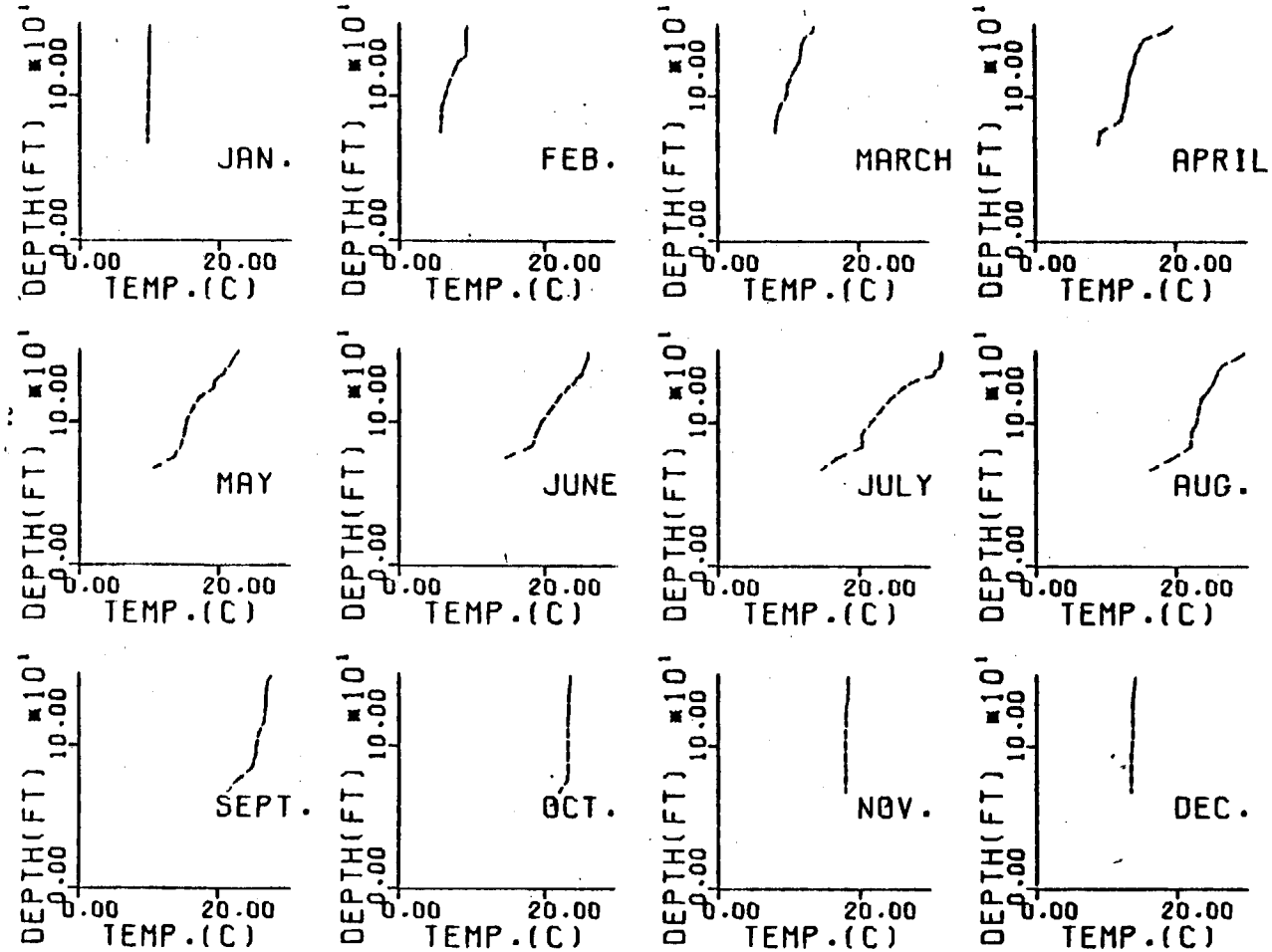

Figure B-23. Lake Keowee measured temperature profiles, 1977 - Station 502

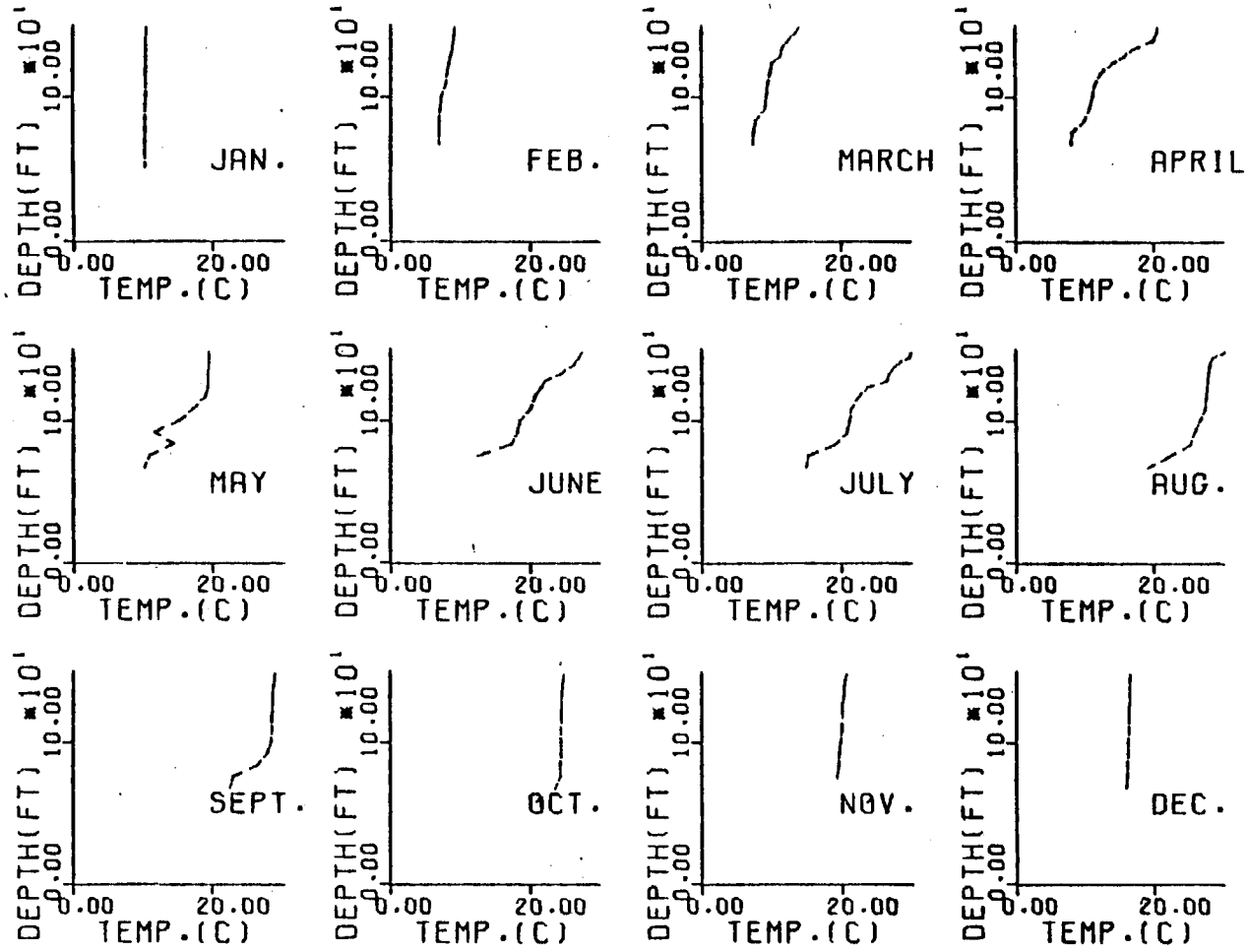

Figure B-24. Lake Keowee measured temperature profiles, 1978 - Station 502

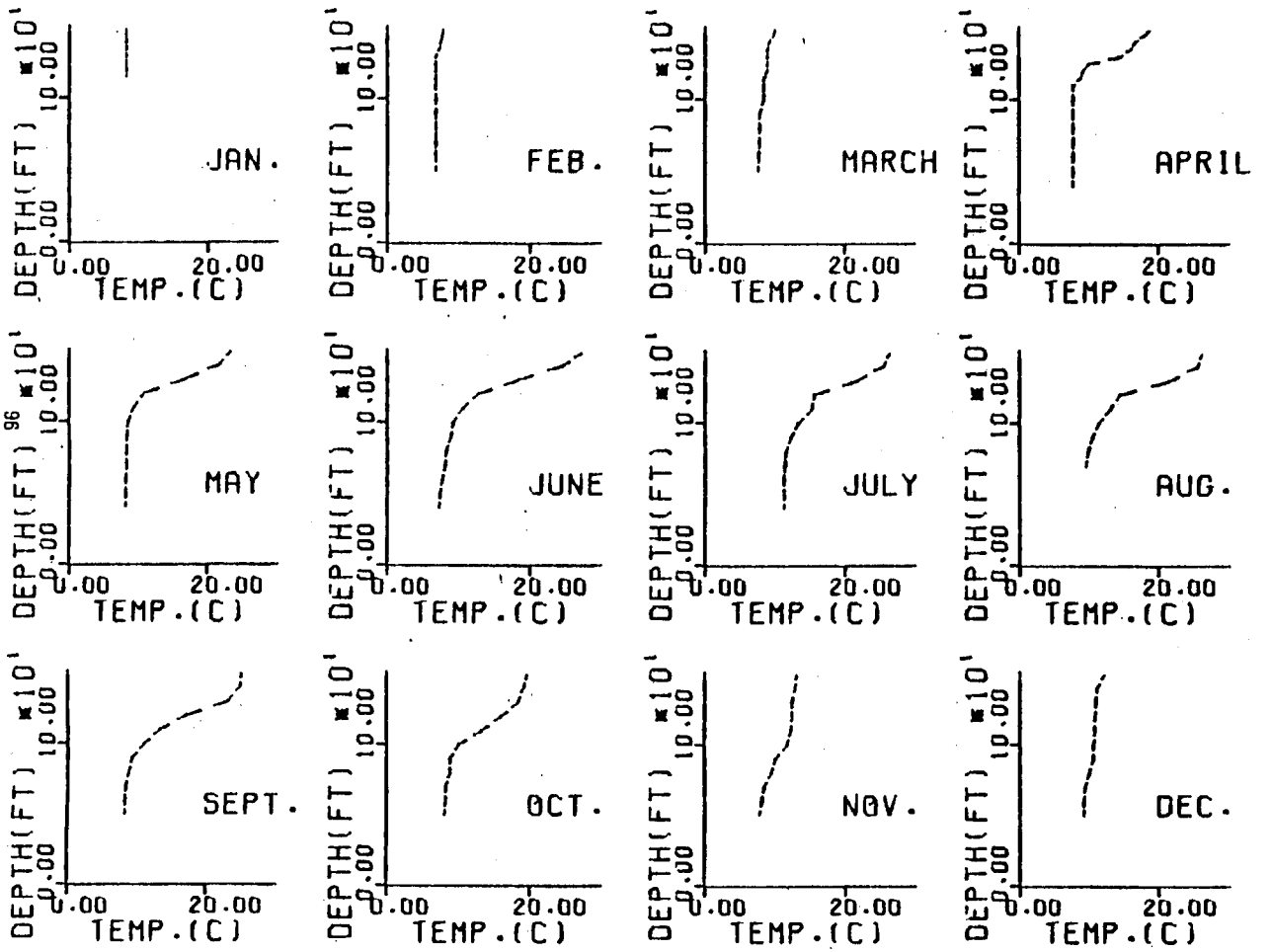

Figure B-25. Lake Keowee measured temperature profiles, 1971 - Station 503

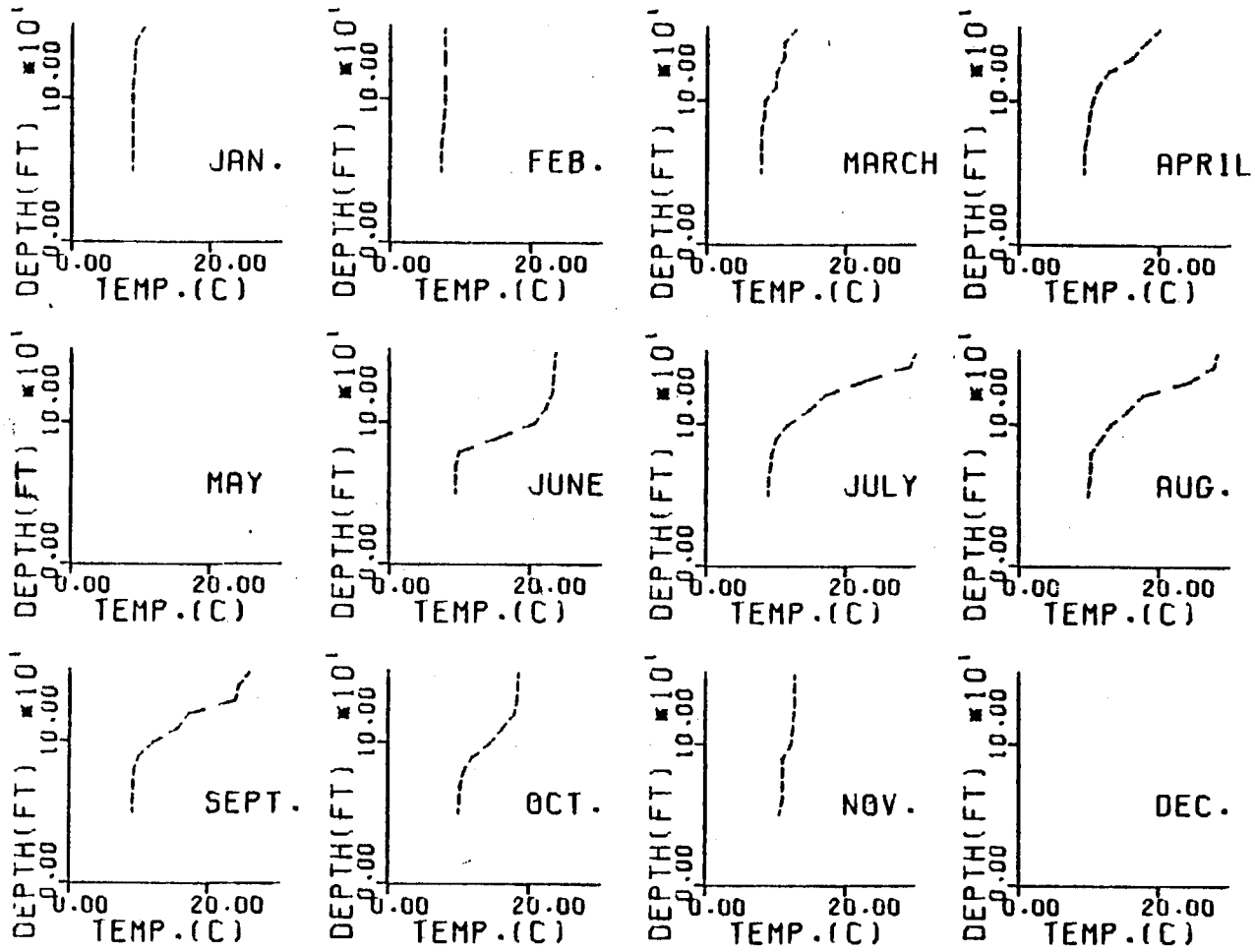

Figure B-26. Lake Keowee measured temperature profiles, 1972 - Station 503

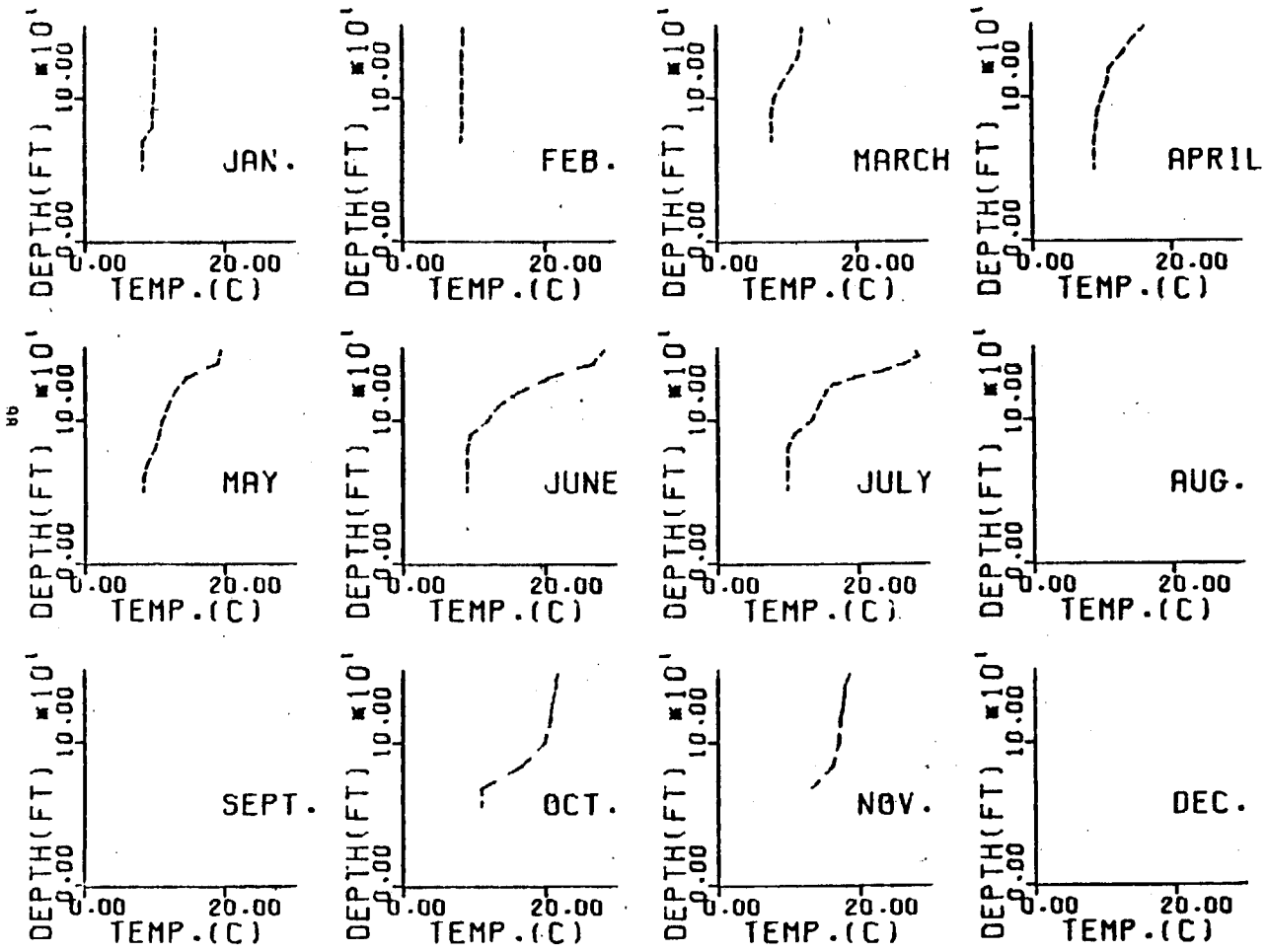

Figure B-27. Lake Keowee measured temperature profiles, 1973 - Station 503

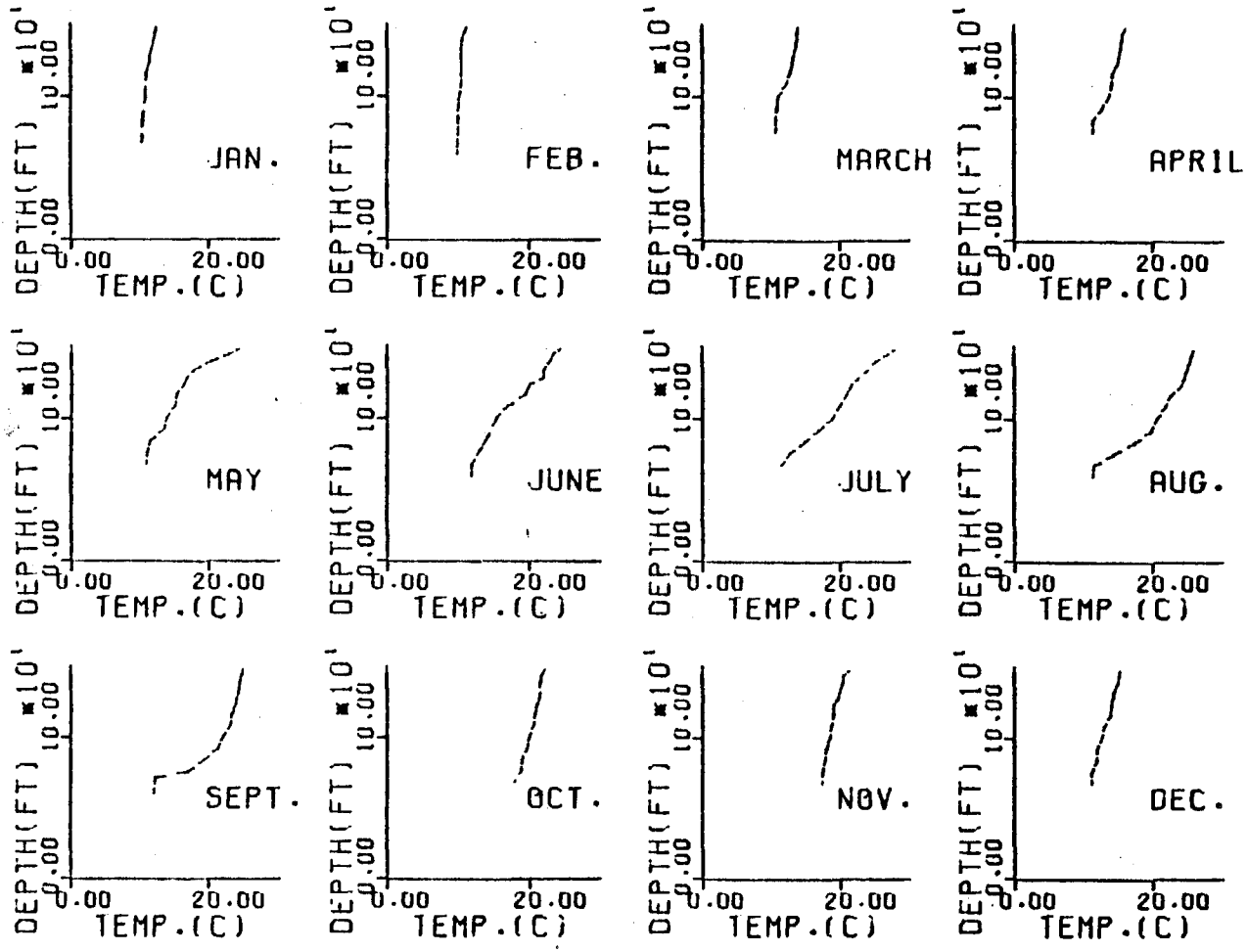

Figure B-28. Lake Keowee measured temperature profiles, 1974 - Station 503

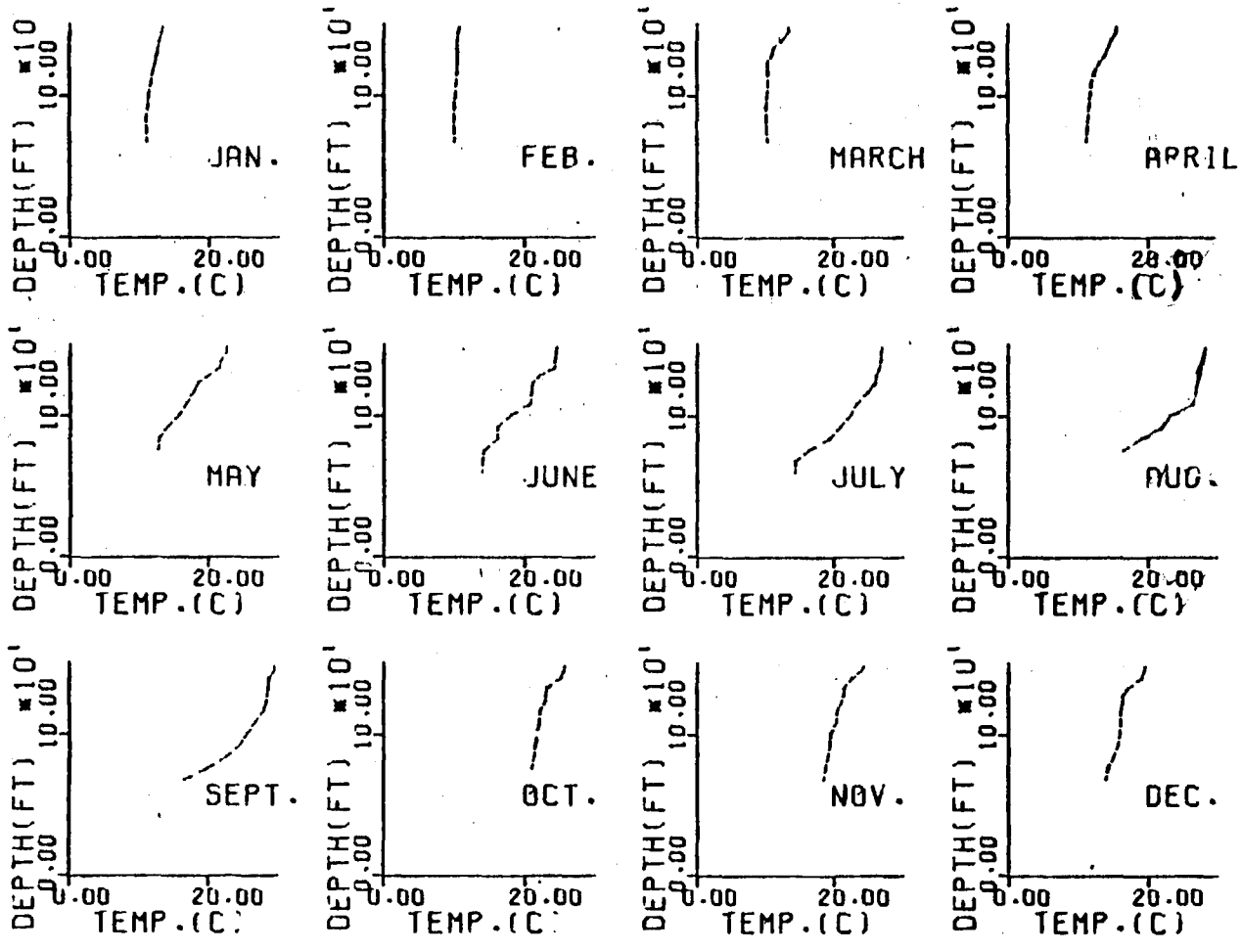

Figure B-29. Lake Keowee measured temperature profiles, 1975 - Station 503

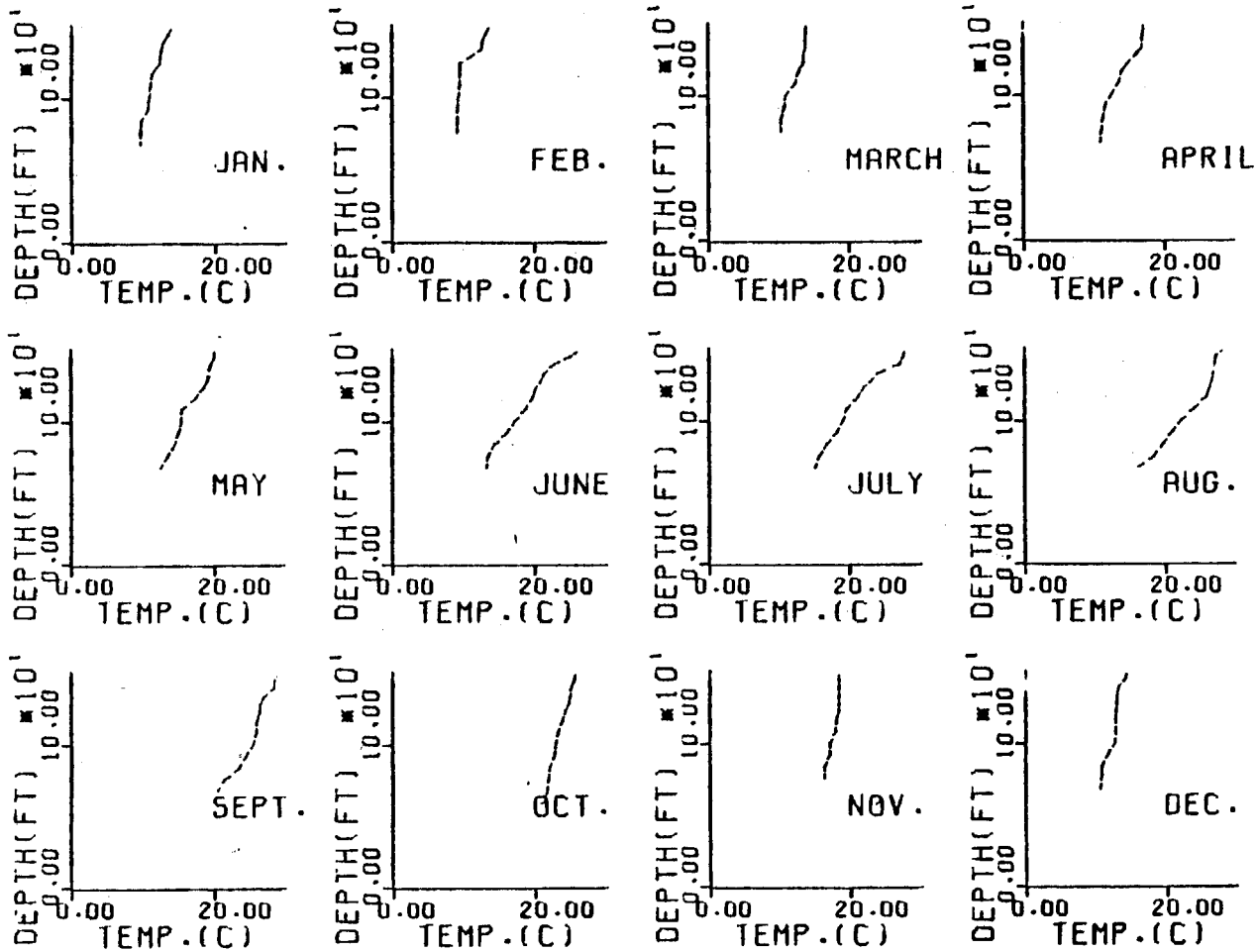

Figure B-30. Lake Keowee measured temperature profiles, 1976 - Station 503

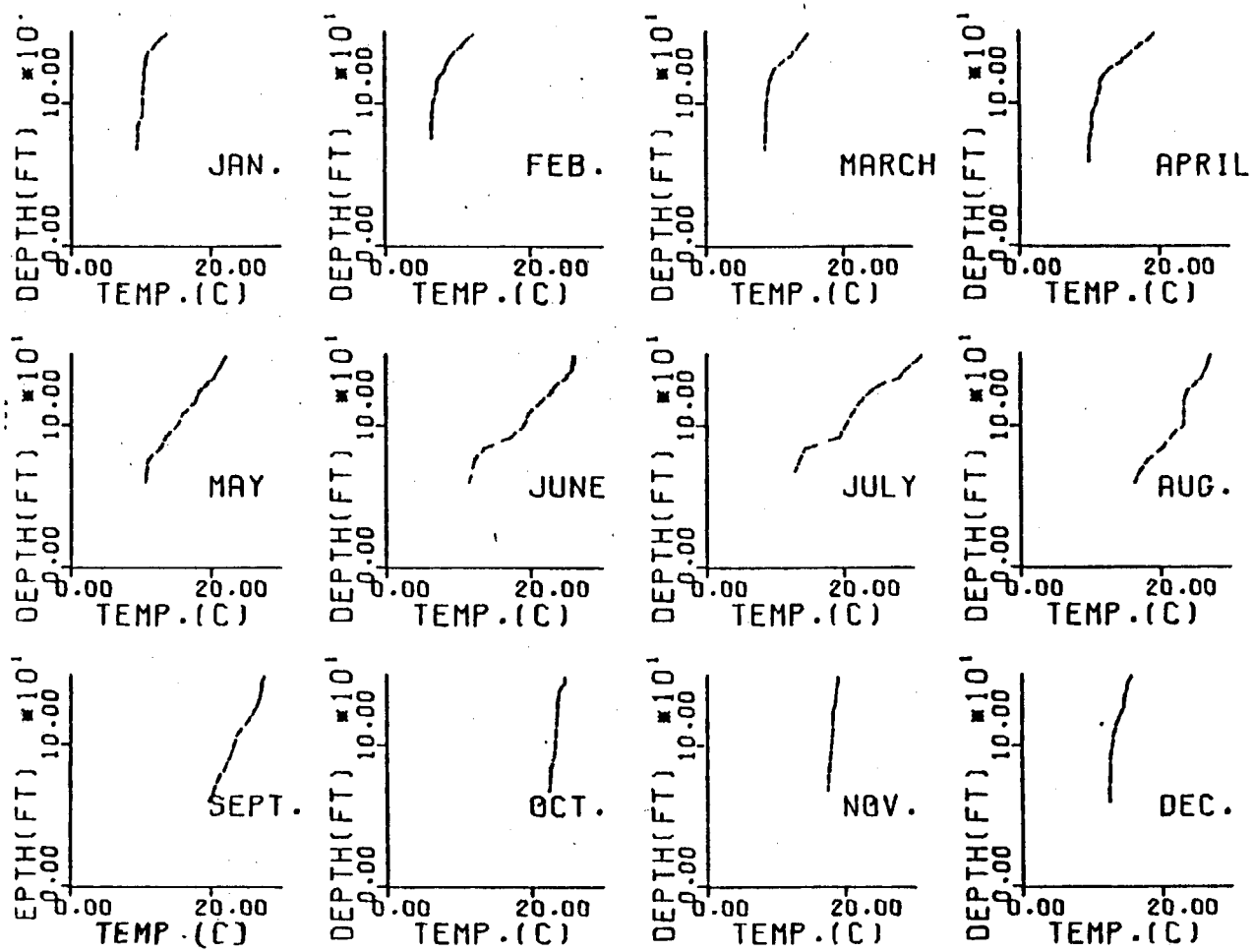

Figure B-31. Lake Keowee measured temperature profiles, 1977 - Station 503

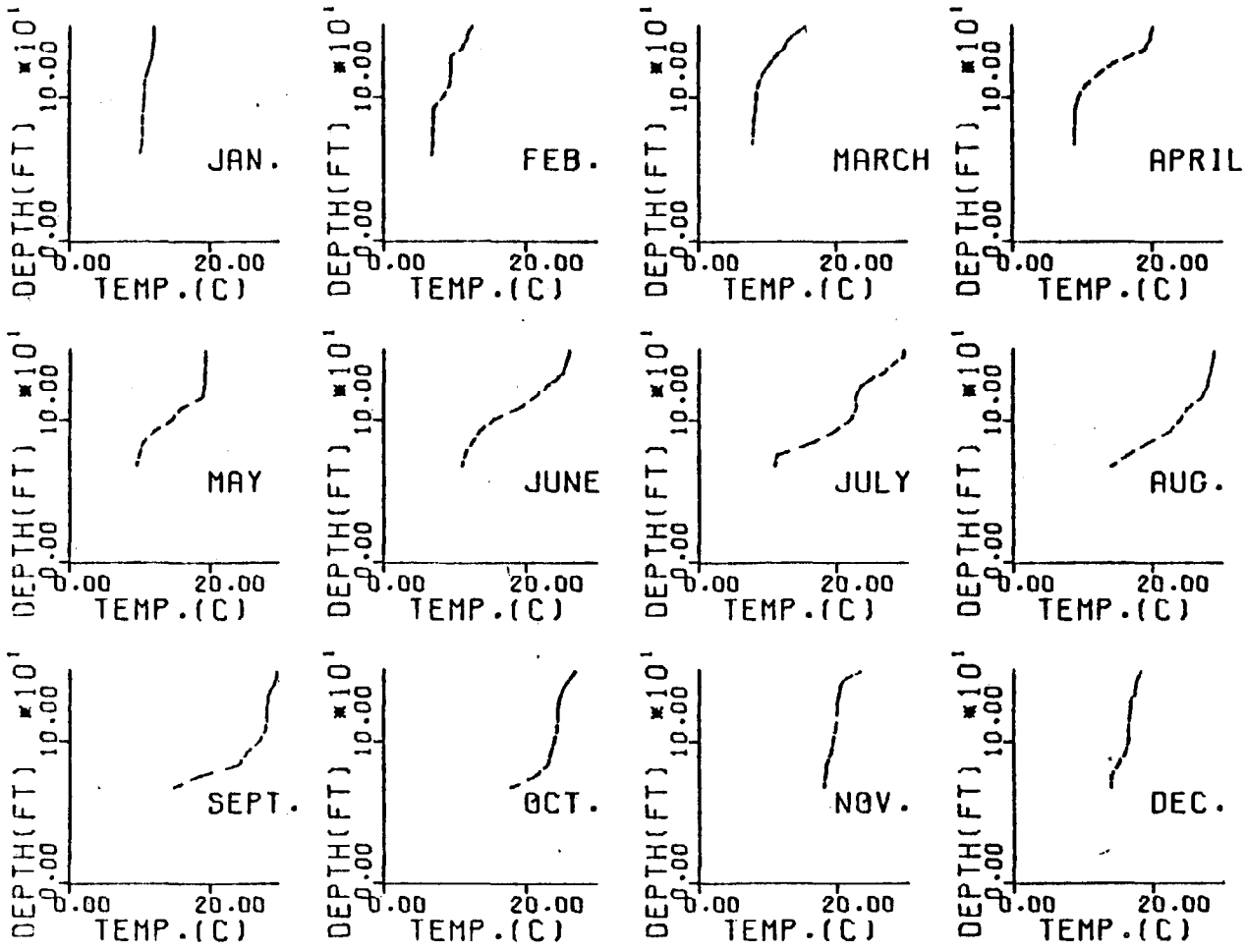

Figure B-32. Lake Keowee measured temperature profiles, 1978 - Station 503

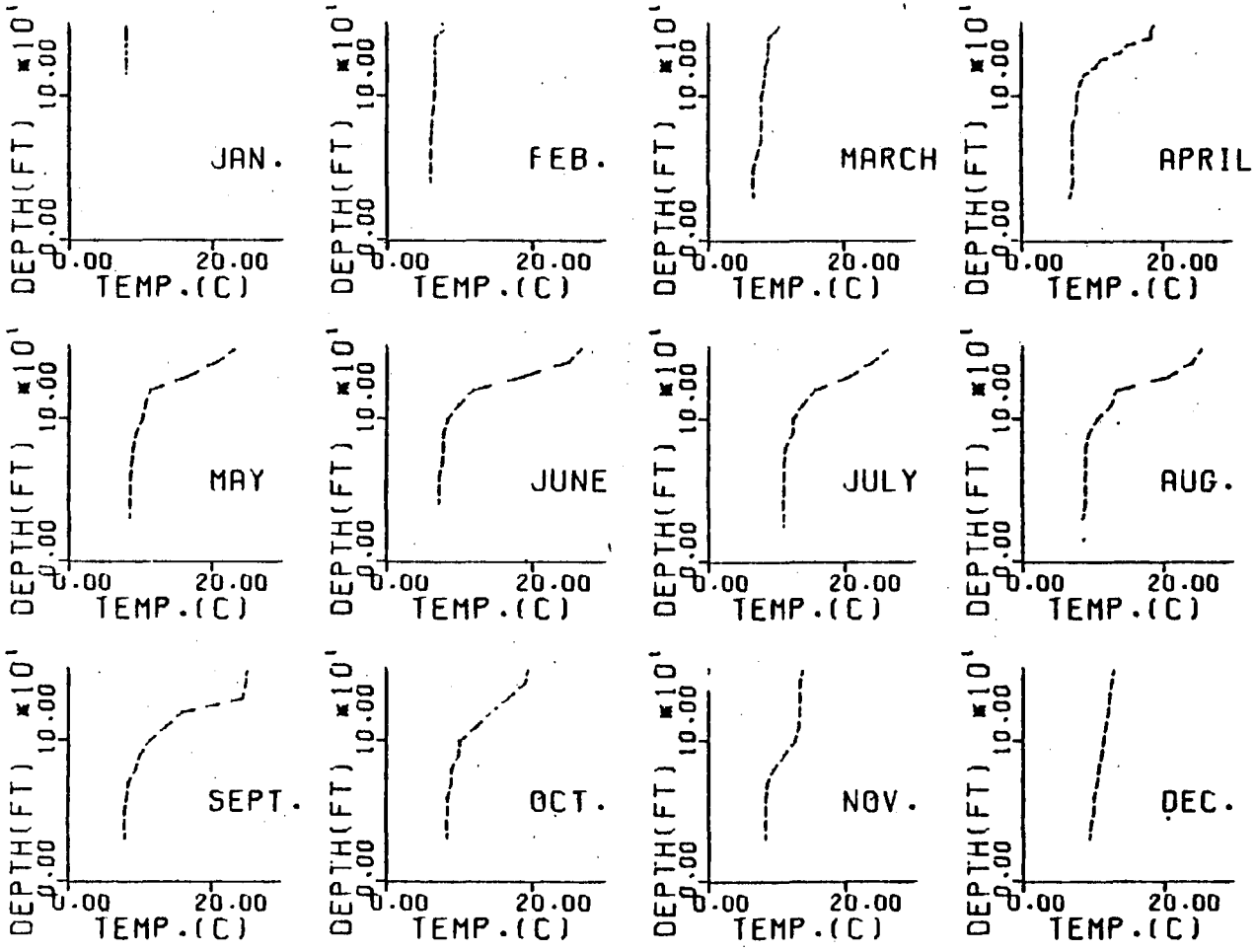

Figure B-33. Lake Koewee measured temperature profiles, 1971 - Station 504

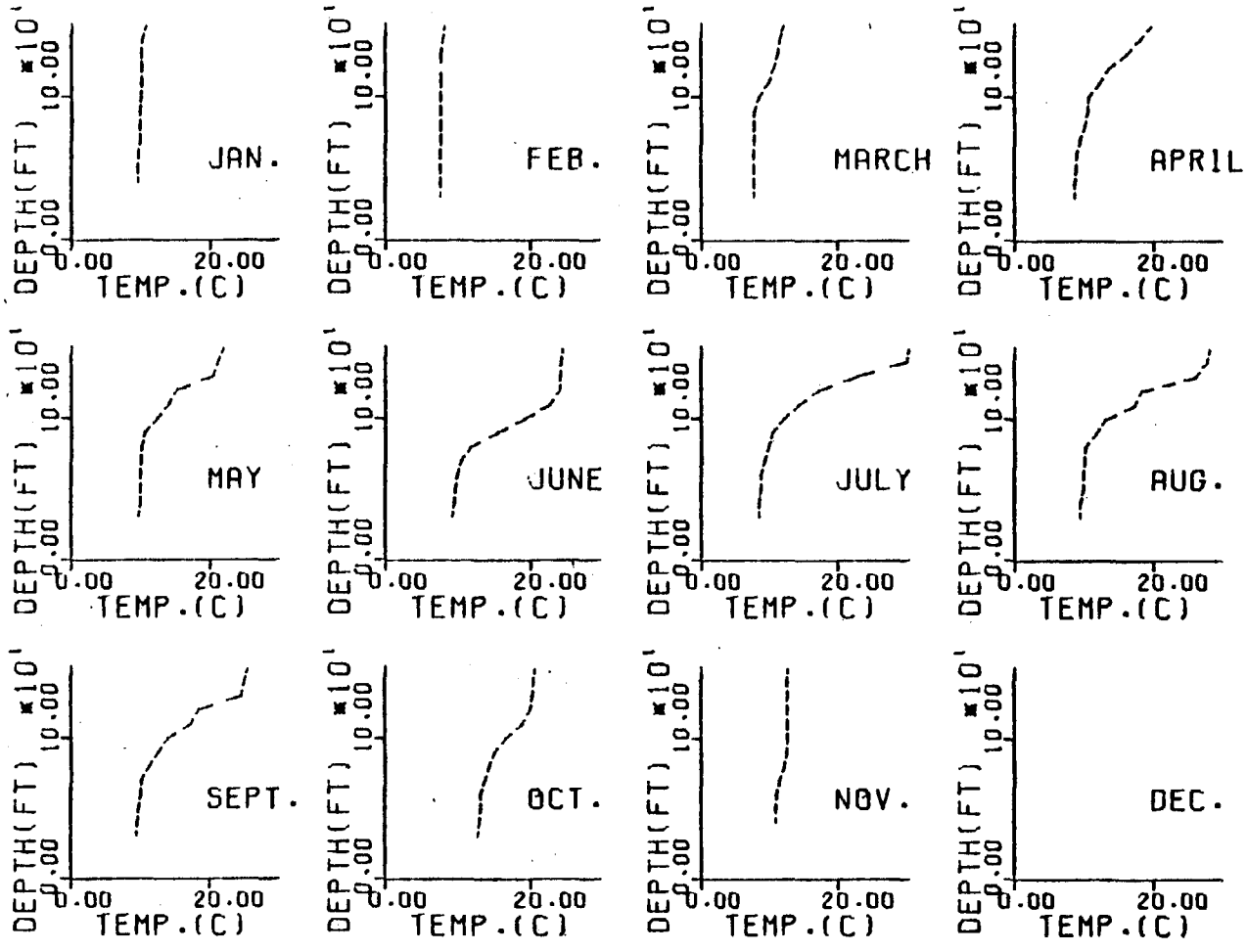

Figure B-34. Lake Keowee measured temperature profiles, 1972 - Station 504

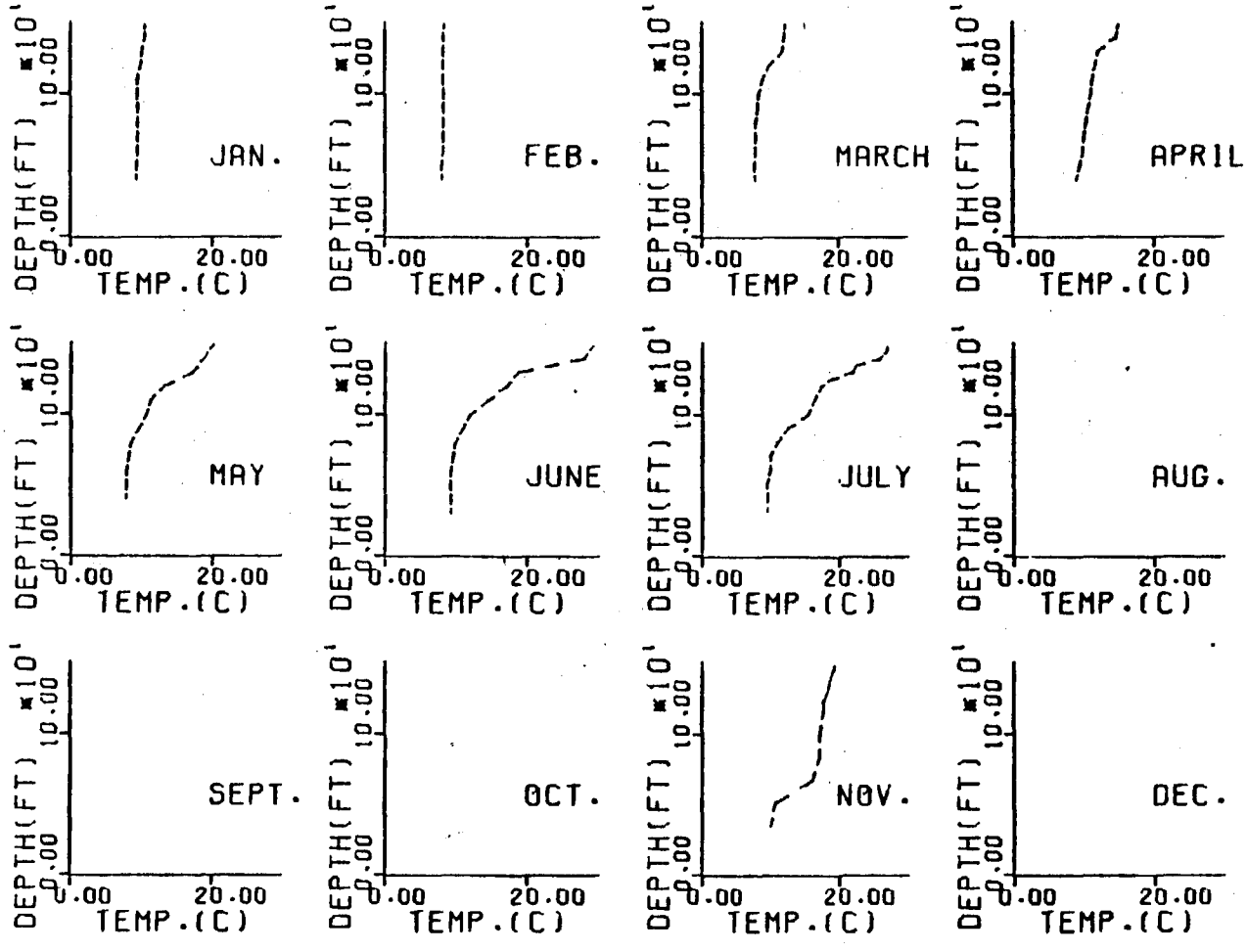

Figure B-35. Lake Keowee measured temperature profiles, 1973 - Station 504

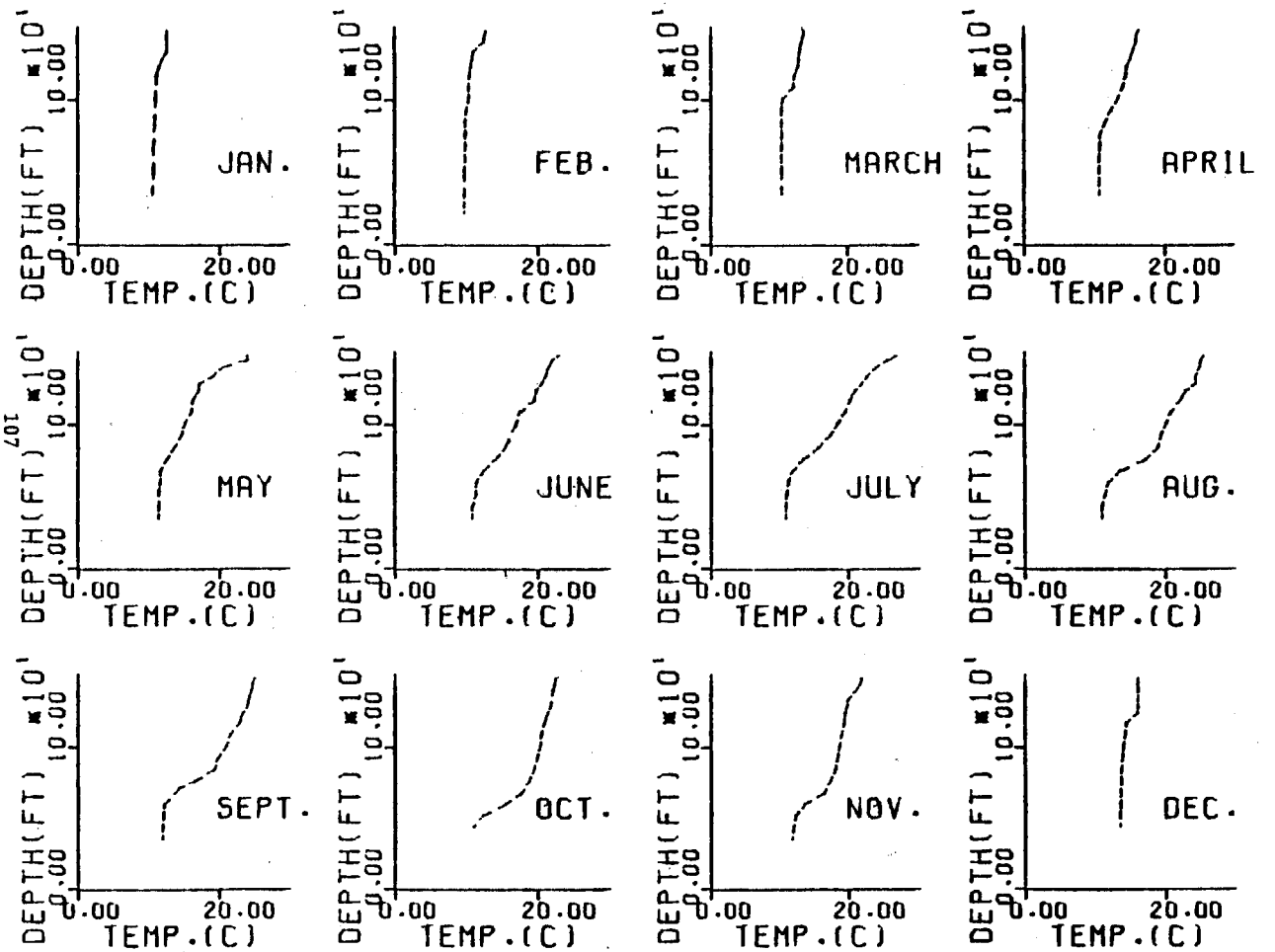

Figure B-36. Lake Keowee measured temperature profiles, 1974 - Station 504

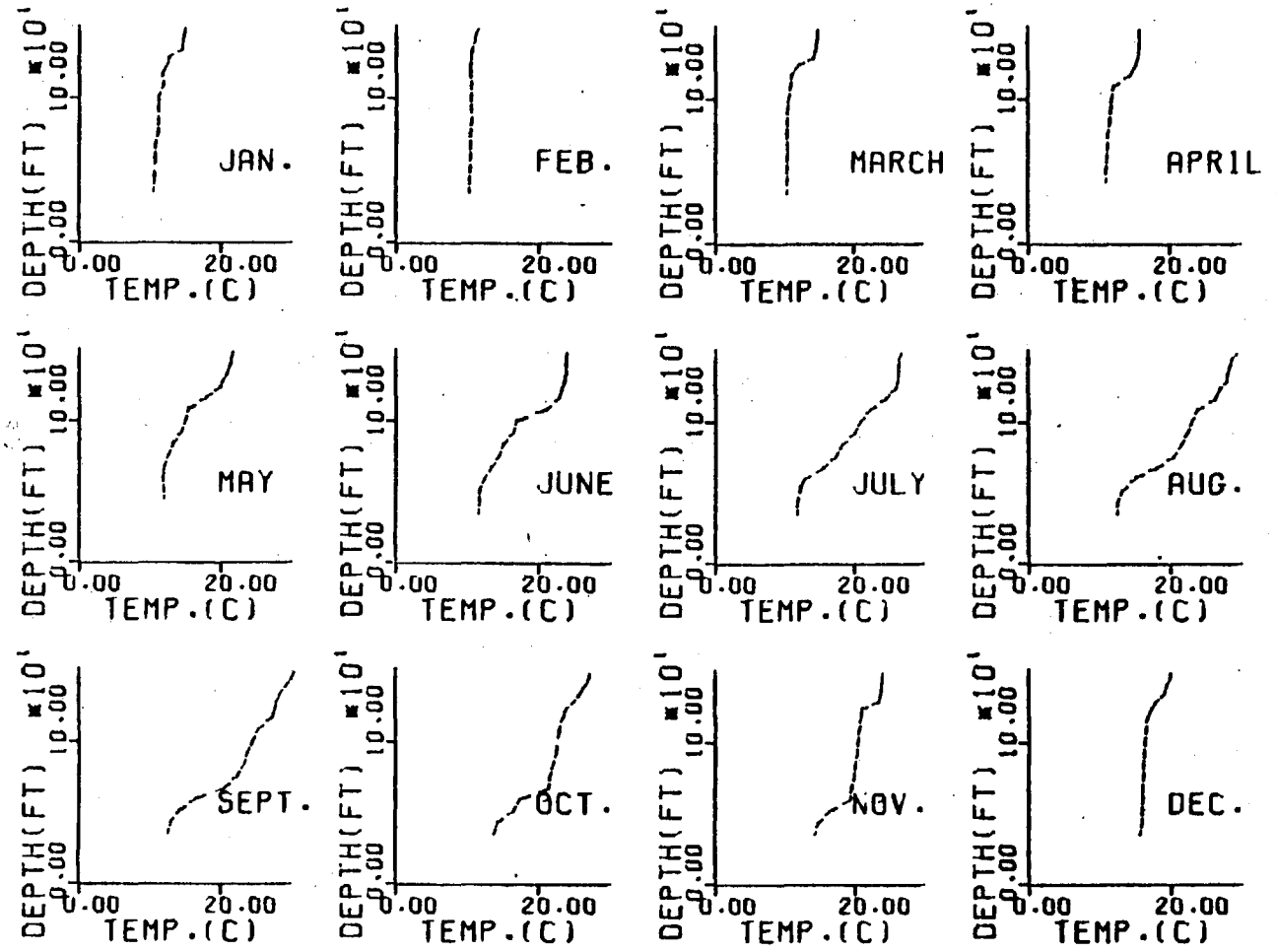

Figure B-37. Lake Keowee measured temperature profiles, 1975 - Station 504

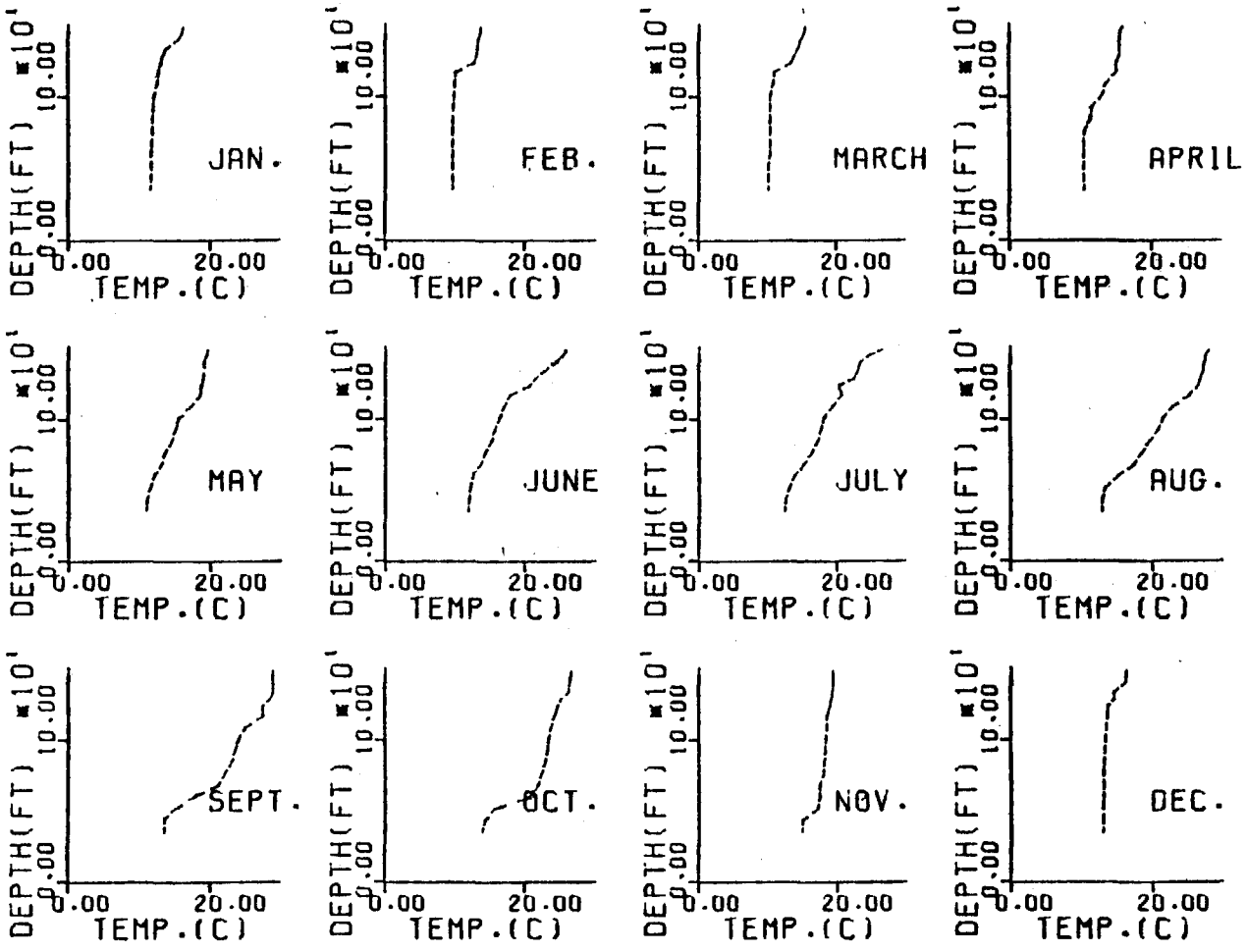

Figure B-38. Lake Keowee measured temperature profiles, 1976 - Station 504

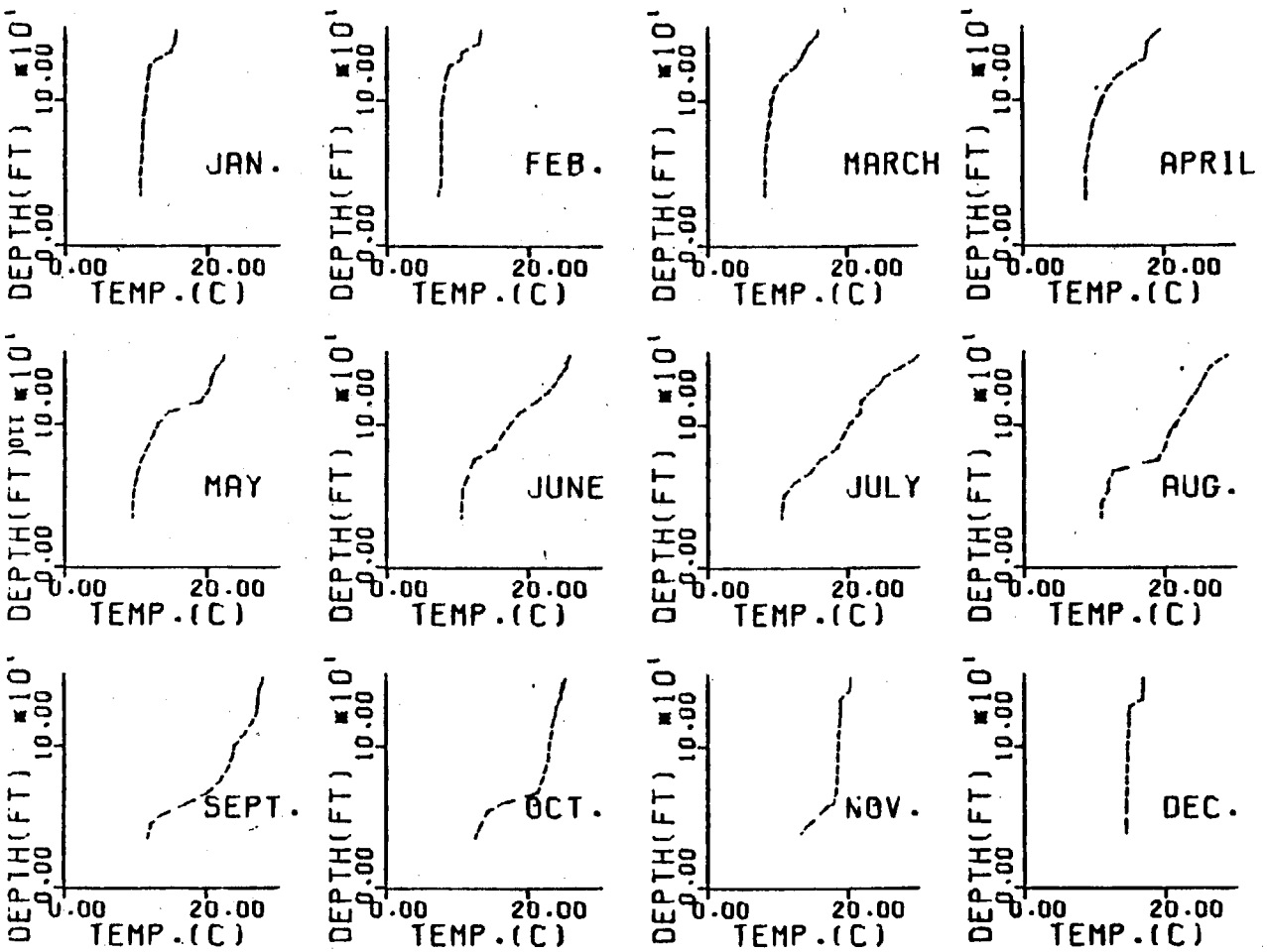

Figure B-39. Lake Keowee measured temperature profiles, 1977 - Station 504

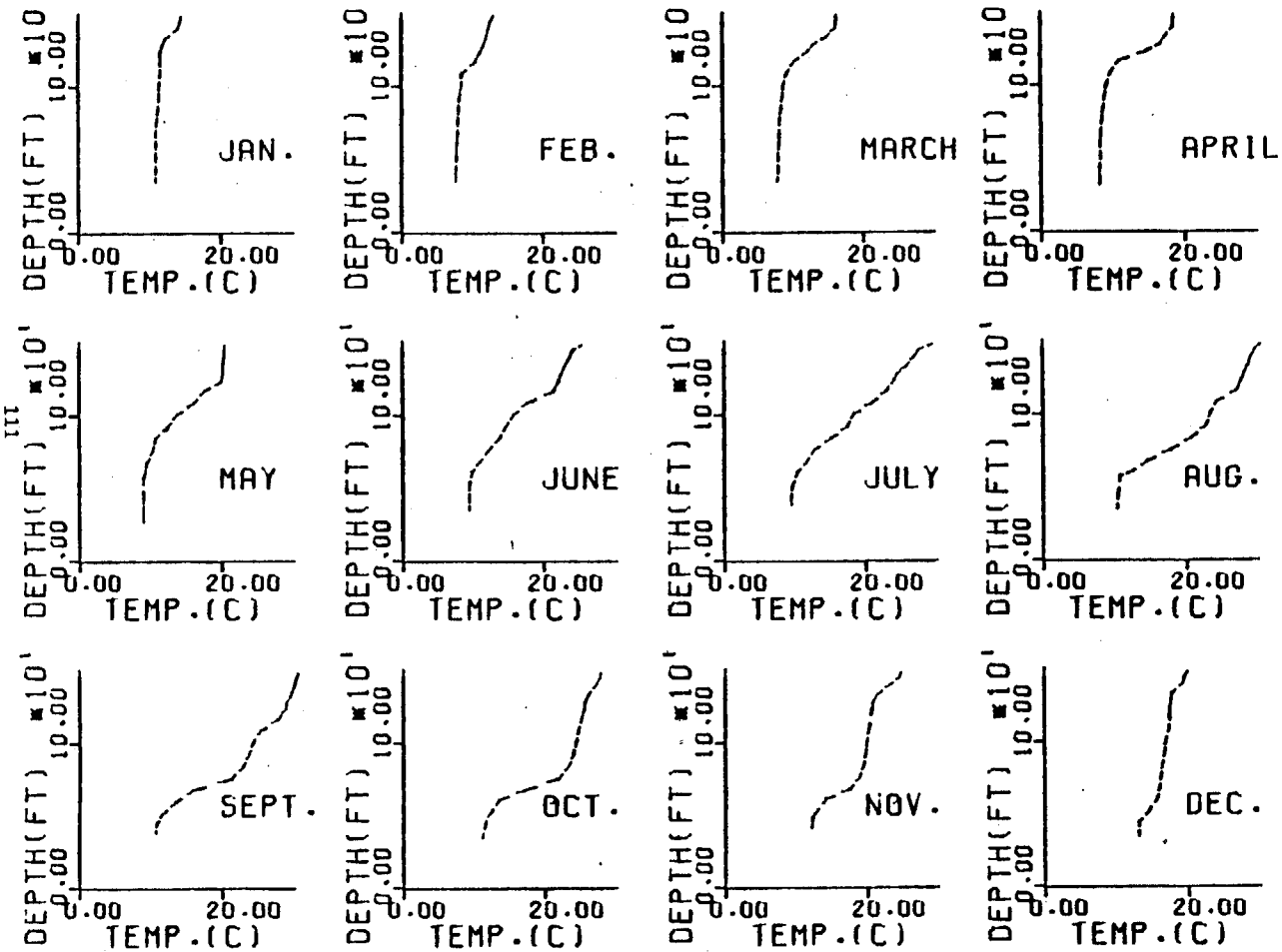

Figure B-40. Lake Keowee measured temperature profiles, 1978 - Station 504

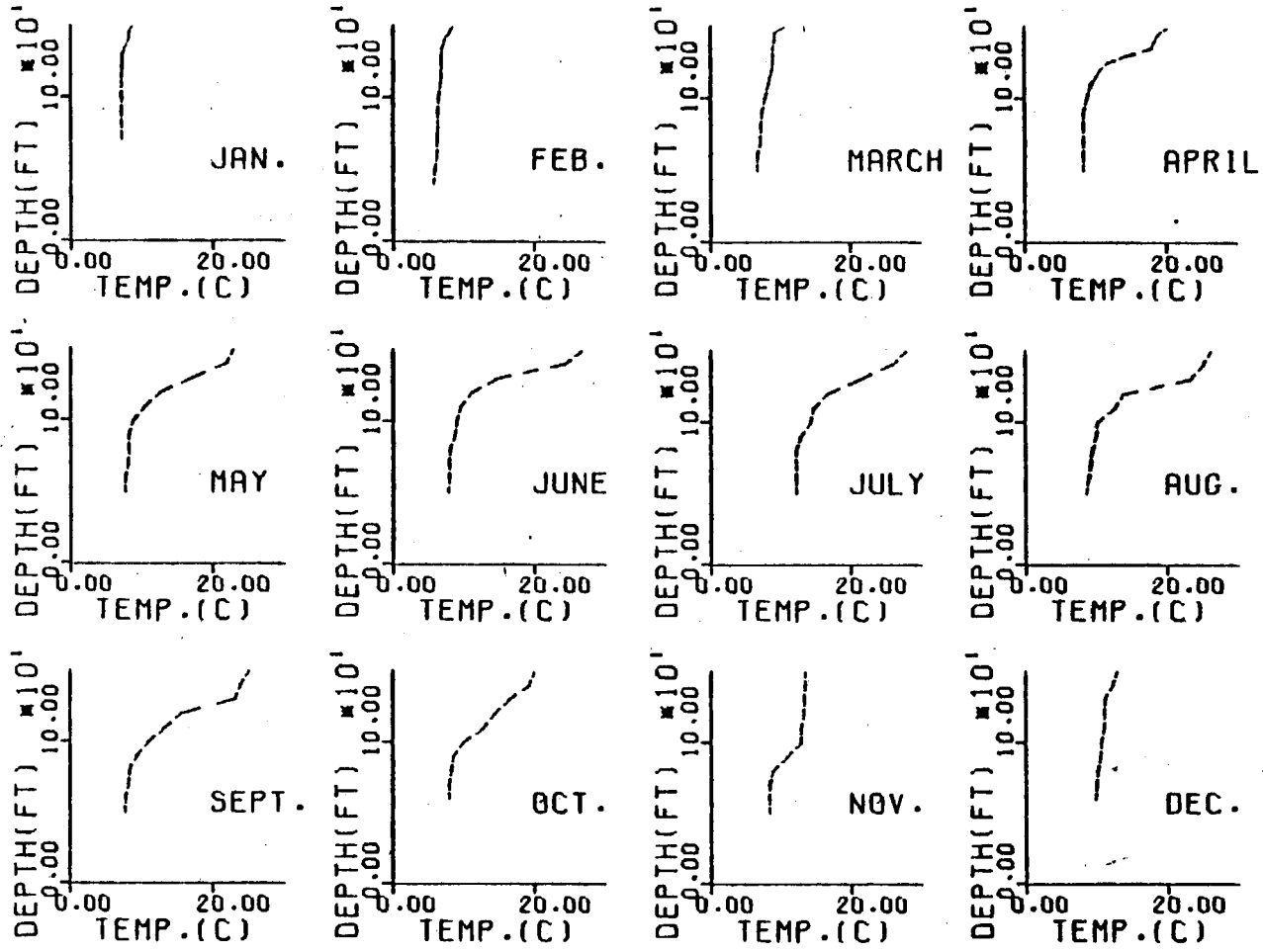

Figure B-41. Lake Keowee measured temperature profiles, 1971 - Station 505

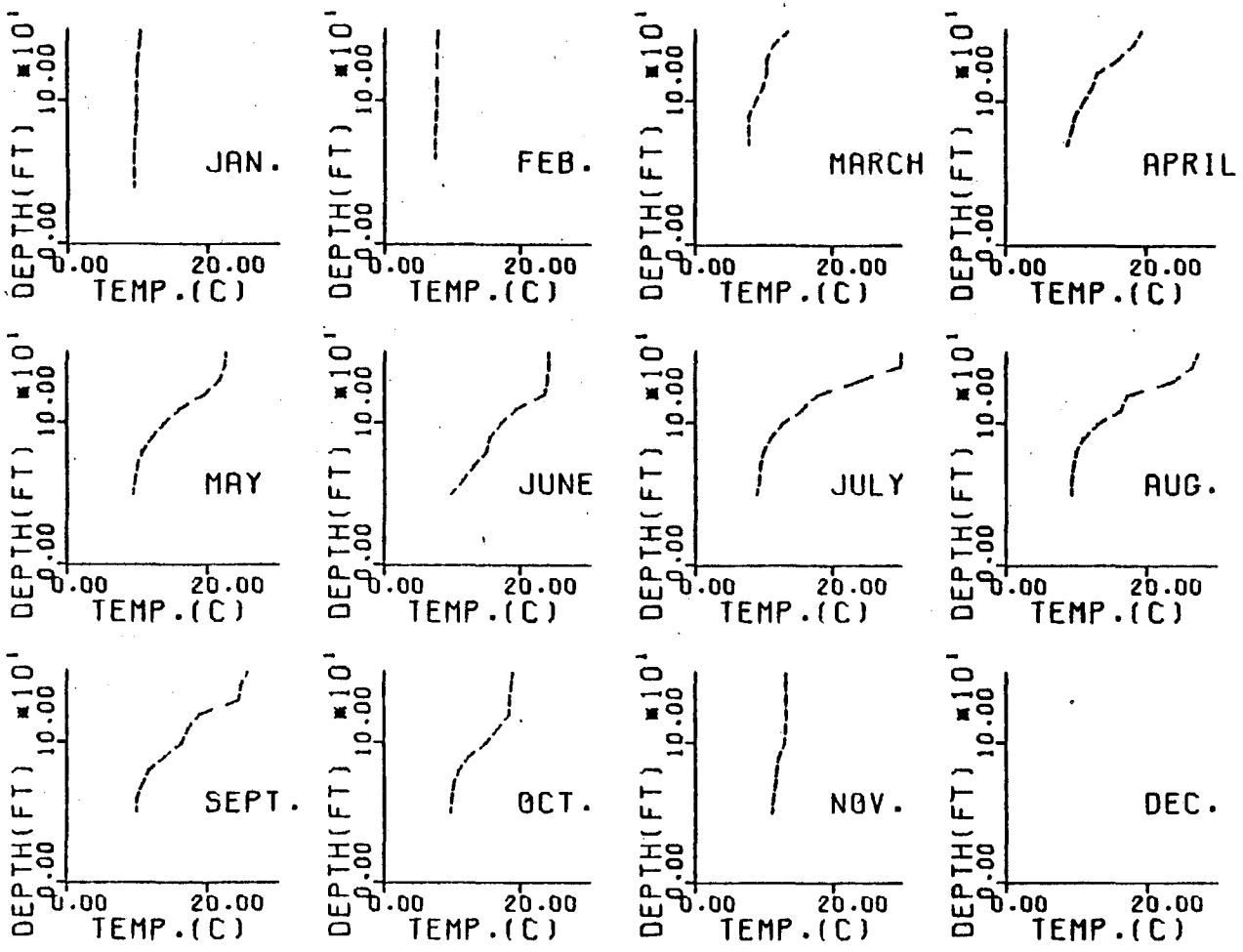

Figure B-42. Lake Keowee measured temperature profiles, 1972 - Station 505

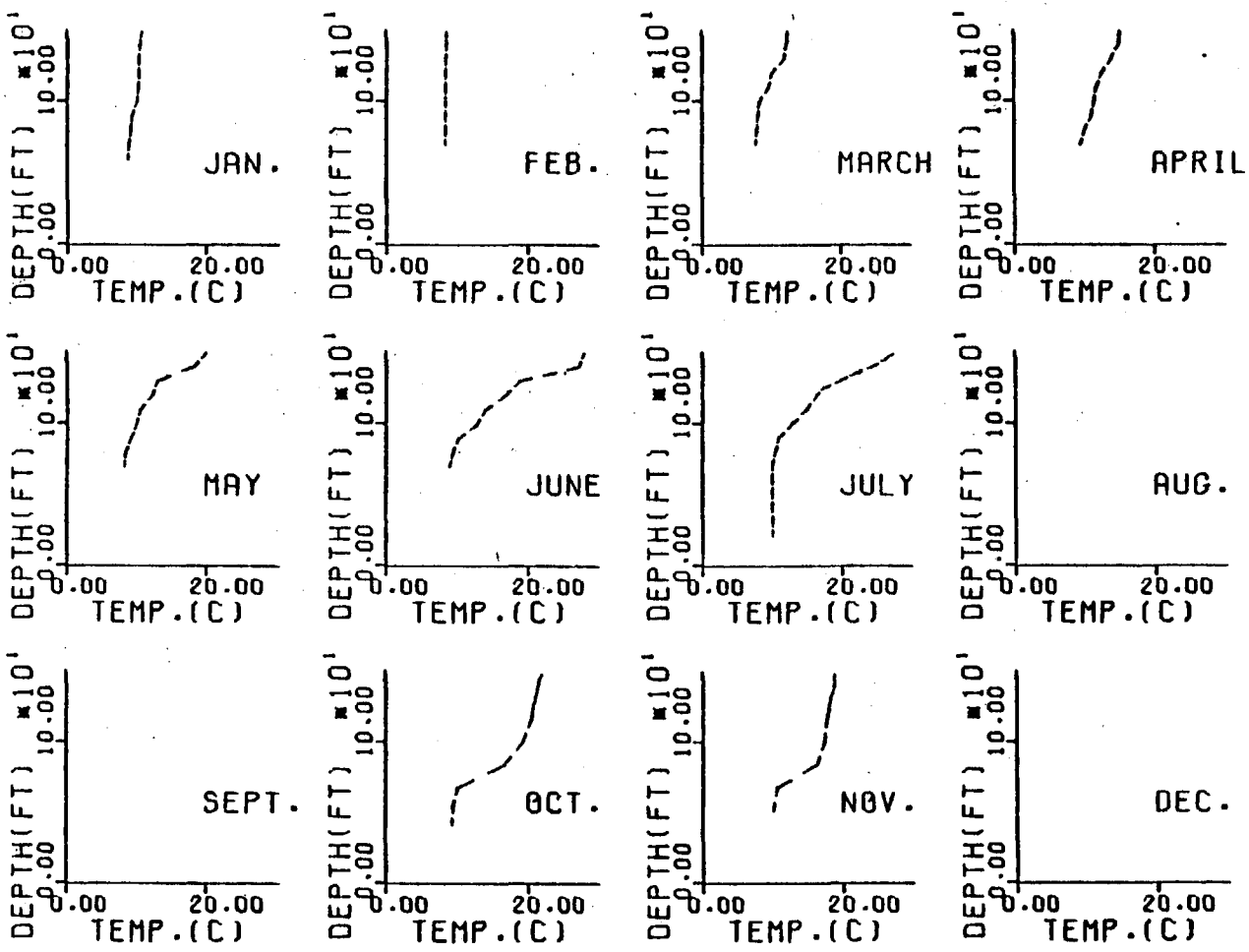

Figure B-43. Lake Keowee measured temperature profiles, 1973 - Station 505

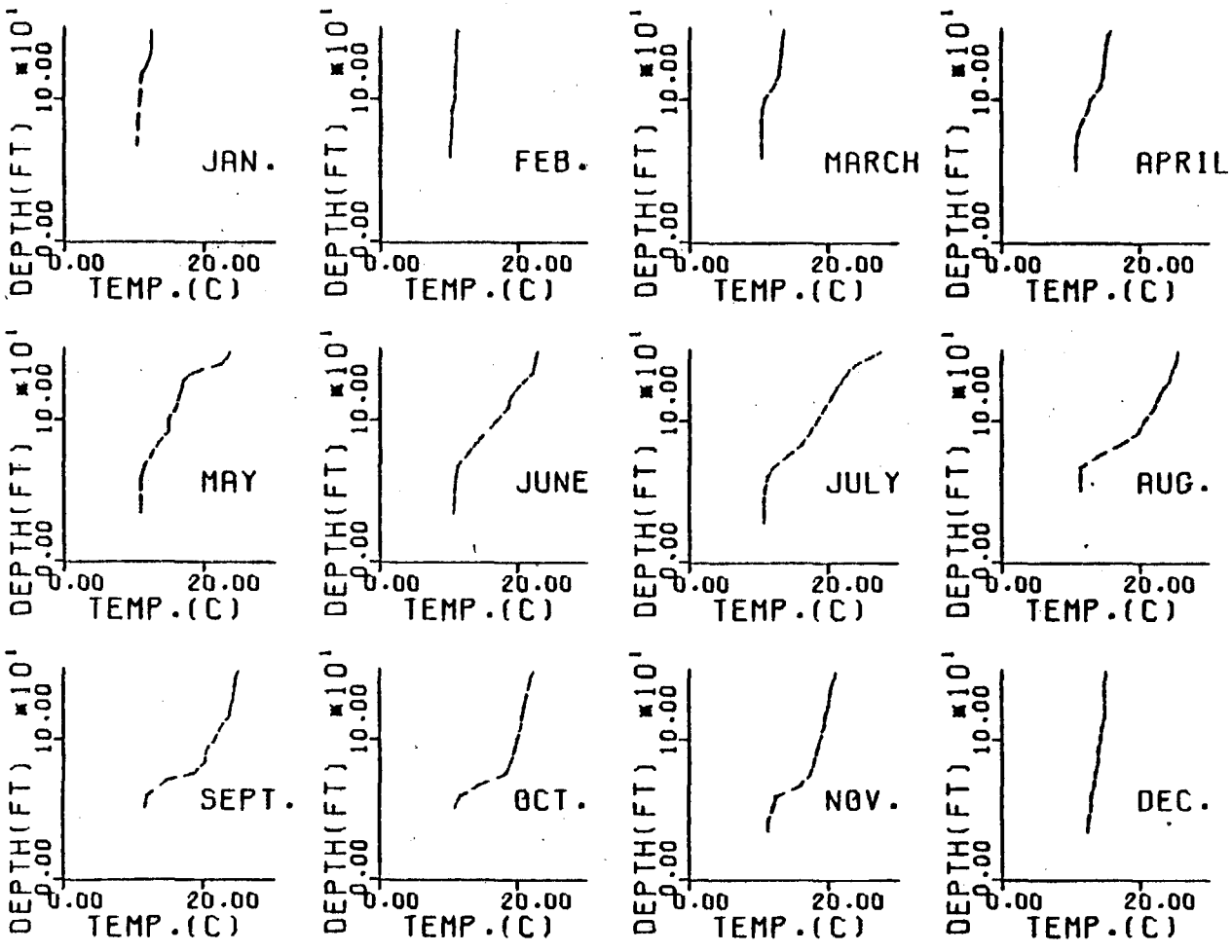

Figure B-44. Lake Keowee measured temperature profiles, 1974 - Station 505

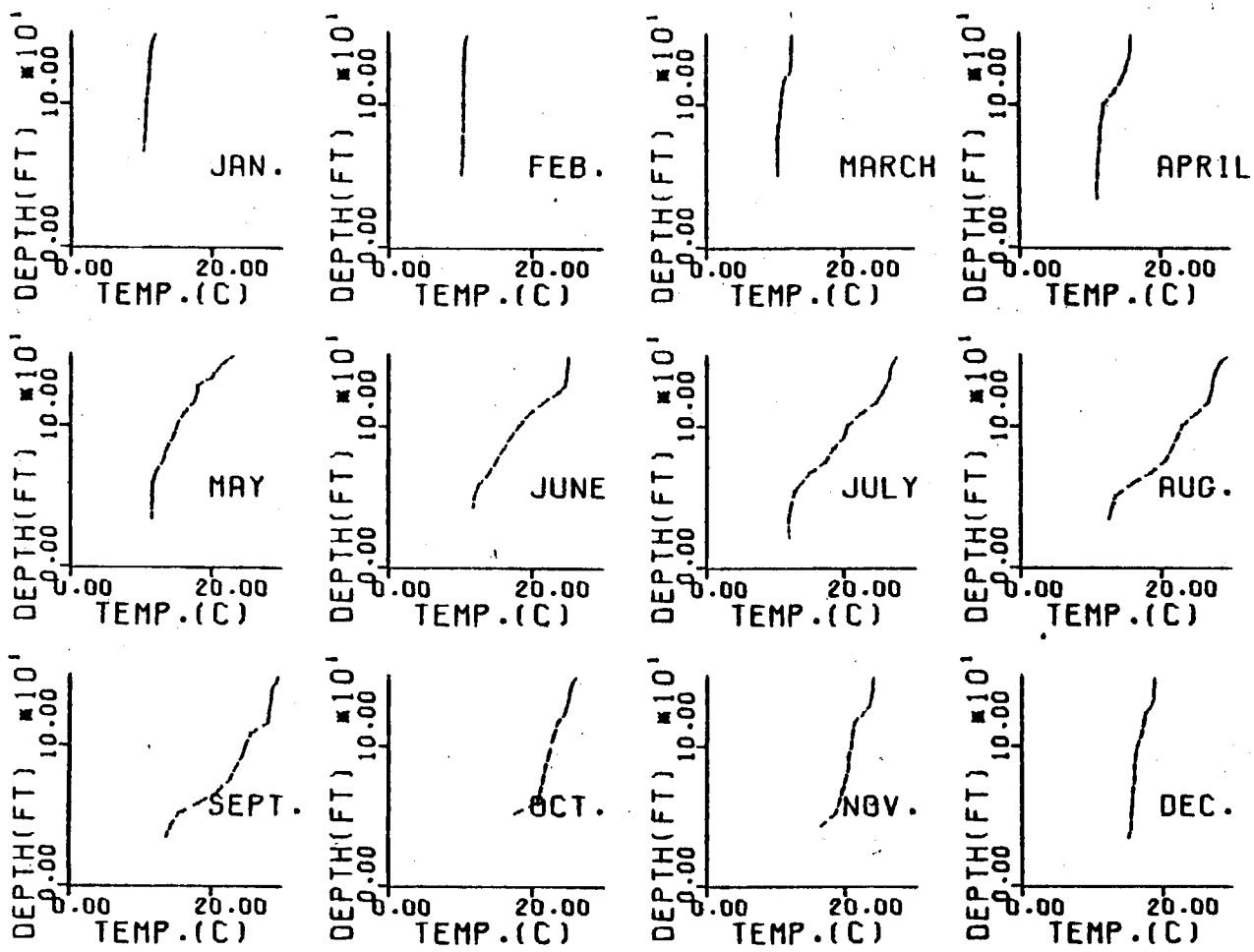

Figure B-45. Lake Keowee measured temperature profiles, 1975 - Station 505

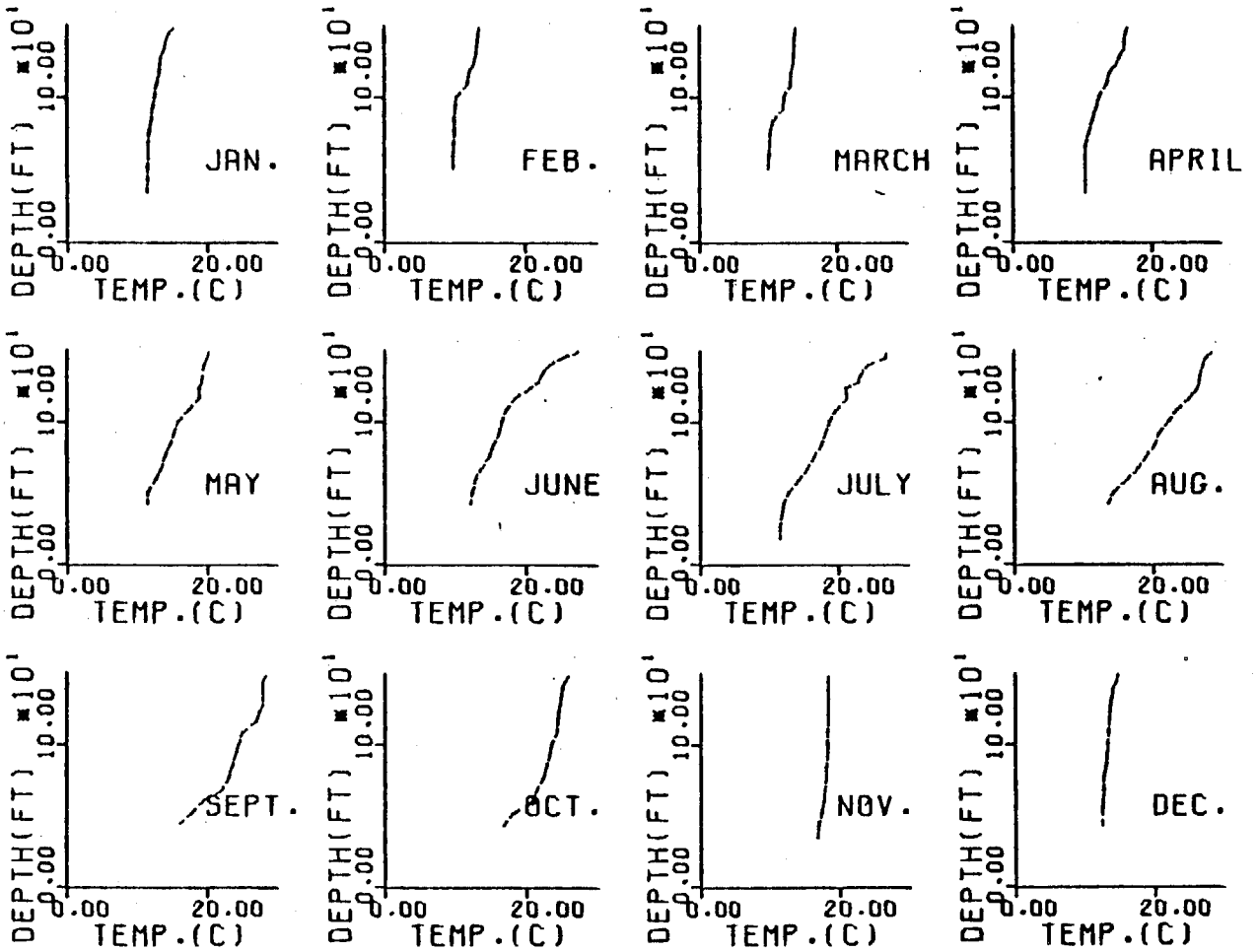

Figure B-46. Lake Keowee measured temperature profiles, 1976 - Station 505

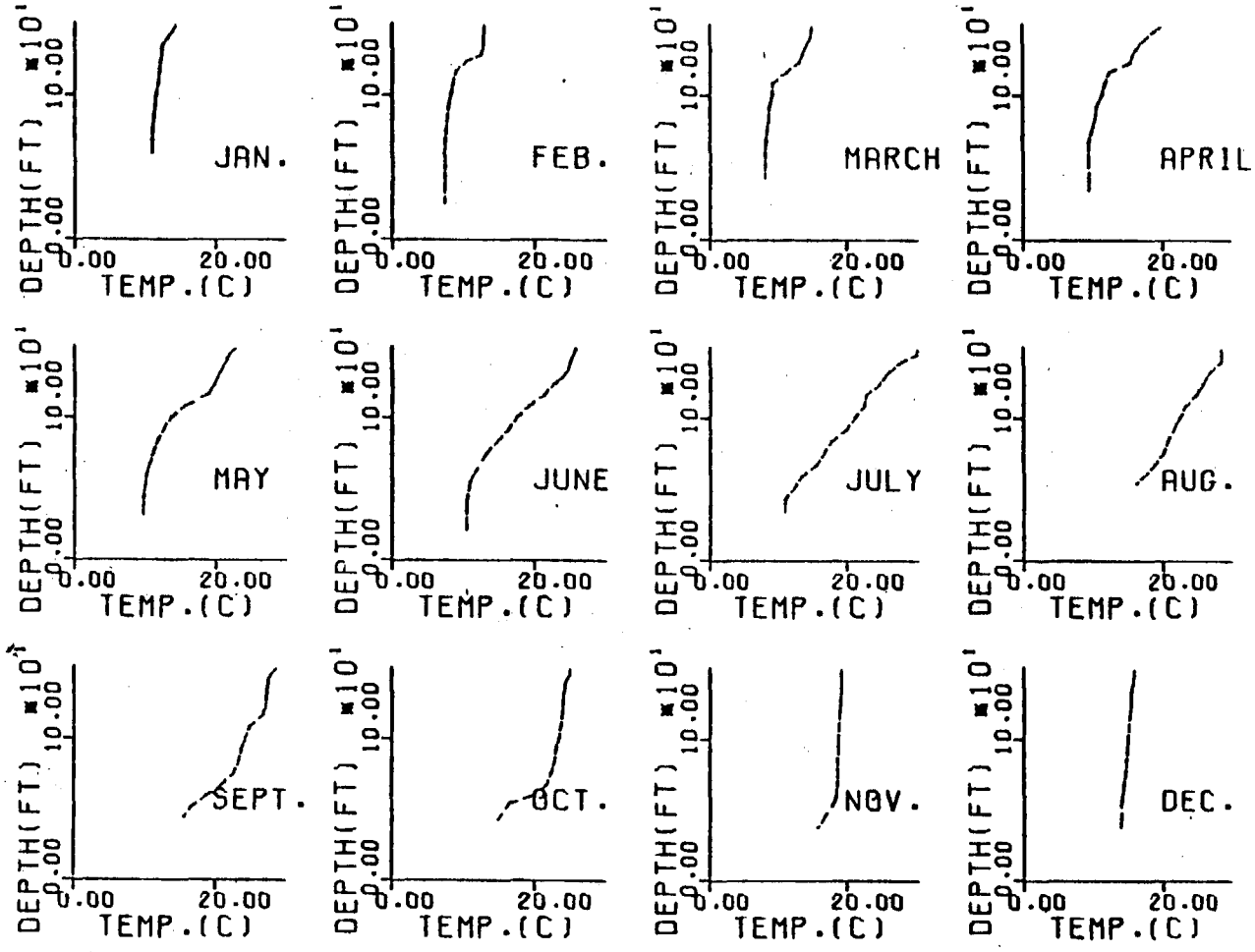

Figure B-47. Lake Keowee measured temperature profiles, 1977 - Station 505

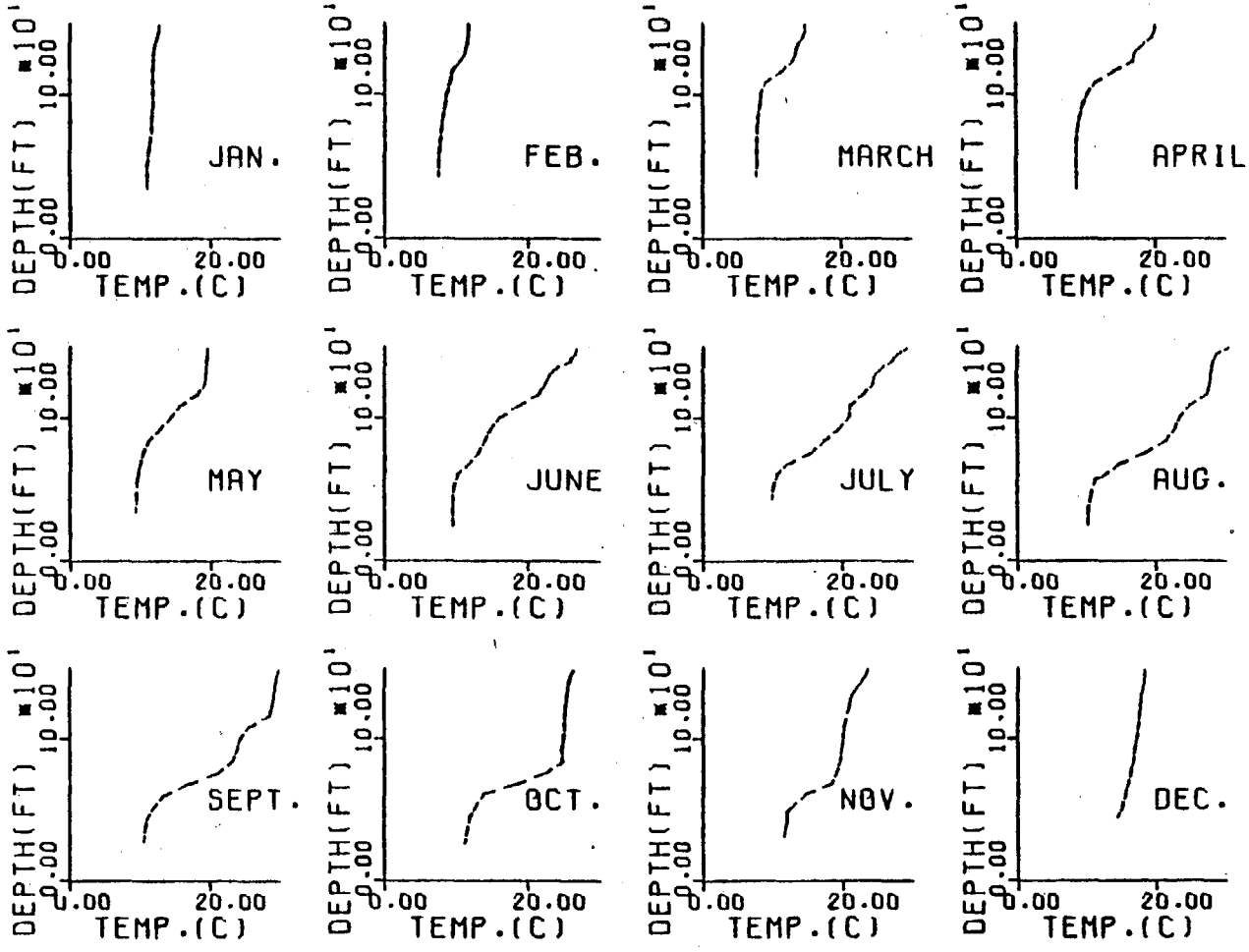

Figure B-48. Lake Keowee measured temperature profiles, 1978 - Station 505

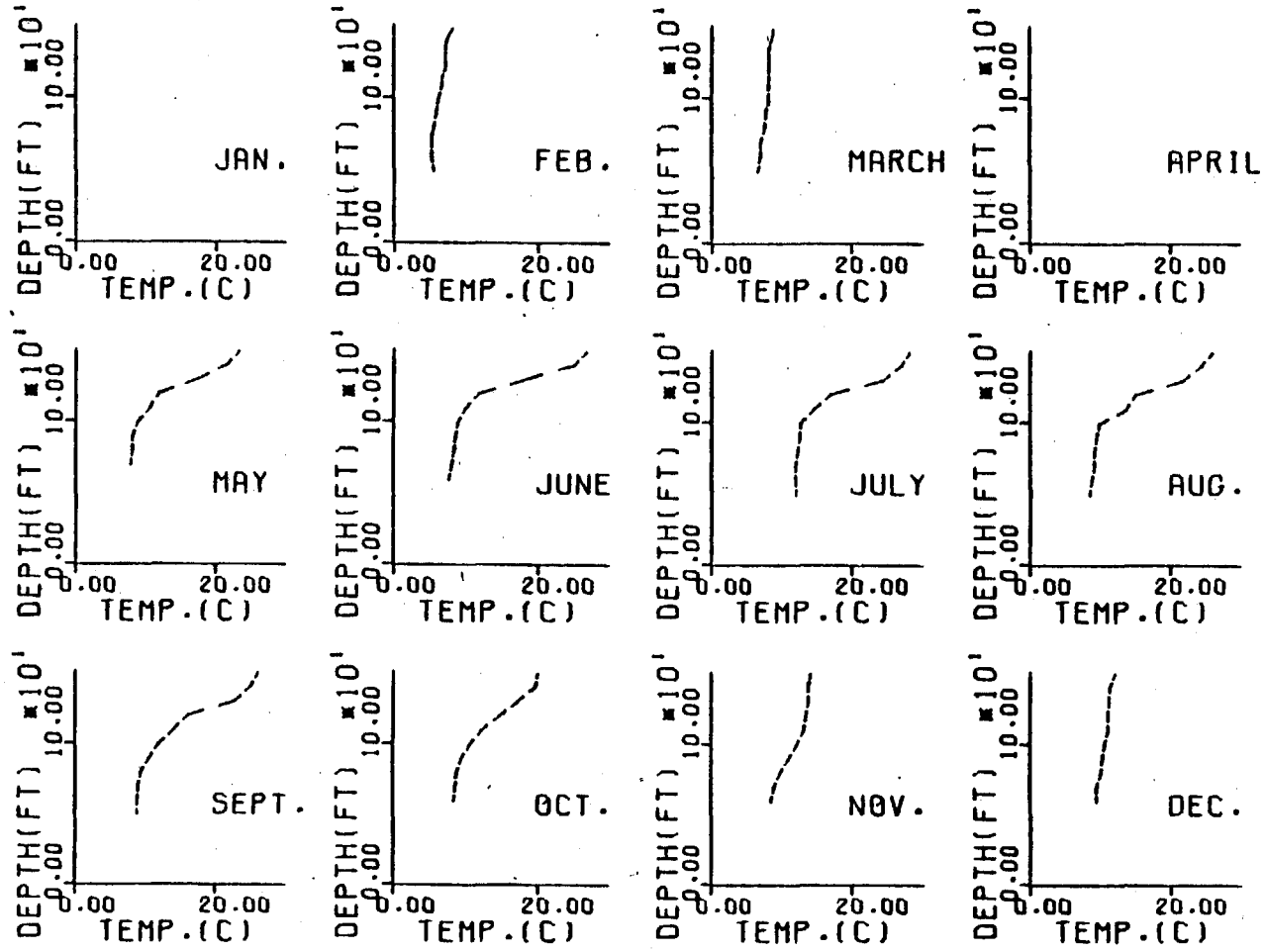

Figure B-49. Lake Keowee measured temperature profiles, 1971 - Station 506

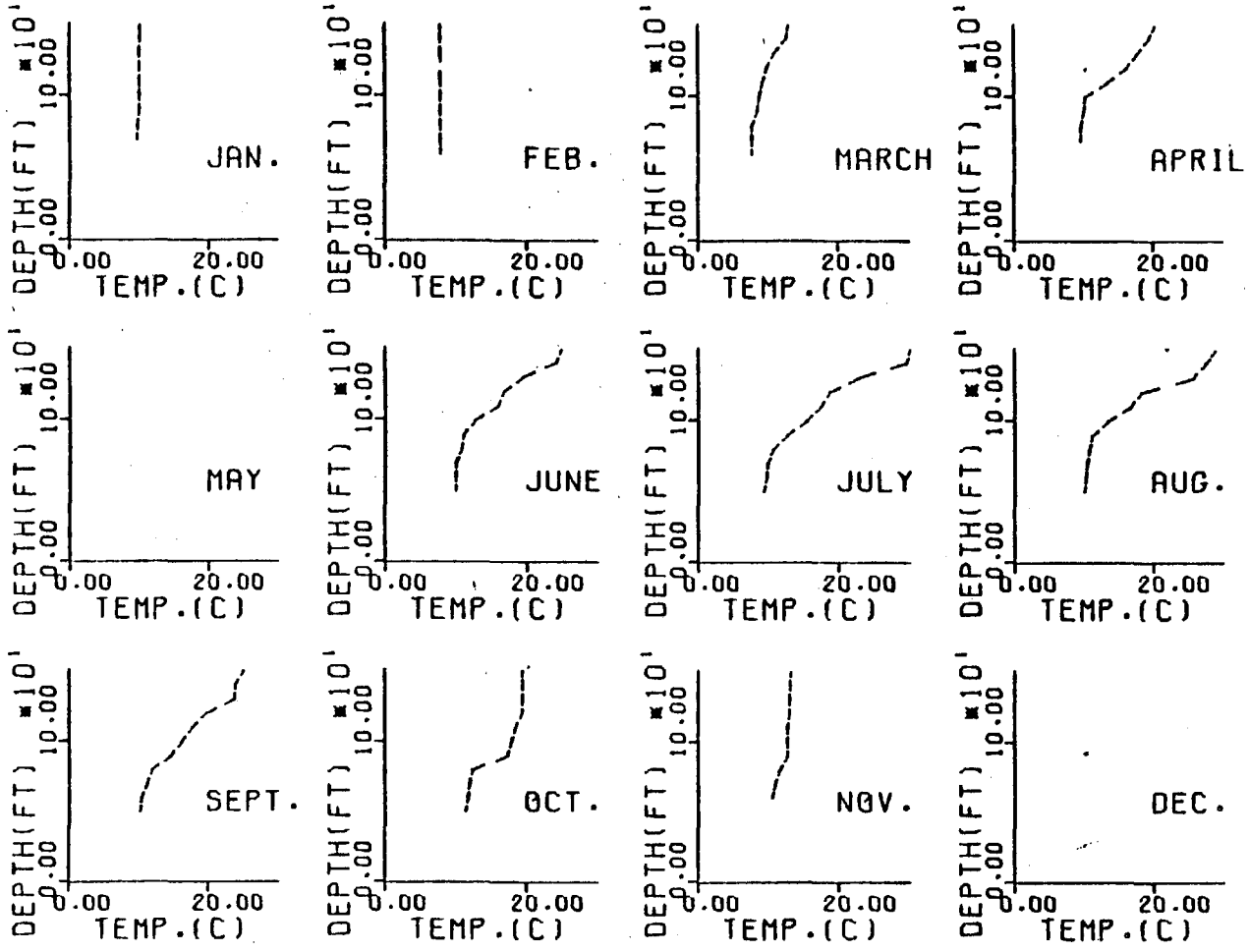

Figure B-50. Lake Keowee measured temperature profiles, 1972 - Station 506

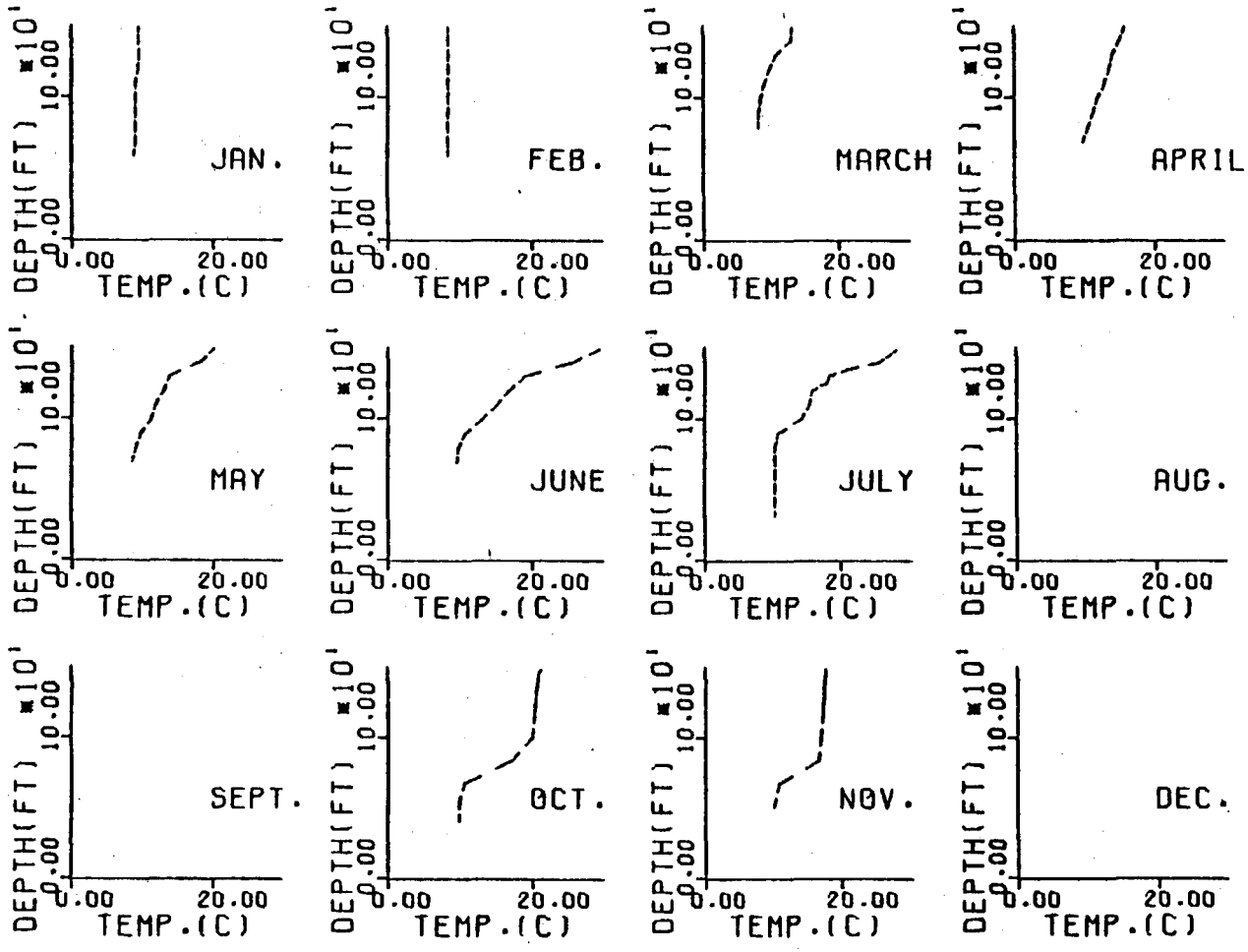

Figure B-51. Lake Koewee measured temperature profiles, 1973 - Station 506

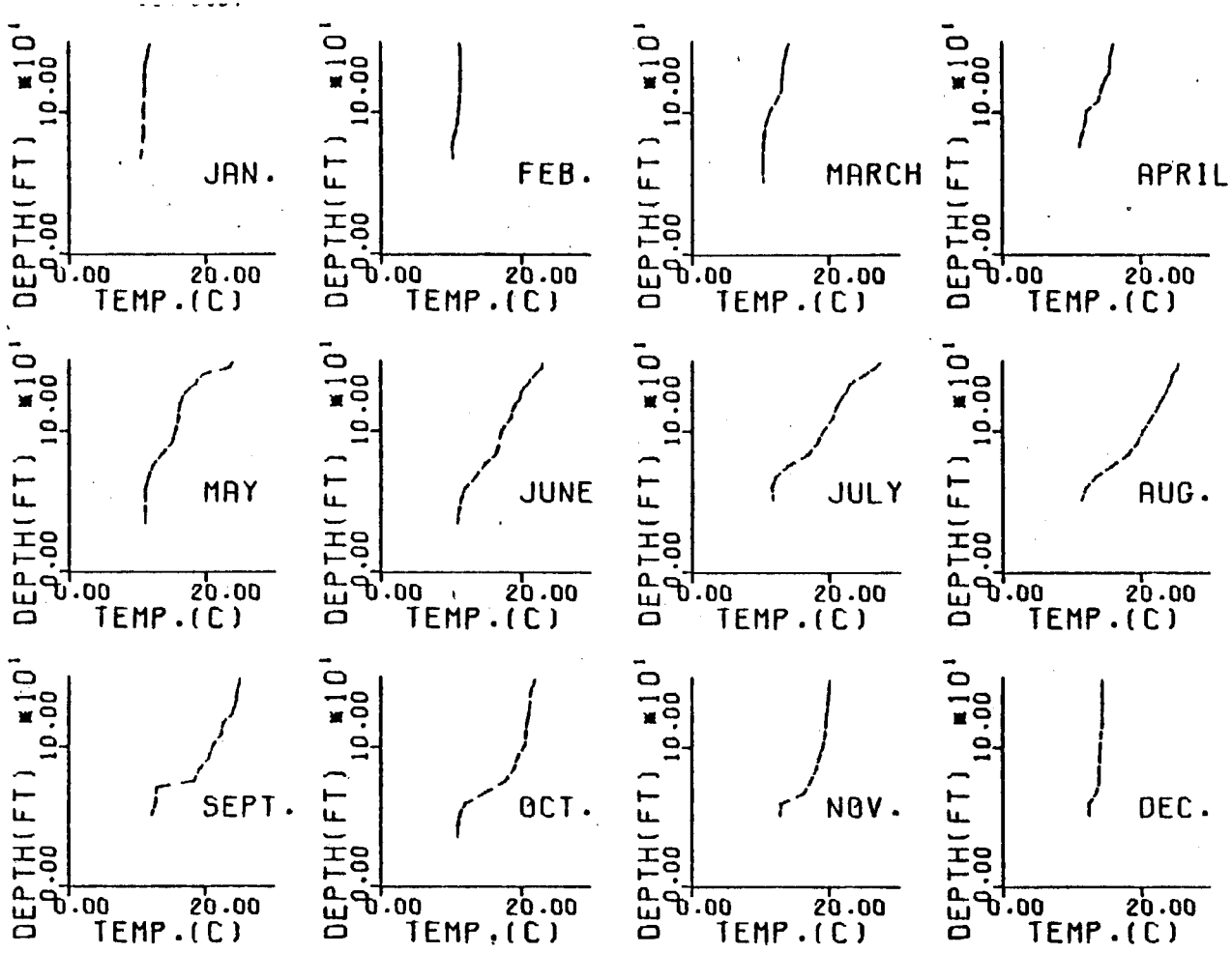

Figure B-52. Lake Keowee measured temperature profiles, 1974 - Station 506

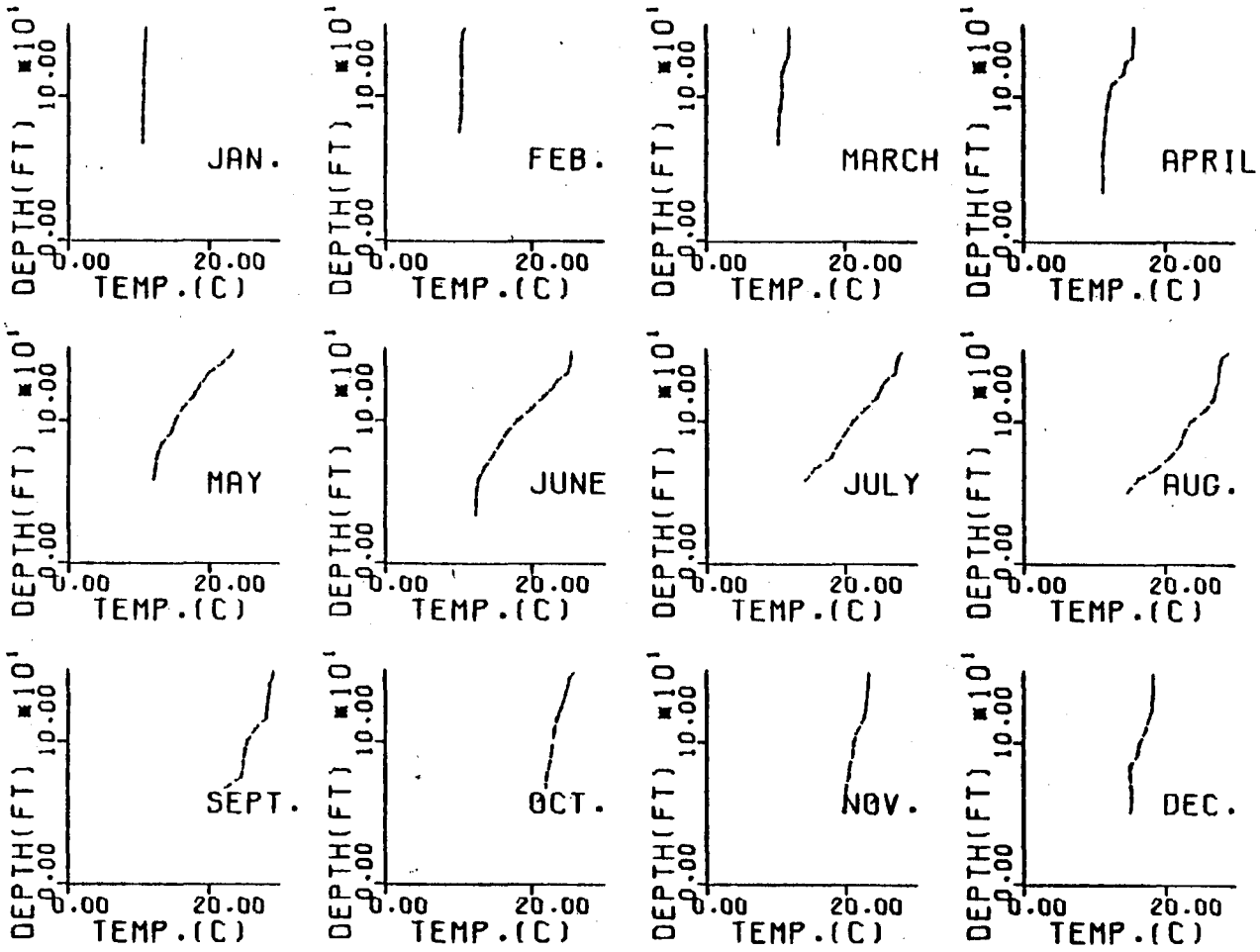

Figure B-53. Lake Keowee measured temperature profiles, 1975 - Station 506

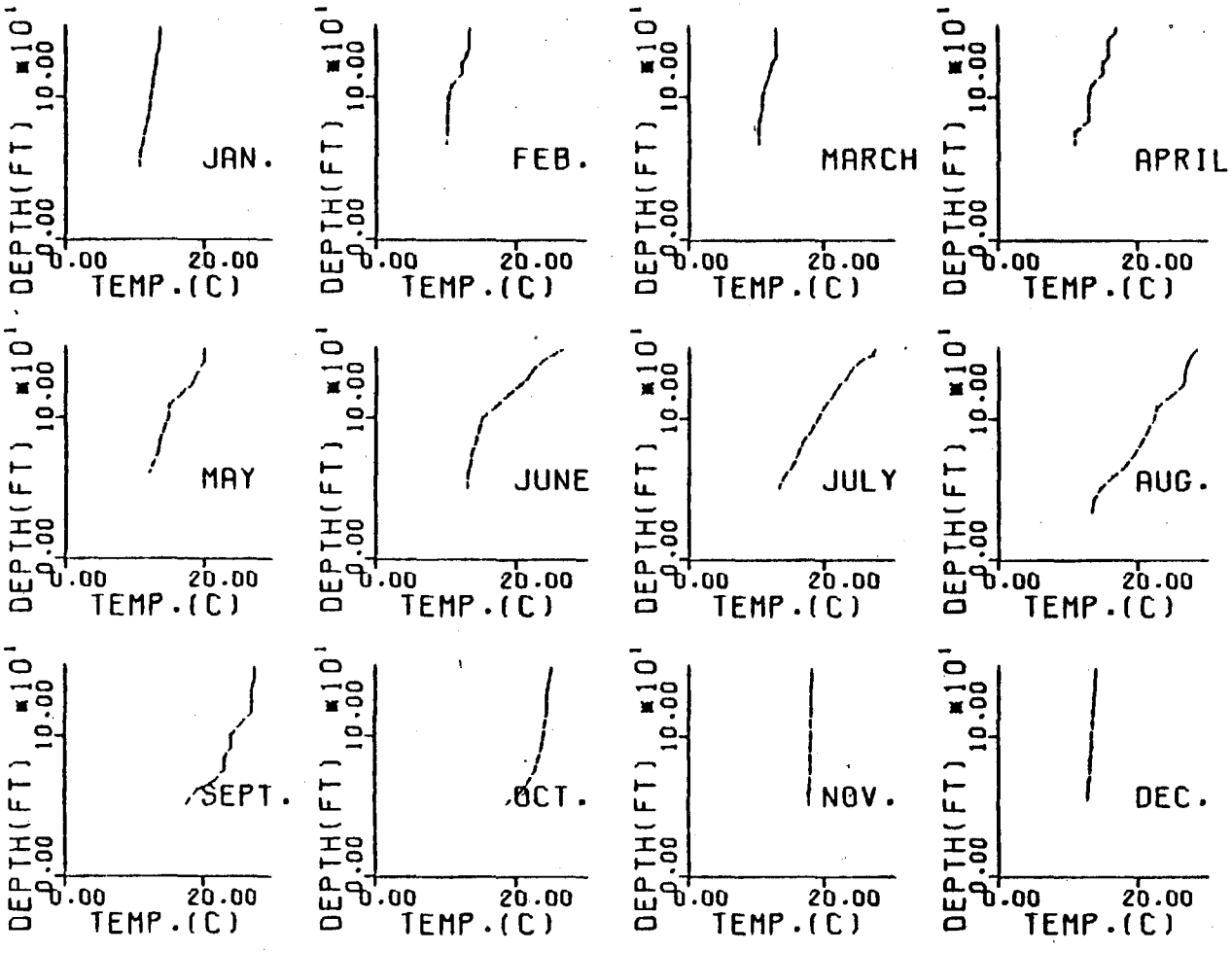

Figure B-54. Lake Koewee measured temperature profiles, 1976 - Station 506

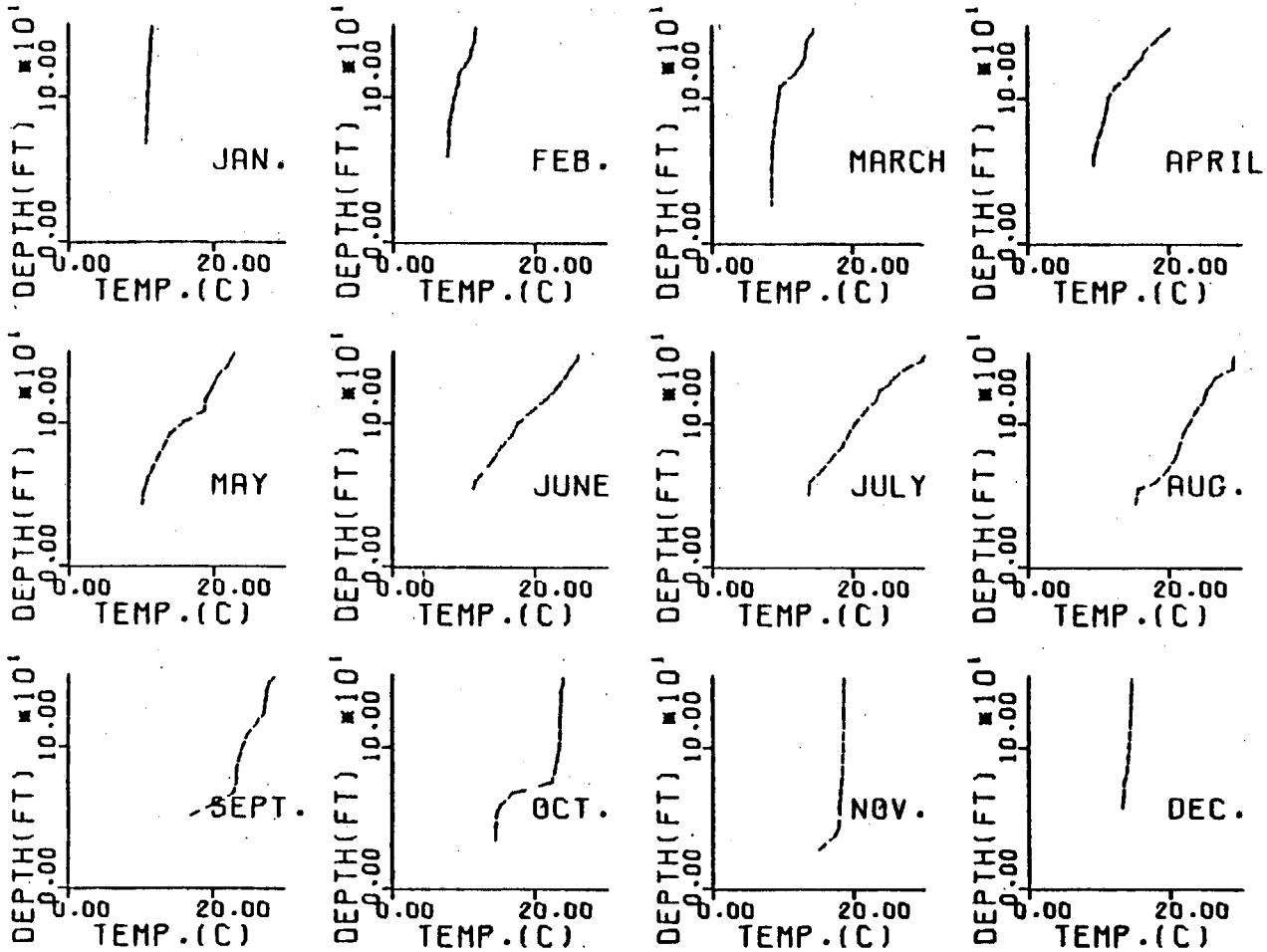

Figure B-55. Lake Keowee measured temperature profiles, 1977 - Station 506

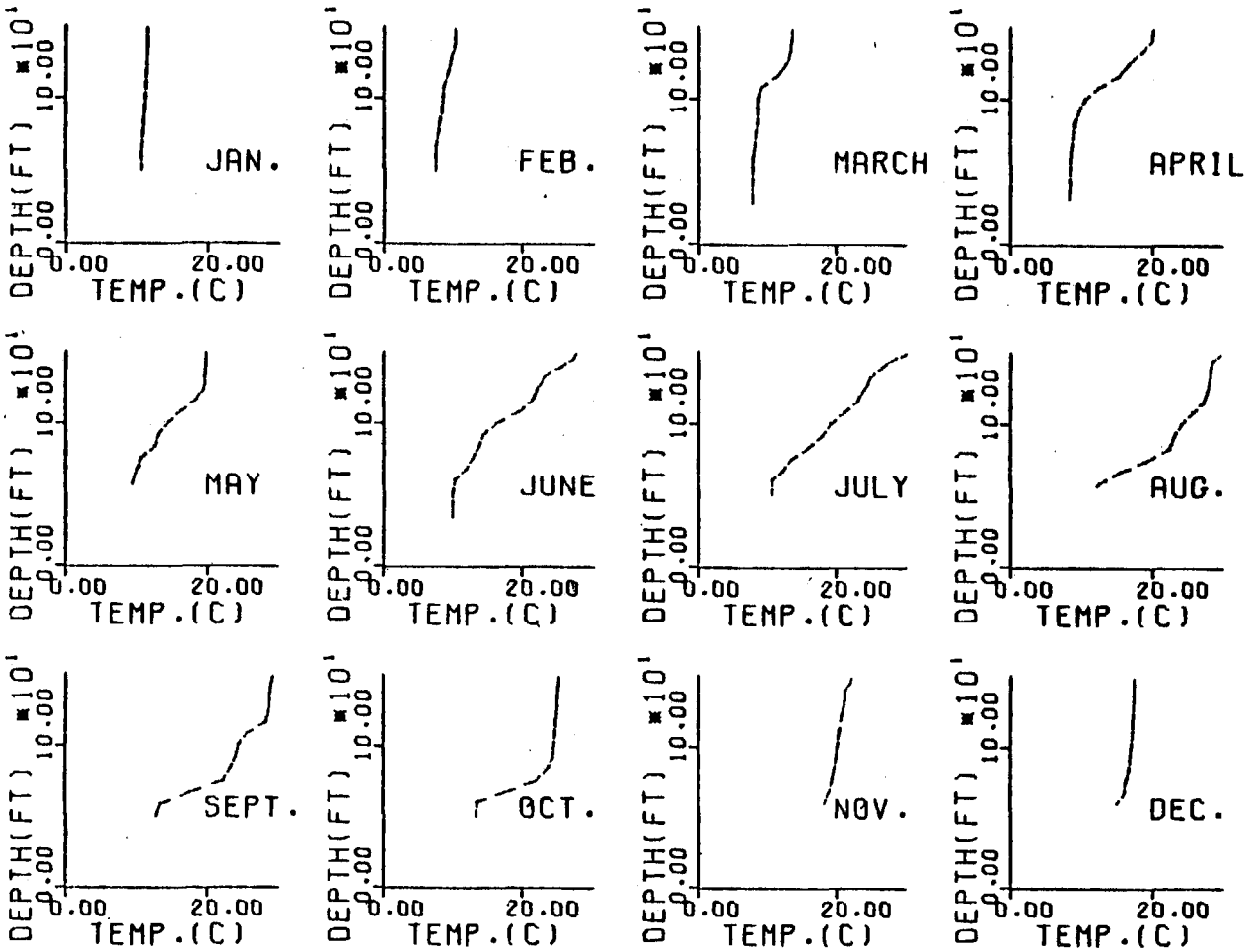

Figure B-56. Lake Keowee measured temperature profiles, 1978 - Station 506

APPENDIX C

MEASURED TEMPERATURE PROFILES
(Average of Stations 500 Through 506)

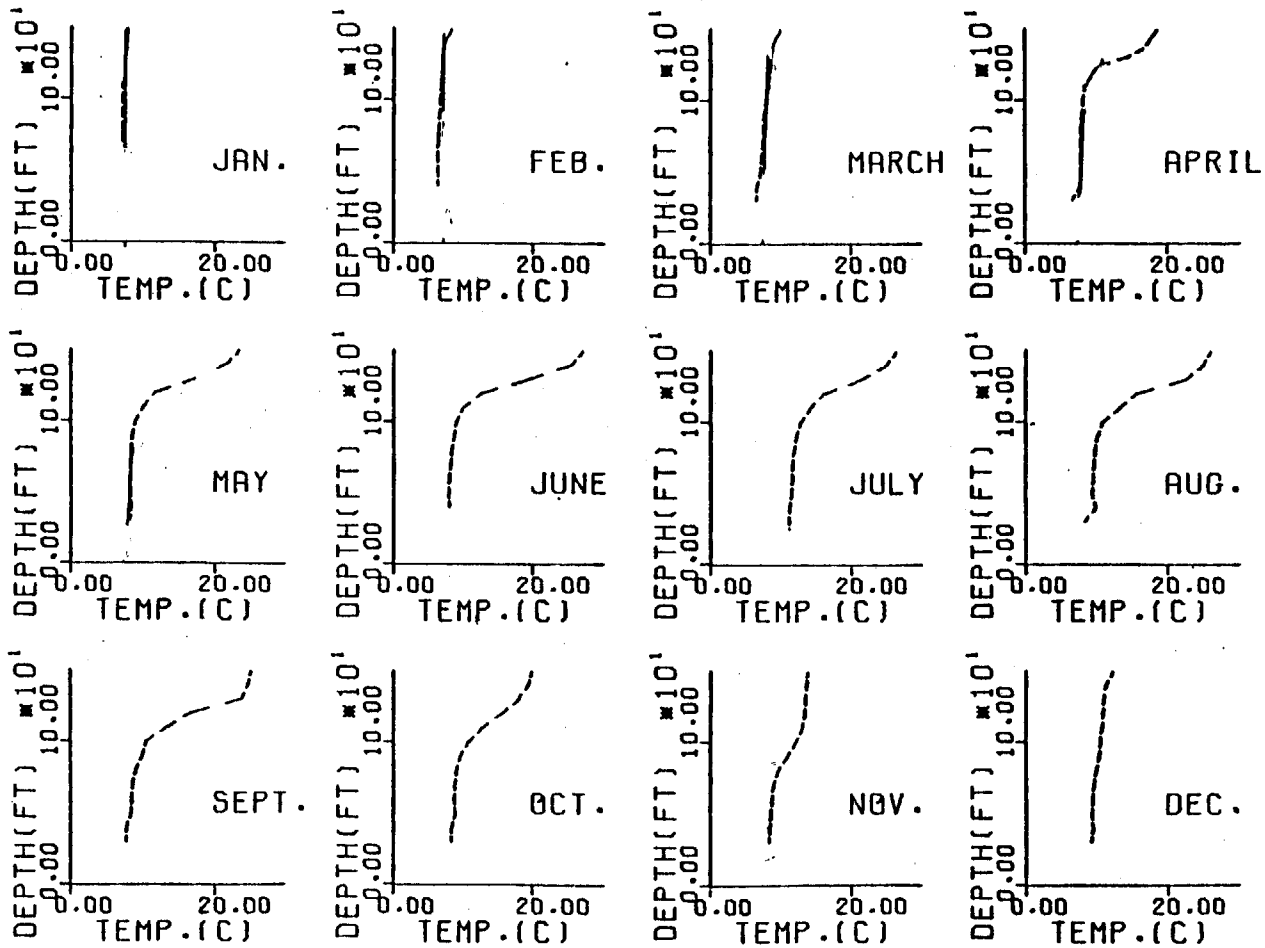

Figure C-1. Lake Keowee averaged measured temperature profiles, Stations 501-506, 1971

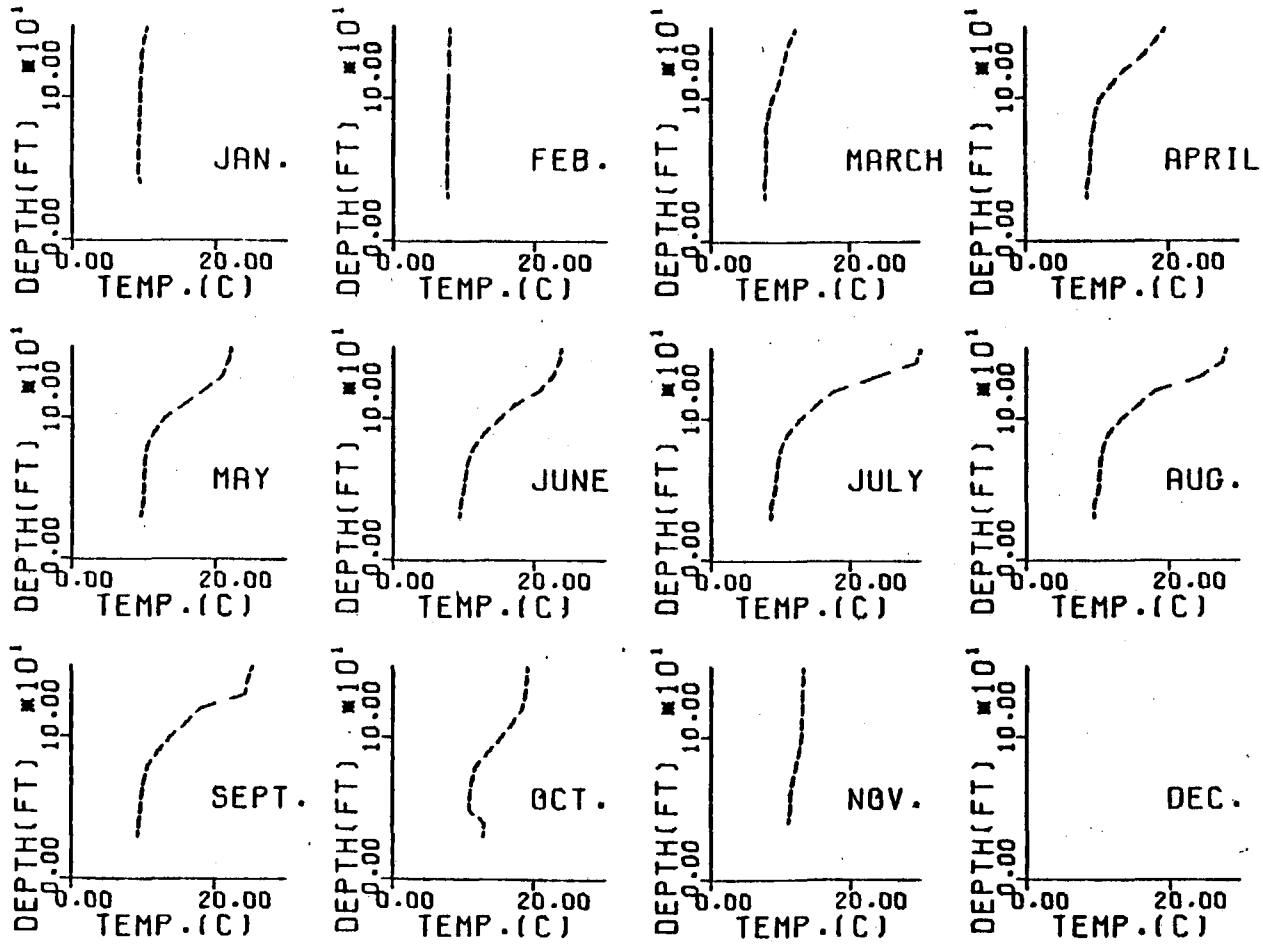

Figure C-2. Lake Keowee averaged measured temperature profiles, Stations 501-506, 1972

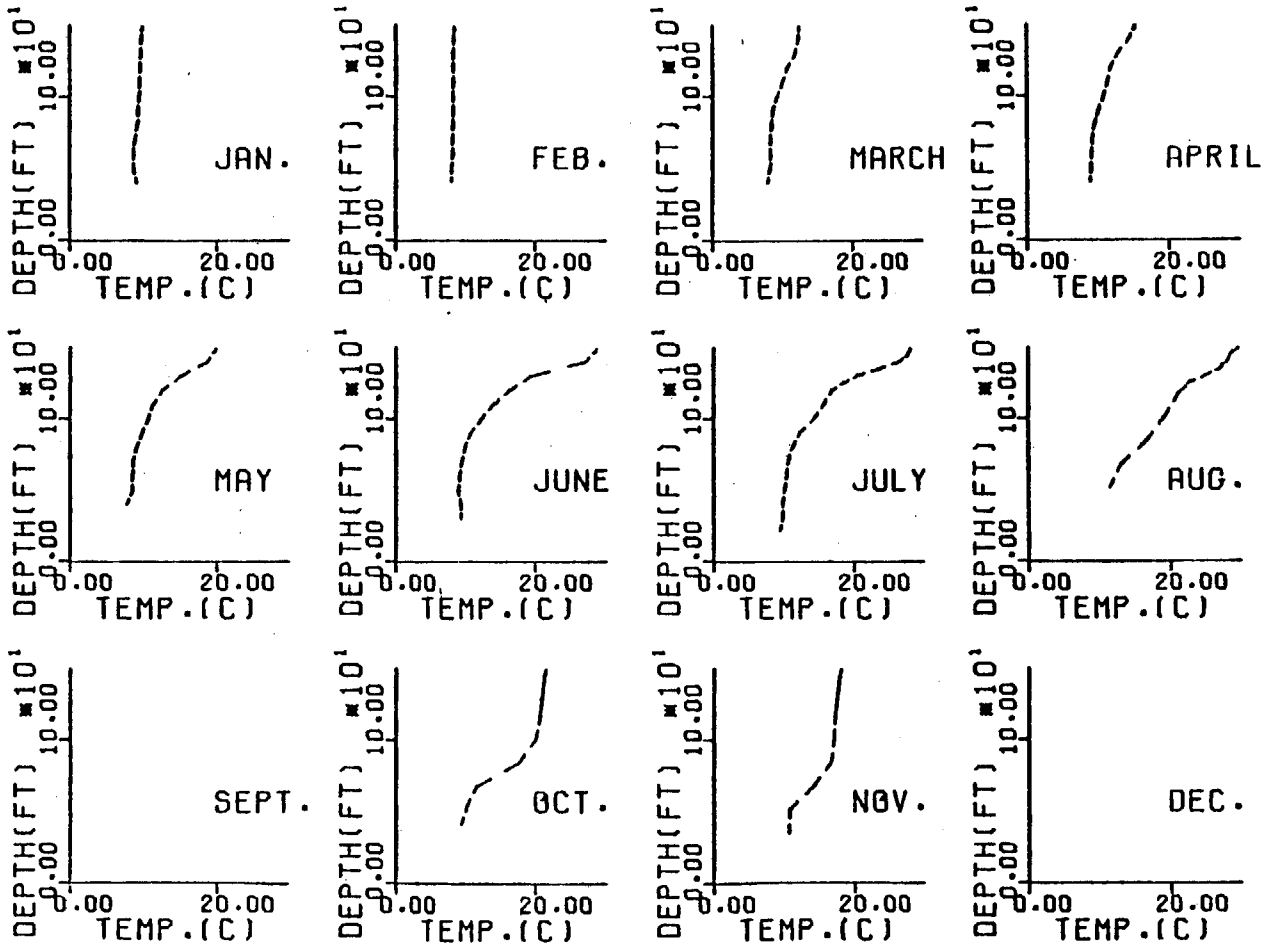

Figure C-3. Lake Keowee averaged measured temperature profiles, Stations 501-506, 1973

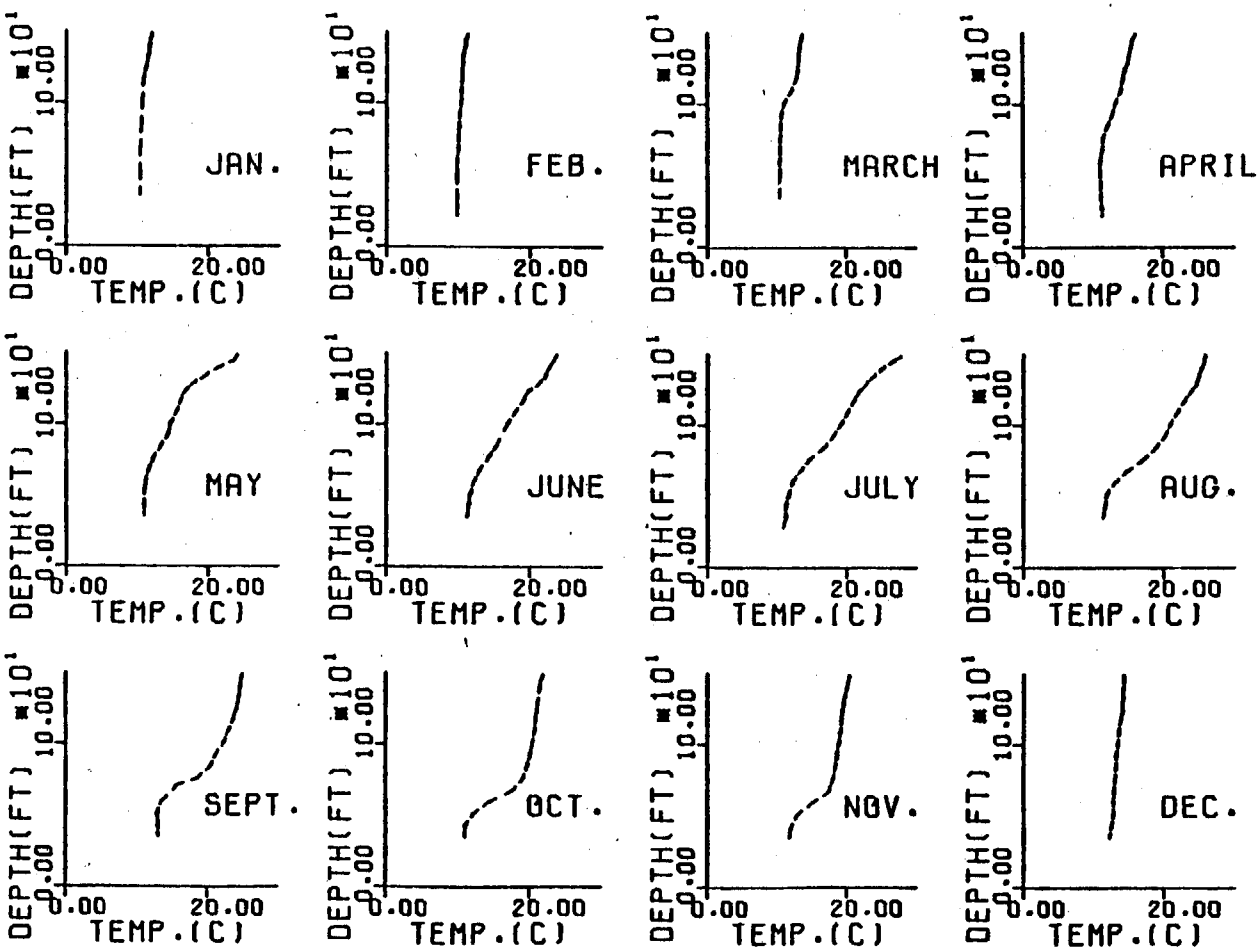

Figure C-4. Lake Keowee measured temperature profiles, Stations 501-506, 1974

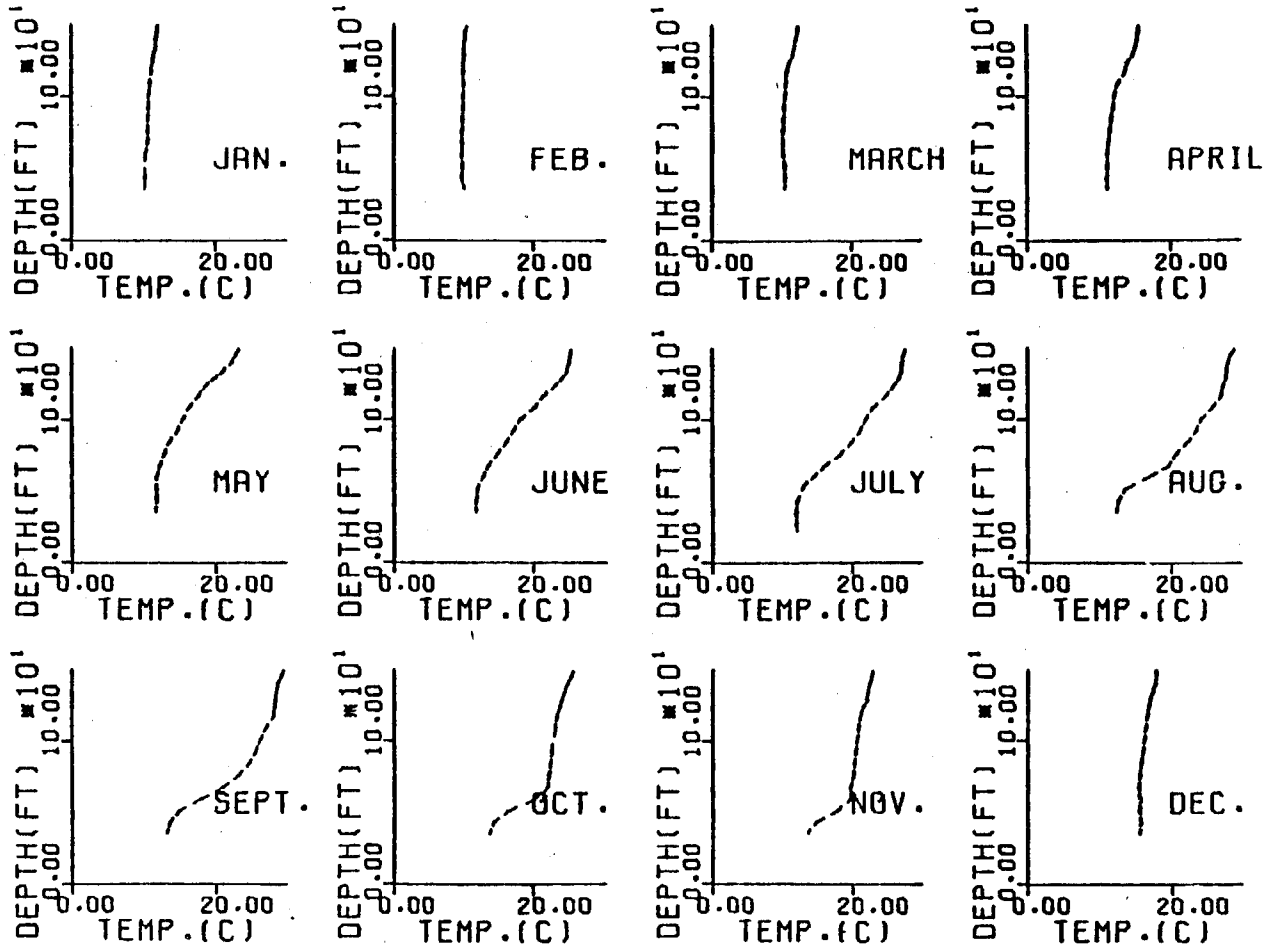

Figure C-5. Lake Keowee measured temperature profiles, Stations 501-506, 1975

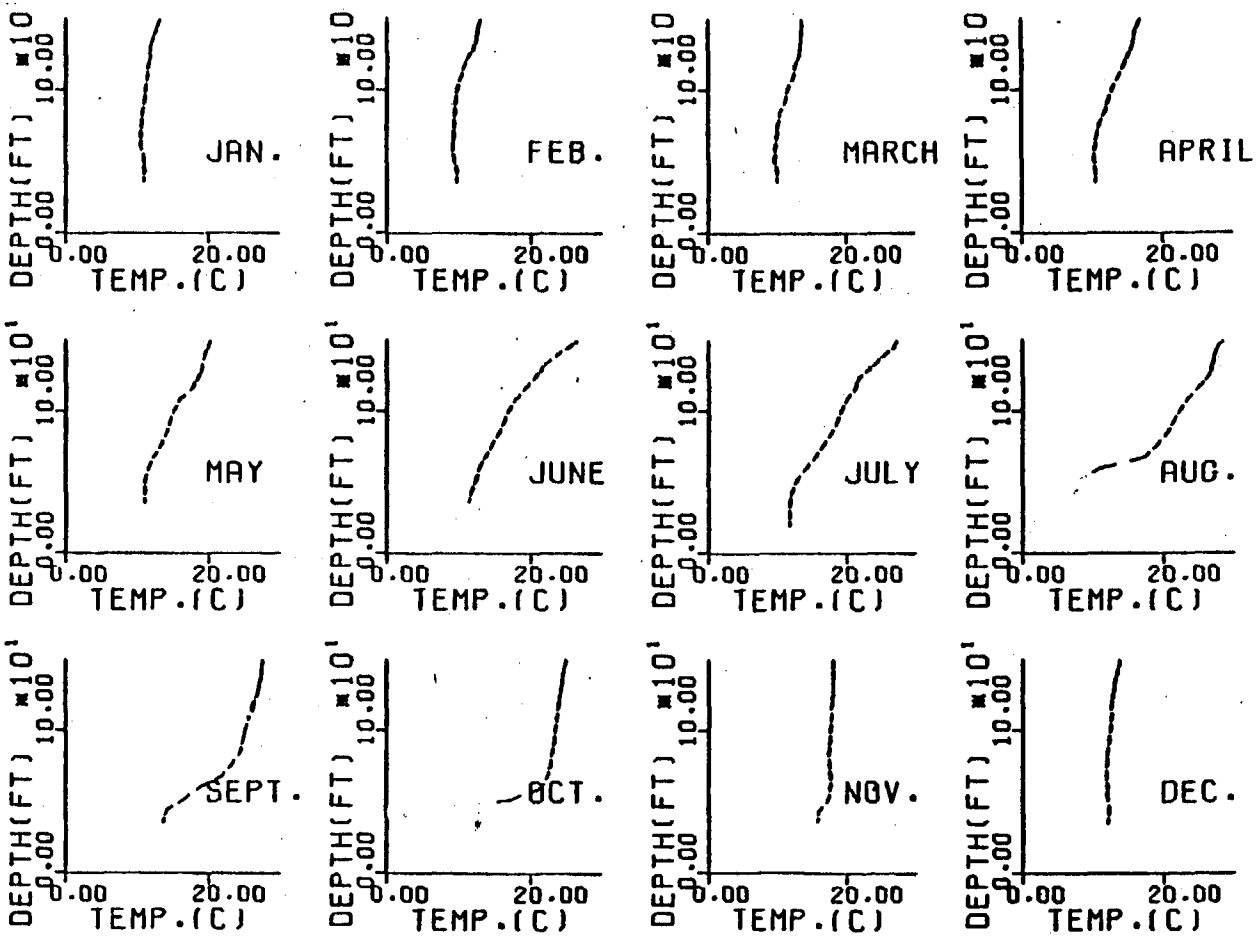

Figure C-6. Lake Keowee measured temperature profiles, Stations 501-506, 1976

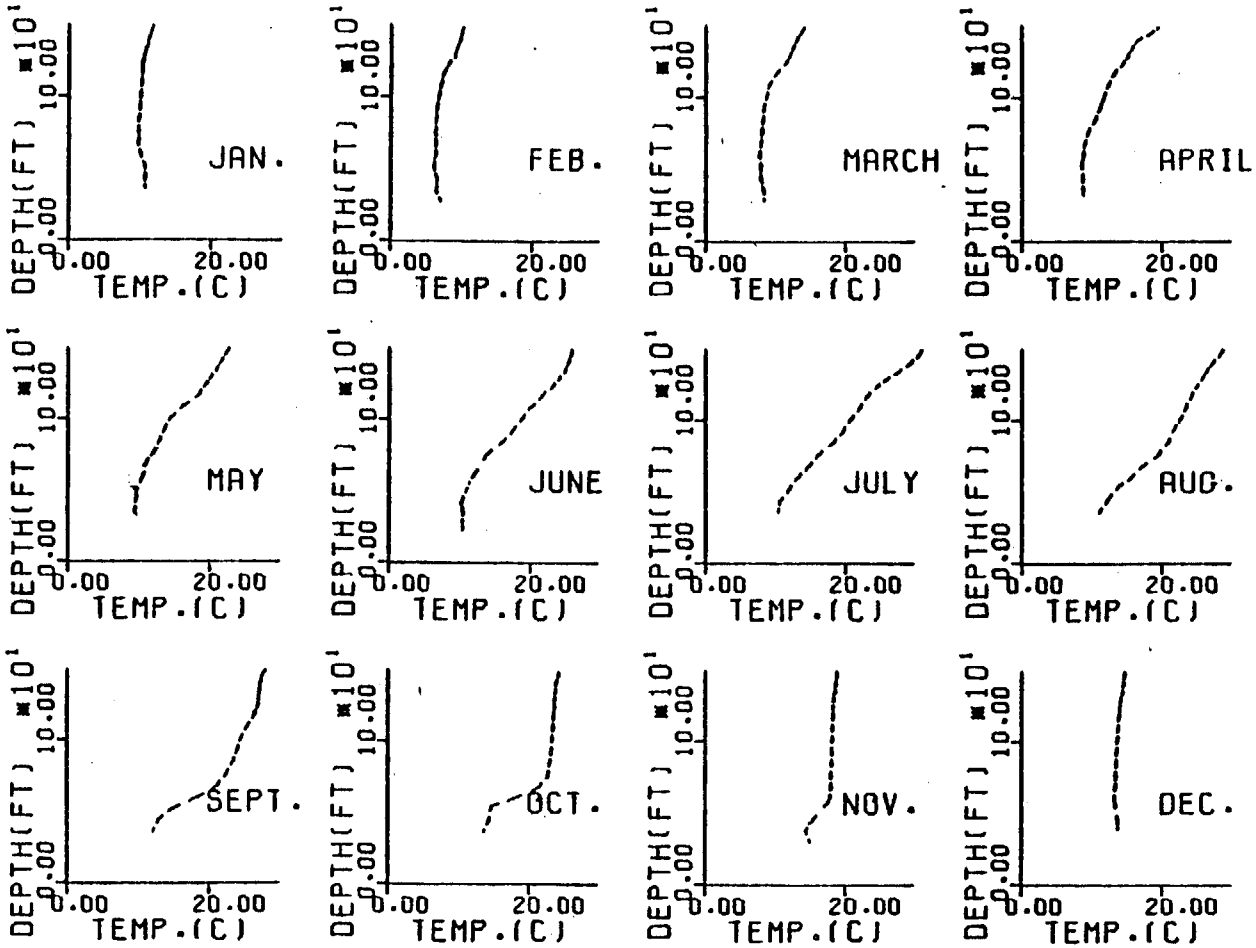

Figure C-7. Lake Keowee measured temperature profiles, Stations 501-506, 1977

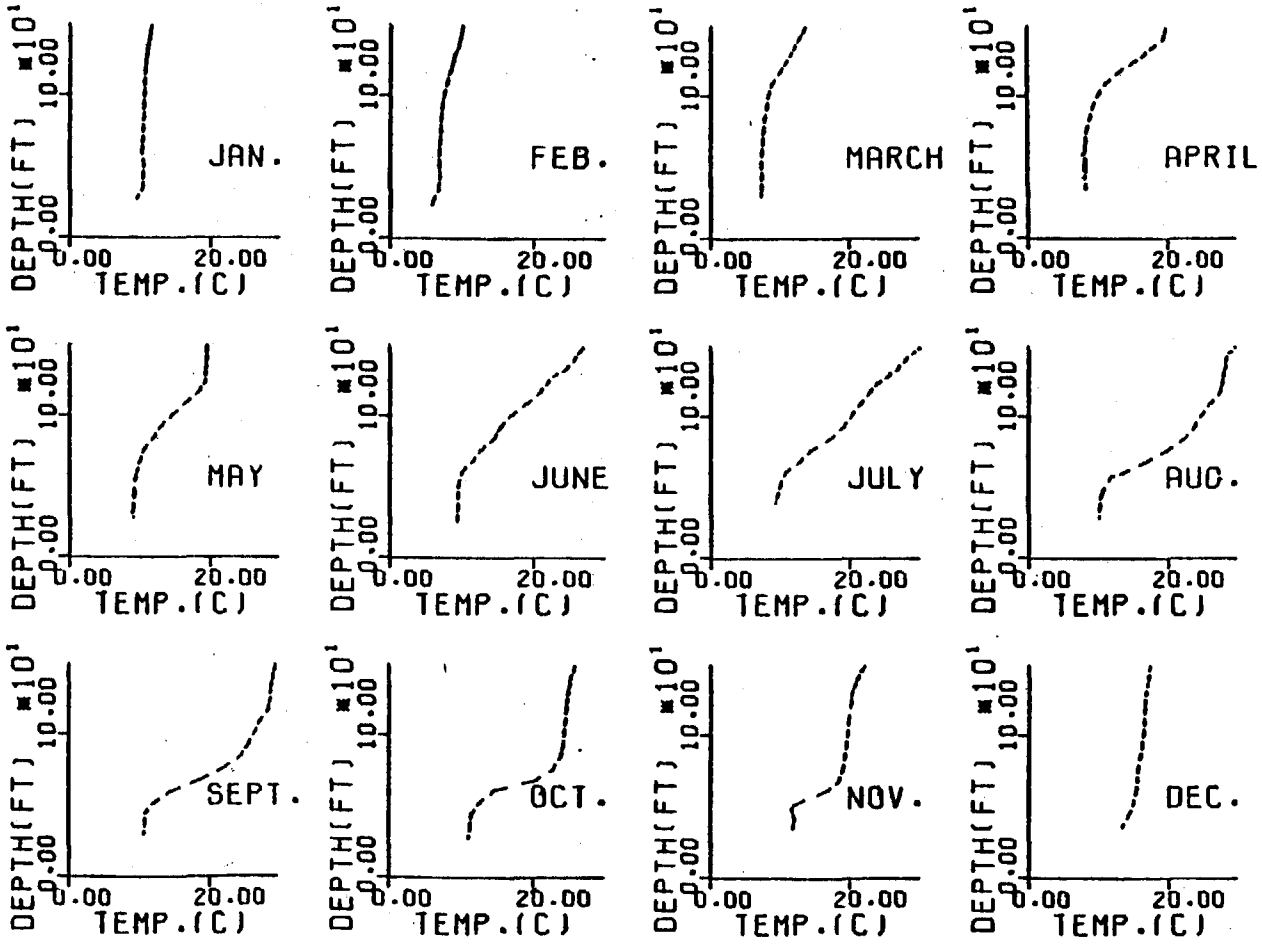

Figure C-8. Lake Keowee measured temperature profiles, Stations 501-506, 1978